Nanoparticles-Infused Lithium Manganese Phosphate Coated With Magnesium-Gold Composite Thin Film - A Possible Novel Material for Lithium Ion Battery Olivine Cathode

UNIVERSITY *of the*
WESTERN CAPE

Ntuthuko Wonderboy Hlongwa
(BSc Honours)

A mini-thesis submitted in partial fulfilment of the requirements for the degree of

Magister Scientiae in Nanoscience

Faculty of Science

University of the Western Cape

Bellville, Cape Town, South Africa

Supervisor: Prof Emmanuel Iwuoha

Co-supervisors: Dr Chinwe Ikpo

December, 2014

Nanoparticles-Infused Lithium Manganese Phosphate Coated With Magnesium-Gold Composite Thin Film - A Possible Novel Material for Lithium Ion Battery Olivine Cathode

Keywords

Energy

Lithium-ion batteries

Cathode

Olivine cathode

Coating

Thin film

Composite

Magnesium-gold

Charge/discharge capacity

Electrochemical impedance spectroscopy

Cyclic voltammetry

Conductivity

Abstract

Nanoparticles-Infused Lithium Manganese Phosphate Coated With Magnesium-Gold Composite Thin Film - A Possible Novel Material for Lithium Ion Battery Olivine Cathode

Ntuthuko Wonderboy Hlongwa

Msc mini Thesis, Department of Chemistry, University of the Western Cape,

December 2014

Architecturally enhanced electrode materials for lithium ion batteries (LIB) with permeable morphologies have received broad research interests over the past years for their promising properties. However, literature based on modified porous nanoparticles of lithium manganese phosphate ($LiMnPO_4$) is meagre. The goal of this project is to explore lithium manganese phosphate ($LiMnPO_4$) nanoparticles and enhance its energy and power density through surface treatment with transition metal nanoparticles. Nanostructured materials offer advantages of a large surface to volume ratio, efficient electron conducting pathways and facile strain relaxation. The material can store lithium ions but have large structure change and volume expansion during charge/discharge processes, which can cause mechanical failure. $LiMnPO_4$ is a promising, low cost and high energy density (700 Wh/kg) cathode material with high theoretical capacity and high operating voltage of 4.1 V vs. Ag/AgCl which falls within the electrochemical stability window of conventional electrolyte solutions. $LiMnPO_4$ has safety features due to the presence of a strong P–O covalent bond. The $LiMnPO_4$ nanoparticles were synthesized via a sol-gel method followed by coating with gold nanoparticles to enhance conductivity. A magnesium oxide (MgO) nanowire was then coated onto the $LiMnPO_4$/Au, in order to form a support for gold nanoparticles which will then form a thin film on top of $LiMnPO_4$ nanoparticles crystals. The formed products will be $LiMnPO_4$/Mg-Au composite. MgO has good electrical and thermal conductivity with improved corrosion resistance. Thus

the electronic and optical properties of MgO nanowires were sufficient for the increase in the lithium ion diffusion. The pristine $LiMnPO_4$ and $LiMnPO_4$/Mg-Au composite were examined using a combination of spectroscopic and microscopic techniques along with cyclic voltammetry (CV) and electrochemical impedance spectroscopy (EIS). Microscopic results revealed that the $LiMnPO_4$/Mg-Au composite contains well crystallized particles and regular morphological structures with narrow size distributions. The composite cathode exhibits better reversibility and kinetics than the pristine $LiMnPO_4$ due to the presence of the conductive additives in the $LiMnPO_4$/Mg-Au composite. This is demonstrated in the values of the diffusion coefficient (*D*) and the values of charge and discharge capacities determined through cyclic voltammetry. For the composite cathode, *D* = 2.0 x 10^{-9} cm^2/s while for pristine $LiMnPO_4$ D = 4.81 x 10^{-10} cm^2/s. The charge capacity and the discharge capacity for $LiMnPO_4$/Mg-Au composite were 259.9 mAh/g and 157.6 mAh/g, respectively, at 10 mV/s. The corresponding values for pristine $LiMnPO_4$ were 115 mAh/g and 44.75 mAh/g, respectively. A similar trend was observed in the results obtained from EIS measurements. These results indicate that $LiMnPO_4$/Mg-Au composite has better conductivity and will facilitate faster electron transfer and therefore better electrochemical performance than pristine $LiMnPO_4$. The composite cathode material ($LiMnPO_4$/Mg-Au) with improved electronic conductivity holds great promise for enhancing electrochemical performances, discharge capacity, cycle performance and the suppression of the reductive decomposition of the electrolyte solution on the $LiMnPO_4$ surface. This study proposes an easy to scale-up and cost-effective technique for producing novel high-performance nanostructured $LiMnPO_4$ nanopowder cathode material.

Declaration

I declare that "*Nanoparticles –infused lithium manganese phosphate coated with magnesium-gold composite thin film - a possible novel material for lithium ion battery olivine cathode*" is my own work, that it has not been submitted before for any degree or examination in any other university, and that all the sources I have used or quoted have been indicated or acknowledged as complete references.

Ntuthuko Wonderboy Hlongwa December 2014

Signed……

Dedication

This work is dedicated to: my late mother and father; Zandile Hlongwa and Thembinkosi David Hlongwa, my grandmother Phanjiwe Ntu Mbotho and my aunt Phumlile Mbotho.

Acknowledgements

To God almighty that created and gave me mental and physical strength to complete this project and the One behind all my successes, be the glory and honour.

I would like to thank my supervisor, Prof Emmanuel Iwuoha, for the care, encouragement and support that he has been giving throughout the course of the year, may God richly bless him. To my co-supervisors, Dr Chinwe Ikpo and Dr Natasha Ross, thank you for your advice and guidance for this project. To the SensorLab family, it has been fun working with you guys though frustrating at times, thanks to everyone who was ever willing to help. To the 2013 Nanoscience group I would like to express my sincere gratitude to all for their insight and guidance. I am honoured to have worked with such ingenious individuals thanks for your encouragements. To my family and friends, I say a big thank you for your love, motivation and support throughout the period of the study.

I also would like to acknowledge National Nanosciences Postgraduate Teaching and Training Platform (NNPTTP) for the award of MSc Scholarship, and lastly but not the least, the Chemistry Department and UWC, for providing me the opportunity to study for this postgraduate degree.

Table of Contents

Title page.....i

Keywords.....ii

Abstract.....iii

Declaration.....v

Dedication.....vi

Acknowledgements.....vii

Table of Contents.....viii

Acronyms and abbreviations.....xi

List of figures.....xii

List of tables.....xiv

Chapter 1.....1

1 **Introduction**.....1

1.1 **Research background**.....1

1.1.1 Need for renewable energy production.....2

1.1.2 Energy storage technology the solution to renewable energy production.....2

1.2 **Problem statement**.....5

1.3 **Motivation or rationale**.....6

1.4 **Research aims**:.....7

1.5 **Thesis lay-out**.....8

Chapter 2.....9

2 **Literature review**.....9

2.1 **Battery technology and operating principle**.....9

2.1.1 Primary batteries.....10

2.1.2 Secondary batteries.....10

2.1.2.1 Lead-acid batteries.....11

2.1.2.2 Nickel based batteries.....12

2.1.2.3 Lithium ion polymer (Li-ion polymer).....13

2.1.2.4 Lithium ion batteries.....13

2.2 **Cathode functionality** 18
2.2.1 Lithium manganese phosphate ($LiMnPO_{4)}$ cathode material 19
2.2.1.1 Synthesis on high- performance $LiMnPO_4$ olivine cathode……..21
2.3 **Electrolytes** 22
2.3.1 Aqueous electrolyte 23
2.3.2 Organic electrolyte 24
2.4 **Surface modification by doping and coating** 24
2.5 **Nanomaterials and relevance of nanotechnology** 25
2.6 **Gold nanoparticles and magnesium oxide nanowires for surface modification** 26
Chapter 3 29
3 **Materials and methods** 29
3.1 **Reagents** 29
3.2 **Methodology** 29
3.2.1 Preparation of $LiMnPO_4$ nanoparticles 29
3.2.2 Preparation of gold nanoparticles (AuNPs) 30
3.2.3 Coating $LiMnPO_4$ nanoparticles with gold nanoparticles 30
3.2.4 Synthesis of MgO nanowires 30
3.2.5 MgO nanowire coated onto $LiMnPO_4$/Au 31
3.3 **Material characterization techniques and instrumentation** 31
3.3.1 Structural characterisation and crystal structure identification 31
3.3.2 UV-Vis spectroscopy 35
3.3.1.1 X-ray diffraction (XRD)……..31
3.3.1.2 Surface morphology by SEM and HRTEM……32
3.3.1.3 Energy dispersive x-ray spectroscopy(EDS)…….……..33
3.3.1.4 Fourier transform infrared spectroscopy (FTIR)…….…34
3.3.1.5 Raman spectroscopy……34
3.3.3 Electrochemical techniques 35
Chapter 4: 40
4 **Results and discussion** 40
4.1 **Characterisation and analysis of nano-$LiMnPO_4$ olivine cathode** ... 40
4.1.1 Particle morphology and chemical composition 40

4.1.2 Crystal structure and phase composition analyses by X-ray diffraction (XRD) 44
4.1.3 $LiMnPO_4$ fourier-transform infrared and Raman vibrational spectroscopic analysis 46
4.1.4 Electrochemical characterisation of $LiMnPO_4$ 49
Chapter 5 52
5 **Analysis of lithium manganese phosphate coated with magnesium-gold composite thin film** 52
5.1 **Magnesium nanowire and gold nanoparticles** 52
5.1.1 Synthesis and characterisation of magnesium oxide nanowires 52
5.1.2 Characterisation of gold nanoparticles 57
5.2 **Lithium manganese phosphate coated with magnesium-gold composite thin film** 60
5.2.1 Particle morphology and chemical composition of composite of $LiMnPO_4$/Mg-Au 60
5.2.2 Crystal structure and phase composition analysis by x-ray diffraction (XRD) for the composite of $LiMnPO_4$/Mg-Au thin film 63
5.2.3 Fourier-transform infrared $LiMnPO_4$ coated with Mg-Au thin film analysis 65
5.2.4 Electrochemical characterisation for composite of $LiMnPO_4$ coated with magnesium-gold composite 65
5.2.4.1 Cyclic voltammetry for redox reaction analysis……..66
5.2.4.2 Electrochemical impedance spectroscopy……72
Chapter 6 78
6 **Conclusion and Recommendations** 78
6.1 **Conclusion** 78
6.2 **Recommendations** 81
References 82

Acronyms and abbreviations

CV	Cyclic voltammetry
EIS	Electrochemical Impedance spectroscopy
XRD	X-ray diffraction
SEM	Scanning electron microscopy
EDS	Energy dispersive x-ray spectroscopy
TEM	Transmission electron microscopy
HRTEM	High resolution transmission electron microscopy
$LiMnPO_4$	Lithium manganese phosphate
Au	Gold
Mg	Magnesium
MgO	Magnesium oxide
AuNps	Gold nanoparticles
NW	Nanowire
$LiMnPO_4$/Mg-Au	Lithium manganese phosphate coated with magnesium-gold composite thin film

List of figures

Figure 2.1: Comparison of different battery technologies in terms of volumetric and gravimetric energy density. (www.nexergy.com/media/BatteryGraph.JPG 2011). 14

Figure 2.2: Schematic of the electrochemical process in a lithium ion cell. (http://tuprints.ulb.tu-darmstadt.de/1864/1/Dissertation_Stefan_Laubach.pdf 2011). 16

Figure 2.3: Structure of the LiMnPO4 with Pnma space group (Bakenov and Taniguchi, 2011). 20

Figure 3.1: Nyquist Plot with impedance vector (Barsoukov and Macdonals 2005). 38

Figure 3.2: Typical Bode plot (Barsoukov and Macdonals 2005). 39

Figure 3.3: Randles circuit equivalent electrical circuit. 39

Figure 4.1: High resolution scanning electron micrographs (HRSEM) of $LiMnPO_4$ powder calcined at 580 °C. 41

Figure 4.2: TEM images of $LiMnPO_4$ powders calcined at 580 °C at (a) - (b) with lattice image or HRTEM (c) and selected area electron diffraction (SAED) patterns (d). 43

Figure 4.3: EDS of the synthesized nano-$LiMnPO_4$ on the copper grid 44

Figure 4.4: XRD patterns of $LiMnPO_4$ samples calcined at different temperatures for 3 h: (a)400 °C; (b) 450 °C; (c) 500 °C;(d) 550 °C and (e) 580 °C 46

Figure 4.5: FTIR spectra of olivine $LiMnPO_4$ calcinated at 580 °C 48

Figure 4.6: Raman spectra of olivine $LiMnPO_4$ 48

Figure 4.7: Cyclic voltammograms of the bare GCE and that of GCE modified with the $LiMnPO_4$ in 1 M $LiSO_4$ 50

Figure 4.8: Cyclic voltammetry of $LiMnPO_4$ in 1 M $LiSO_4$ electrolyte 51

Figure 5.1: SEM images of the MgO nanowires 53

Figure 5.2: (a) TEM image of the MgO nanowires and (b) SAED patters of the MgO nanowires 54

Figure 5.3: MgO nanowires TEM energy dispersive x-ray (EDS). 55

Figure 5.4: X-ray pattern of the MgO nanowire network 56

Figure 5.5: Absorbance spectra of the MgO nanowires 56

Figure 5.6: TEM images of the gold nanoparticles. 58
Figure 5.7: TEM/EDS of the gold nanoparticles. 59
Figure 5.8: Gold nanoparticles UV-Vis absorption..... 59
Figure 5.9: HRSEM of $LiMnPO_4$/Mg-Au nanoparticles at magnification of 2 µm. 61
Figure 5.10: HRSEM of $LiMnPO_4$/Mg-Au nanoparticles at magnification of 300 nm. 62
Figure 5.11: HRSEM of $LiMnPO_4$/Mg-Au nanoparticles at magnification of 1µm with the use of SE detector. 62
Figure 5.12: Energy dispersive x-ray (EDS) of $LiMnPO_4$/Mg-Au nanoparticles 63
Figure 5.13: XRD pattern of $LiMnPO_4$ coated Mg-Au composite thin film..... 64
Figure 5.14: FTIR spectra for olivine $LiMnPO_4$/Mg-Au composite 65
Figure 5.15: Comparative cyclic voltammograms of $LiMnPO_4$/Mg-Au thin film composite and pristine $LiMnPO_4$ in 1 M $LiSO_4$. Scan rate 10 mV/s (voltage range: -1000 mV/s – 1000 mV/s). 68
Figure 5.16: The effect of potential scan rate on the cyclic voltammograms of $LiMnPO_4$/ Mg-Au composite in 1 M $LiSO_4$ 1 – 10 mV/s. Voltage range: -1000–1000 mV. 70
Figure 5.17: The plots of the anodic peak current as a function of potential scan rates and cathodic current as a function of potential scan rate for $LiMnPO_4$..... 71
Figure 5.18: The plots of the anodic peak current as a function of potential scan rates and cathodic current as a function of potential scan rate for $LiMnPO_4$/Mg-Au thin film composite. 72
Figure 5.19: Comparative Nyquist plots of $LiMnPO_4$ and $LiMnPO_4$/Mg-Au thin film composite at formal potential..... 74
Figure 5.20: Comparative Bode phase-impedance diagrams of $LiMnPO_4$ and $LiMnPO_4$/Mg-Au composite at formal potential..... 75

List of tables

Table 5.1: Chemical composition by EDS/SEM……...…….…….. 63

Table 5.2: Kinetic parameters of composite $LiMnPO_4$ and $LiMnPO_4$ obtained from electrochemical impedance spectroscopy ……..……..….77

Chapter 1

1 Introduction

1.1 Research background

Energy is a central societal issue impacting our way of life, world, economy and human health. Primary energy can be divided into non-renewable and renewable energy source groups. The non-renewable sources are mostly the energy that is formed or found in nature. Fossil fuels are classified as non-renewable energy resources because they took millions of years to form naturally yet their reserves are easily depleted (Mann *et al*., 2009). The escalating use of fossil fuels brings about increase in environmental concerns (Winter and Brodd, 2005). The world coal consumption seems to increase year after year which is mainly due to the need and the much increasing population. Concurrently, the increase in demand for electricity will cause coal to be depleted much sooner than predicted therefore; there is a great need for alternative energy sources. The South African economy is largely coal-driven which is grossly unsustainable and at a serious risk due to the continuous increase in demand for fossil fuels (coal, oil and gas) as well as depletion of non-renewable resources. A major issue of local and global concern on fossil fuel energy economy is also associated with carbon dioxide (CO_2) emissions upon fossil fuel combustion during electricity generation. Environmental concerns for CO_2 stem from the fact that it is the major greenhouse gas, which contribute to global warming and climate change (Hadjipaschalis *et al.*, 2009; Scrosati and Garche, 2010). As the South African population grows; a more than proportionate increase in energy demand is anticipated.

The energy economy is at a serious risk because of a series of factors including the continuous increase in the demand for oil. A global increase in energy demand will cause a dramatic rise of prices of conventional energy sources as we have seen in the last ten years and the dependence of national economies on a continuous and undistorted supply of such sources has become critical. Due to

these many mentioned factors that arise from non-renewable sources, there is a need for global movements towards the generation of renewable energy which can help meet increased energy needs and demands.

1.1.1 Need for renewable energy production

Renewable energy sources generally come from resources such as sunlight, wind, geothermal heat. The use of this energy source has increased worldwide as potential general source of energy. Renewable energy sources have advantages over non-renewable methods, but these types of energy sources relying on the weather or climate to work effectively. Renewable sources currently provide 4% of electricity production which mostly come from solar energy, this is estimated to grow by more than 25% by 2030 (Alotto *et al.*, 2014). The power of these renewable sources ranges from the hourly time –scale which is definitely related to the daily sun-light through the year, typical of photo- voltaic (PV) systems, down to the min–s time-scale that is characteristic of wind generators (Alotto *et al.*, 2014). They operate by harnessing the power of nature and as such their peak power outputs may not match the power requirements (Jacobson *et al.*, 2009). Therefore, for renewable energy sources to be considered as the new source of energy they must be completely reliable as primary sources of energy. When excess is produced, energy from these sources needs to be stored and released when needed. Energy storage technologies form therefore, an important and essential part of a reliable and effective renewable unit for plant distribution at full capacity and efficiency (Chen, 2013).

1.1.2 Energy storage technology the solution to renewable energy production

Energy storage is done by devices or physical media that store energy to perform useful operation at a later stage or time. A device that stores energy is sometimes called an accumulator. It is believed that the use of renewable energy source could be environmentally friendly and energy storage could also be useful in reducing electrical costs for distributors and consumers (Hadjipaschalis *et al.*, 2009). The

most important part of energy storage is the ability to have charge/discharge cycles which have short timescale (s-min). There are different types of energy storage methods; some are available and others are still under development or are still being researched, which are: PHES (pumped hydro energy storage), CAES (compressed air energy storage), TES (thermal energy storage), FES (Flywheel energy storage), SMES (superconducting magnetic energy storage), EDLC (electric double layer capacitor) and ECES (electrochemical energy storage) (Alotto *et al.*, 2014). Energy storage technology must not only ensure response time and storage capacity which are suitable for meeting both the generation and grid needs, but should be able to withstand a large number of charge/discharge cycles and they need to have a long lifetime (Hadjipaschalis *et al.* 2009). The different energy storage technologies are suitable to store energy differently and meet different localization needs.

Prior research has shown that electrochemical energy storage systems (ECES) are the leading candidates in finding a solution to assist renewable energy generators. ECES is one of the technologies used to store energy in different plants. There are three different types of ECES and conversion which are batteries, fuel cells, and electrochemical capacitors (ECs). These devices differ in application, energy scale and conversion mechanisms but have similar electrochemical operating principles where the electrode/electrolyte interface energy-providing processes occur at phase boundaries with the separation of electron and ion transport (Winter and Brodd, 2005).

Batteries and fuel cells work by converting chemical energy via redox reactions at the anode and cathode to produce or generate electrical energy (Winter and Brodd, 2005). Anode is an electrode where electric current flows into a polarized electrical device, while cathode is electrode where electric current flows out of a polarized electrical device. The only difference between batteries and fuel cells is that batteries are in a closed system with both cathode and anode being in charge-transfer medium. Energy storage and energy conversion in a fuel cell is separated due to the fact that it contains fuels such as hydrogen and hydrocarbons.

Electrochemical capacitors do not work by redox reaction; anode and cathode aren't appropriate (Winter and Brodd, 2005). Electrolyte ions are orientated at the electrolyte/electrolyte interface, and electrical double layers (EDLs) are formed and released, this will cause parallel movement of electrons in the external will, and that is how energy is delivered (Winter and Brodd, 2005). When supercapacitors and fuels cells are compared against batteries, batteries have enjoyed more application markets and they have established market position.

Batteries as of today are the best positioned technology to handle the challenges of renewable energy technology. This research work is aimed at addressing the current disadvantages of the cathode in lithium- ion batteries and finding an alternative cathode material with better performance. The cathode material that is widely used is lithium cobalt oxide ($LiCoO_2$) but it is however, expensive and also not environment friendly. This research work proposes the use of olivine cathode nanoparticles of lithium manganese phosphate ($LiMnPO_4$) coated with magnesium-gold composite thin film.

The proposed composite cathode material with improved electronic conductivity holds great promise for enhanced electrochemical performances, discharge capacity, cycle performance, rate capacity and suppression of reductive decomposition of electrolyte solution on the $LiMnPO_4$. This study presents an easy scale-up and cost effective route for the production of novel, high-performance nanostructured $LiMnPO_4$ cathode material.

1.2 Problem statement

The olivine $LiMnPO_4$ is an excellent cathode material for lithium ion battery mainly due to its superior redox potential at 4.1 V vs. Li/Li^+ when compared with the already commercialised olivine $LiFePO_4$, layered $LiCoO_2$ and spinel $LiMnO_4$. However, very low electrochemical performance caused by huge volume change between $LiMnPO_4$ and $MnPO_4$ during intercalation; and poor electronic conductivity limits its application. Nanomaterials have been proved to be useful in lithium ion batteries with several advantages like - the reduced dimensions increase significantly the rate of lithium insertion/removal due to the short distances for lithium- ion transport within the material; they increase rate capacity of lithium ion battery as well as improve cycle life. Electron transport within the cathode material is also enhanced by nanometer-sized particles; high surface area allows active material to absorb lithium ions more effectively hence increase capacity. With the decrease in size, the chemical potentials for lithium ions and electrons may be modified, resulting in a change of electrode potential (thermodynamics of the reaction). Nanomaterials will provide new reactions which are not possible with bulk materials. In this research project Nanoparticles-infused $LiMnPO_4$ cathode material will be prepared by coating with gold nanoparticles and magnesium nanowires thereby enhancing its conductivity. The electrochemical characterisation of the prepared materials will be conducted by employing electrochemical impedance spectroscopy (EIS) and cyclic voltammetry (CV). The proposed composite cathode material ($LiMnPO_4$/Mg-Au) with improved electronic conductivity holds great promise for enhanced electrochemical performances, discharge capacity, cycle performance and suppression of the reductive decomposition of the electrolyte solution on the $LiMnPO_4$ surface.

1.3 Motivation or rationale

The South African economy is largely coal-driven which is grossly unsustainable and at a serious risk due to the continuous increase in demand for fossil fuels (coal, oil and gas) as well as depletion of non-renewable resources. A major issue of local and global concern on fossil fuel energy economy is associated with carbon dioxide (CO_2) emissions upon fossil fuel combustion during electricity generation. Environmental concerns for CO_2 stem from the fact that it is the major greenhouse gas contributing to global warming and climate change. As the South African population grows; a more than proportionate increase in energy demand is anticipated. This therefore places an urgent need for sustainable and efficient energy systems. The two principal renewable energy sources are solar and windmills. Solar and wind power systems convert natural sources of energy (sunlight and wind kinetic energy) into electricity. They are regarded as major future sources of electrical energy. However, intermittent supply of energy from these renewable sources as a result of seasonal and tidal variations makes the development of efficient energy storage systems inevitable. Therefore there is a need for suitable energy storage system and in this project the use of lithium ion battery is proposed. The lithium ion battery with its outstanding features including high energy density, high voltage, long cycle life, and short charge time, is designed to spearhead the modern revolution in batteries. South Africa has large deposits of much of the chemical raw materials such as manganese, iron, cobalt, nickel and vanadium, required for the manufacture of lithium ion batteries. Hence, the development of this technology in the country will reduce dependence on fossil fuels, cause increased participation in nanotechnology and nanoscience research, provide opportunities for human resource capacity development and benefit the environment.

1.4 Research aims:

The goal of this project is to explore lithium manganese phosphate ($LiMnPO_4$) modified by being coated with magnesium-gold composite thin film as cathode materials and study the conductivity of the $LiMnPO_4$ vs. $LiMnPO_4$/Mg-Au composite.

The study has the following objectives:

1.2.1. Synthesis of lithium manganese phosphate ($LiMnPO_4$) nanoparticles.

1.2.2 Preparation of gold nanoparticles (AuNps).

1.2.3 The coating of $LiMnPO_4$ with AuNps.

1.2.3. Synthesis of magnesium (MgO) nanowire.

1.2.4 The coating of $LiMnPO_4$/Au with MgO nanowire to form $LiMnPO_4$/Au/MgO nanocomposite.

1.2.5. Characterization of $LiMnPO_4$/Au/MgO nanocomposite by Transmission Electron Microscopy (TEM), Scanning Electron Microscopy (SEM), Electrochemical Impedance Spectroscopy (EIS), Cyclic Voltammetry (CV), X-ray Diffraction (XRD), Fourier-transform Infra-red Spectroscopy *(*FTIR*)*, Raman Spectroscopy and Energy Dispersive X-ray Spectroscopy (EDS).

1.5 Thesis lay-out

This thesis is presented in six chapters.

Chapter 1: Gives brief background information on the project, problem statement and motivation as well as aims and objectives.

Chapter 2: Provides a detailed literature review .

Chapter 3: Consists of reagents, procedures and instrumentations used for the success of this study.

Chapter 4: Provides results and discussion of the formed $LiMnPO_4$ nanoparticles illustrating the morphological, structural, spectroscopic, electrochemical properties.

Chapter 5: Provides results and discussion of MgO nanowire synthesized, Au nanoparticles synthesised and nanoparticle-$LiMnPO_4$ coated with magnesium-gold thin film composite and their structural, spectroscopic and electrochemical characterisations.

Chapter 6: Conclusion and recommendations.

Chapter 2

2 Literature review

2.1 Battery technology and operating principle

Batteries are electrochemical devices that produce energy by converting chemical energy into electrical energy to power a variety of applications by using electrochemical redox reactions which occur at the anode and cathode (Hadjipaschalis *et al.*, 2009). The fundamental part of a battery is the electrochemical cell which consists of three main components: the electrodes: cathode and anode; and the electrolyte. The anode is where oxidation chemical reaction takes place in a cell; electrons are donated to an external circuit, a good anode material should be efficient as a reducing agent with good conductivity, stability, easy to fabricate and at low cost. Basically metals are used as the anode material. The cathode is where reduction chemical reactions take place in a cell; it accepts electrons from the external circuit, the cathode material must be an efficient oxidizing agent, have a useful working voltage and show good stability when in contact with the electrolyte (Winter and Brodd, 2005). Common cathode materials are metal oxides. An electrolyte is a material that provides pure ionic conductivity between the anode and cathode of a cell. Its main function is to provide a transport medium for ions to travel from one electrode to the other. It must also prevent short- circuiting by acting as a physical barrier between the electrodes. The electrolyte should not undergo any net chemical changes during the operation of the battery.

Batteries are one of the electrochemical energy storage devices which have found many applications in the market (Winter and Brodd, 2005). Batteries are classified as primary or secondary depending on their capability of being electrically recharged. The classification of batteries differs with chemicals as well as the operation of a battery. The chemical idea works by having two different chemicals in a battery which have different loads and are connected with a negative

(cathode) and the other with a positive electrode (anode) (Winter and Brodd, 2005). Mainly the negative electrode supplies a current of electrons that flow through the appliance and are accepted by positive electrode, which can be used in appliances.

2.1.1 Primary batteries

Primary batteries are not rechargeable. They are discharged once and discarded, and this is due to the fact that reactions at the electrodes are not reversible. They are convenient and cost less per battery, with the downside of costing more over the long term (Winter and Brodd, 2005). The disadvantage is that they have short life time with uneconomical energy sources since they only produce 2 % of the power used in their manufacture. Examples include: zinc-alkaline-manganese-dioxide (the leclanche' cell), zinc-mercuric-oxide, zinc-silver oxide, zinc-air, magnesium-manganese dioxide and primary lithium batteries. These types of batteries are losing market share to newer technology therefore, there is not much current research going on in this area hence the need for other alternatives that can be used time and time again. In this report the focus is on rechargeable batteries, which have found a lot of interest recently in the past decade for storing energy efficiently and having long life time.

2.1.2 Secondary batteries

Secondary batteries are reversible in electrochemical reactions and the cells are rechargeable. They have higher initial cost but their maintenance in terms of recharging is very cheap and they can be used many times. They have found a lot of applications in automotive and aircraft systems, emergency no-fail and standby (UPS) power sources, hybrid electric vehicles and stationary energy storage (SES) systems for electric utility load levelling. They are also used in portable consumer electronics, power tools and electric vehicles. Examples include: lead-acid, nickel cadmium (NiCd), nickel metal hydride (NiMH), lithium ion (Li-ion) and lithium ion polymer (Li-ion polymer) batteries.

2.1.2.1 Lead-acid batteries

They are the oldest known type of rechargeable battery which was invented in 1959 by French physicist Gaston Plante'(Rand and Moseley, 2015). After over 150 years of the concept, lead-acid batteries are still been used due to their cost-effectiveness. Today, they are used widely in motor vehicles (automobile starter motors), wheel chairs and golf carts (Rand and Moseley, 2009). Lead-acid batteries have large power-to weight ratio that is why they can supply high surge current in large scale. Lead-acid designs can be used for storage backup power supplies in cell phone towers, high availability settings like hospitals, and stand-alone power systems (Moncada *et al.,* 2014). Lead-acid batteries like any other electrochemical cell are based on chemical reactions with the use of lead dioxide as the cathode, lead as the anode electrode and sulphuric acid as the electrolyte (Winter and Brodd, 2005) The energy density of lead-acid is around 30 Wh/kg with power density around 180 W/kg and the rated voltage is 2 V delivered from several in-series connection of the cells (Moncada *et al.,* 2014). During the discharge operation of the lead acid battery, the anode and cathode undergo a chemical reaction with the electrolyte and yield a change to lead sulphate that releases electrical energy in the process. The reaction is completely reversed by simply supplying the electrodes with electricity, which is why lead-acid battery can be recharged. Reaction occurring at lead-acid battery:

During discharge

Anode reaction

$$Pb(s) + HSO_4^-(aq) \rightarrow PbSO_4(s) + H^+(aq) + 2e^- \quad (1)$$

Cathode reaction

$$PbO_2(s) + HSO_4^-(aq) + 3H^+(aq) + 2e^- \rightarrow PbSO_4(s) + 2H_2O\,(l) \quad (2)$$

Overall reaction

$$Pb(s) + PbO_2(s) + 2H_2SO_4(aq) \rightarrow 2PbSO_4(s) + 2H_2O(l) \quad (3)$$

During charge

Anode reaction

$$PbSO_4(s) + H^+(aq) + 2e^- \rightarrow Pb(s) + HSO_4^-(aq) \quad (4)$$

Cathode reaction

$$PbSO_4(s) + 2H_2O(l) \rightarrow PbO_2(s) + HSO_4^-(aq) + 3H^+(aq) + 2e^- \quad (5)$$

They have between 85 % and 90 % of energy efficiencies; require low level of maintenance and low investment cost. Self-discharged rates are around 2 % of rated capacity per month (at 25 °C) (Winter and Brodd, 2005). Their drawbacks are that they have relatively low cycle life and battery operational lifetime; have a lifetime which is between 1200 and 1800 charge/discharge cycles or operate for 5-15 years. The depth of discharge and temperature negatively affect the cycle life. Electrode can be damaged by attempts to fully discharge the battery, thus reducing lifetime (Moncada *et al.*, 2014). Regarding temperature levels, using high temperatures like 45 °C which is the maximum limit for battery operation can improve performance of battery by increasing capacity but also they can reduce battery life time as the battery energy efficiency.

2.1.2.2 Nickel based batteries

Nickel based batteries are generally the nickel-cadmium (NiCd), the nickel-metal hydride (NiMH) and the nickel-zinc (NiZn) batteries. These three nickel based batteries use the same material for the positive electrode which is nickel hydroxide and the electrolyte which is an aqueous solution of potassium hydroxide with some lithium hydroxide, respectively (Hadjipaschalis *et al.* 2009). They use a different material for the negative electrode, while NiCd uses cadmium hydroxide, NiMH uses a metal alloy and NiZn uses zinc hydroxide. The energy density of NiCd is 50 Wh/kg; 80 Wh/kg for NiMH and 60 Wh/kg for NiZn which is higher than lead-acid batteries and the rated voltage for the alkaline batteries is 1.2 V (1.65 V for the NiZn) (Hadjipaschalis *et al.*, 2009). NiCd batteries life and cycle life ranges from 1500 cycle for the pocket plate vented type to 3000 cycles for the sinter vented type which is superior to lead-acid batteries but NiMH and

NiZn have lower or similar to lead-acid battery (Hadjipaschalis *et al.,* 2009). The nickel based battery have struggled to penetrate the market in terms of industrial use or for use in supporting renewable energy power systems compared to lead-acid batteries. The cost of NiCd batteries is 10 times higher than the lead-acid battery, which works against the use of this type of battery. The energy efficiencies of nickel based batteries are also lower than that of lead-acid. NiMH has 60 – 70 % and NiZn has 80 % efficiency. For the NiCd batteries, the efficiency varies depending on the type of technology used during manufacture (Shukla *et al.,* 2001), but these values are lower than of lead-acid batteries.

2.1.2.3 Lithium ion polymer (Li-ion polymer)

Lithium ion polymer batteries are usually made up of several identical secondary cells which are arranged in parallel to increase the discharge current capability. They have high energy density which ranges from 100-150 Wh/kg and energy efficiencies which are between 90- 100 %. Lithium polymer has power density which ranges from 50-250 W/kg and the lifetime is about 600 cycles (Hadjipaschalis *et al.,* 2009). This type of battery has found wide applications in mobile phones and other portable electronics.

2.1.2.4 Lithium ion batteries

The failure of metallic lithium as an anode led to the development of rechargeable lithium ion batteries (Barré *et al.,* 2013). Lithium is regarded as the lightest metal with highest potential due to its reactive behaviour. Lithium ion battery uses chemical reaction to release electricity, where lithium ions move from the anode to the cathode during discharge and back when charging, they use an intercalated lithium compound as the electrode material. (Scrosati and Garche, 2010). These intercalation electrodes are electroactive materials that serve as hosts into which guest species are reversibly inserted through the electrolyte. Lithium ion batteries are common in consumer electronics especially in portable electronics and they have the best energy densities when compared with other battery types (comparison shown in **Fig. 2.1**). They have energy densities between 80-150

Wh/kg and energy efficiencies ranging from 90-100 %; their Power densities range from 500-2000 W/kg. The lifetime of lithium ion batteries can reach more than 1500 cycles, and is temperature dependent. At higher temperatures, ageing happens much faster and can be severely shortened due to deep discharge (Hadjipaschalis *et al.,* 2009). Lithium ion battery is made up of three primary functional components which are the anode, cathode and electrolyte. Oxidation reactions occur at the anode where electrons are given up to an external circuit and anode is the reducing electrode, the anode is made from carbon (e.g. graphite), reduction reaction occurs at the cathode where electrons from an external circuit are accepted and the cathode is the oxidizing electrode.

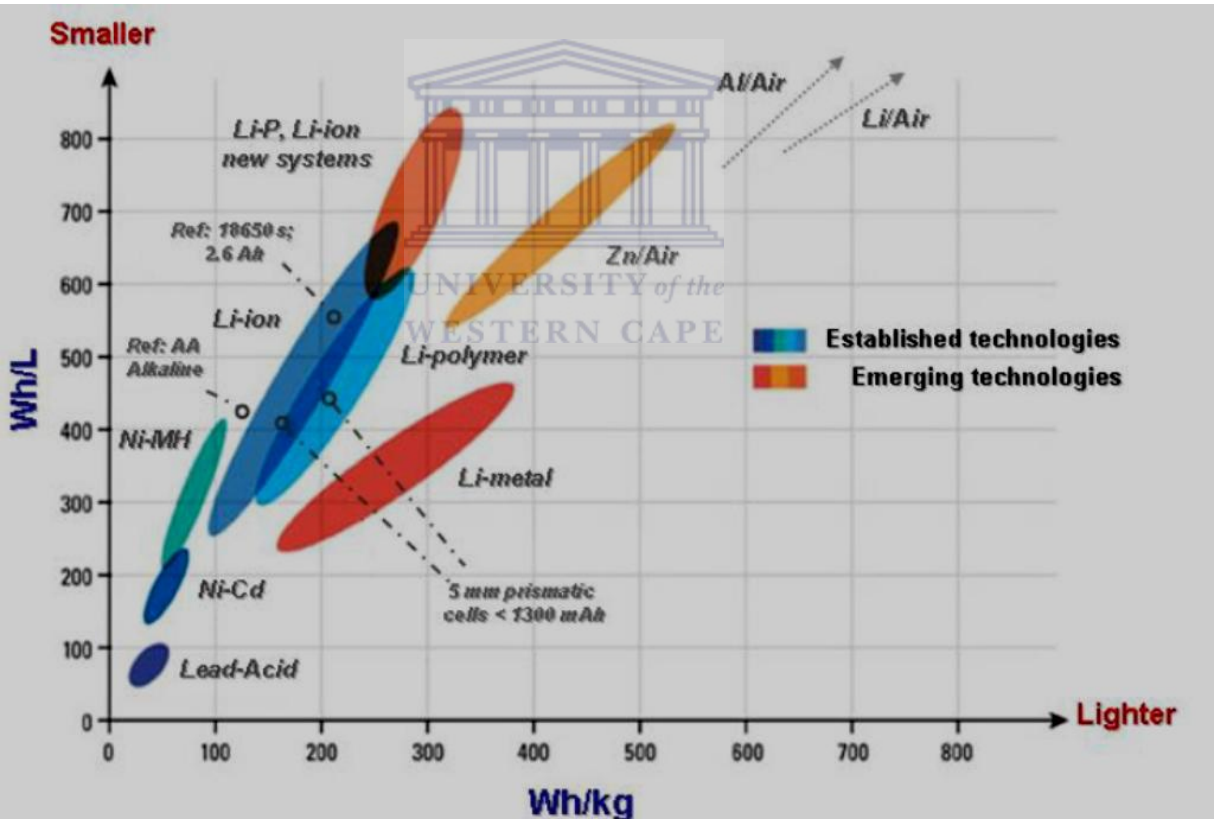

Figure 2.1: Comparison of different battery technologies in terms of volumetric and gravimetric energy density. (www.nexergy.com/media/BatteryGraph.JPG 2011).

Cathode materials are metal oxides ($LiMO_2$ e.g. $LiCoO_2$) (Chen 2013). The electrolyte is a solution of a salt and a solvent such as $LiPF_6$ dissolved in a

mixture of aprotic solvents ethylene carbonates (EC) and diethyl carbonate (Manthriram *et al.*, 2008). The electrolyte is an electronic insulator, but good ionic conductor. Its main function is to provide a transport medium for ions to travel from one electrode to the other.

Lithium ions operation principle is based on reversible de-/intercalation processes of small metal cations, mainly lithium, into the electrode materials (shown in **Fig. 2.2**). The electrochemical role of the electrodes reverses between the anode and the cathode, depending on the direction of current flow through the cell. The operating principle during the discharge process is based on the transfer of current from the negative to the positive electrode through electrolyte and separator diaphragm. While during charging, the current is forced to pass in the reverse direction by applying an over-voltage that is produced by the battery (in **Fig 2.2**) from an external electrical power source (Whittingham, 2004). The lithium ions then move from the positive to the negative electrode, where they become surrounded in the porous electrode material in intercalation (Winter and Brodd, 2005). The operation of the lithium ion battery is based on the intercalation process, a topotactic reaction involving the reversible removal or insertion of lithium ion between the anode and cathode via transport across the electrolyte whereas the electrons generated from the reaction (Manthriram *et al.*, 2008) go through the external circuit to do work.

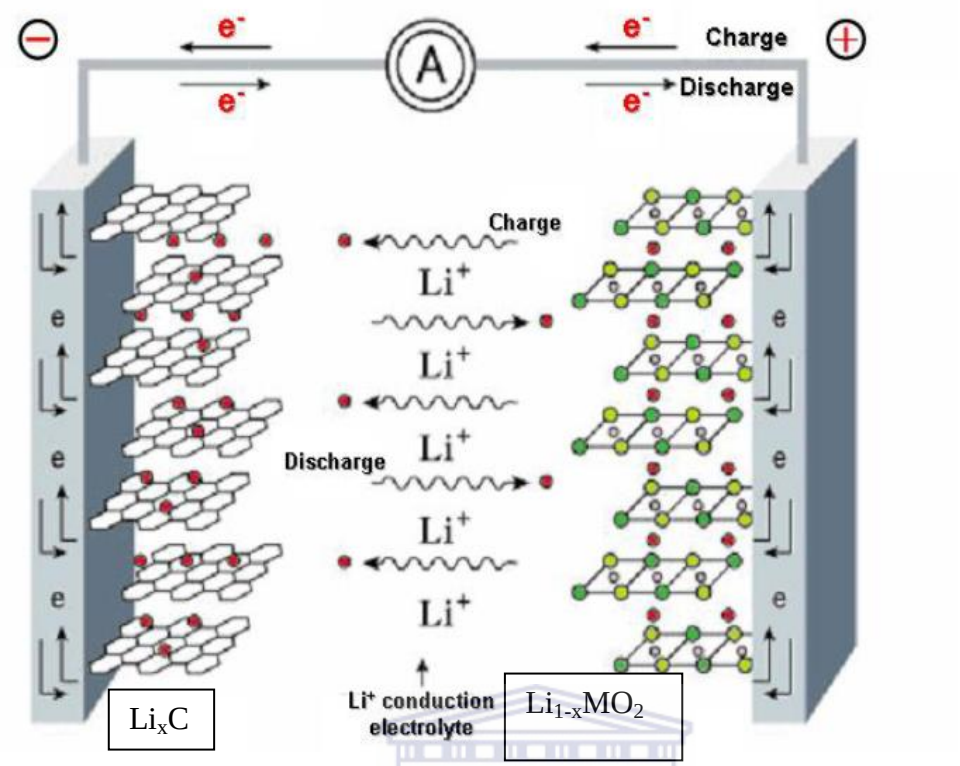

Figure 2.2: Schematic of the electrochemical process in a lithium ion cell. (http://tuprints.ulb.tu-darmstadt.de/1864/1/Dissertation_Stefan_Laubach.pdf 2011).

For more information the reactions at both electrodes in a typical lithium ion cell can be described as follows, where the forward is for the charge and the reverse is for discharge:

Positive: $LiMO_2 \leftrightharpoons Li_{1-x}MO_2 + xLi^+ + xe^-$ (6)

Negative: $C + xLi^+ + Xe^- \leftrightharpoons Li_xC$ (7)

Overall: $LiMO_2 + C \leftrightharpoons Li_xC + Li_{1-x}MO_2$ (8)

$LiMO_2$ represents lithiated transition metal oxide, the forward is for the charge and the reverse is for discharge.

The use of lithium ion batteries in renewable energy plants seem to be problematic with difficulty in scaling up the chemistry of common lithium ion

batteries. Lithium ion batteries suffer drawbacks in terms of safety, cycle life, cost, wide temperature operational range and materials availability (Manthiram *et al*., 2008). The breakthrough for scaling up lithium ion batteries would be achieved by finding electrodes and electrolyte which will serve for renewable energy storage (Aricò *et al*., 2005). There are efforts in the development of improved electrolyte and anode materials but the focus of this research work is on the cathode material due to the fact that the development, performance and cost of lithium-ion batteries are mainly limited by the properties of the cathode material. Part of the challenges is to develop a suitable cathode material that will be able to meet increasingly demands for energy storage. The cathode material must be able to accept and release lithium ions repeatedly (for recharging) and quickly (Novikova *et al.,* 2013).

The goal of the project is to improve the performance of the cathode material through a cost effective technique. Lithium cobalt oxide ($LiCoO_2$) is used currently as cathode material in most lithium ion batteries but it is costly and toxic. (Kim *et al.,* 2008). A search is underway for materials with better capacity, lesser toxicity and lower cost than $LiCoO_2$. Lithium iron phosphate ($LiFePO_4$) has attracted a lot of interest due to its advantages over $LiCoO_2$. It has an orthorhombic olivine structure that is very stable during cycling and is relatively cheaper due to the fact that it contains materials that are available in nature such as iron. However, this material suffers from relatively small voltage at 3.4 V vs. Li^+/Li compared with other olivine types of cathode materials and has a theoretical capacity (170 mAh/g) which limits the energy density. Other members of the olivine type cathode: $LiMPO_4$ (M= Mn; Co; Ni) have higher redox potentials (4.1, 4.8 and 5.1 V vs. Li^+/Li respectively) and therefore will show higher theoretical energy density; however voltages larger than 4.5 V tend to have stability issues for various components of batteries (Fergus, 2010).

2.2 Cathode functionality

A cathode in general electrochemistry is the electrode where reduction occurs. Cathodes are typically oxides of transitions metals. They are the sources of lithium ion in lithium ion batteries (Wang *et al.,* 2006). These materials can be divided into three categories: (a) layered oxides (b) Spinels and (c) Olivines.

The layered transition metal oxides of formula $LiMO_2$ (M= V, Cr, Fe and Ni) consist of empty spaces between the MO_2 layers that can accommodate lithium ions (Whittingham, 2004). One example of this type of cathode material is lithium cobalt oxide ($LiCoO_2$). Layered $LiCoO_2$ is commercially used and is a successful cathode material because it has capacities which is 280 mAh/g and can be larger with 3.6 V and can have larger operating voltages when it is charged to over 4.6 V at room temperature (Kim *et al.,* 2008). But it is unstable compared to other potential electrode materials and can suffer from performance degradation or failure when overcharged. The other disadvantage is that cobalt costs more than the other transition metals.

The spinels and olivines are made up of three dimensional structures with cross-linked channels that are sufficiently large to allow insertion (Whittingham, 2004). Spinels have good structural stability; an example is lithium manganese oxide ($LiMn_2O_4$); a low cost and environmentally friendly material with a charge storage capacity which is 148 mAh/g. It has high abundance, and is a promising candidate to replace layered Ni or Co oxide cathode materials for lithium ion batteries (Manthiram *et al.,* 2008). However, its application is limited due to poor capacity retention during cycling and storage as a result of manganese dissolution in the electrolyte. Research is still ongoing in order to find ways of circumventing this drawback.

The phosphates, $LiMPO_4$ (M= Fe, Mn, Co, Ni) with the olivine structure, are a very promising class of cathode materials. The commonest among them is $LiFePO_4$. This material occurs in nature as the mineral, triphylite and crystallizes in the olivine structure. It has low cost and is environment friendly (Chen, 2013)

with a flat discharge potential at about 3.4 V vs. lithium and a capacity of 170 mAh/g which is higher than that of $LiCoO_2$ and comparable to stabilized $LiNiO_2$. $LiFePO_4$ is much more stable during discharge/charge and with no sign of capacity fading after several cycles (Novikora *et al.*, 2013). It however, has a low electronic and a low ionic conductivity which hampers its electrochemical activity. Work is still ongoing in order to improve its electrochemical performance during charge/discharge cycling.

2.2.1 Lithium manganese phosphate ($LiMnPO_4$) cathode material

Lithium manganese phosphate ($LiMnPO_4$) has received much attention for use in lithium ion batteries because it is cheap and environment friendly. South Africa has large deposits of much of the chemical raw materials such as manganese, iron, cobalt, nickel and vanadium, required for the manufacture of lithium ion battery cathode materials. The potential of $LiMnPO_4$ is compatible with $LiCoO_2$, at 4.1 V vs. Li^+/Li. It has an excellent cycle performance and thermal stability when compared with the lithium transition metal oxides (Aravindan *et al*., 2013).

Fig. 2.3 Shows a schematics diagram of $LiMnPO_4$ olivine. It has an olivine structure, where Mn and Li occupy octahedral 4*c* and 4*a* sites, and P atom in 4*c* site, respectively (Bakenov and Taniguchi, 2011). The O atoms are in a hexagonal close-packed arrangement. The MnO_6 octahedral are separated by PO_4 polyanions (Bakenov and Taniguchi, 2011).

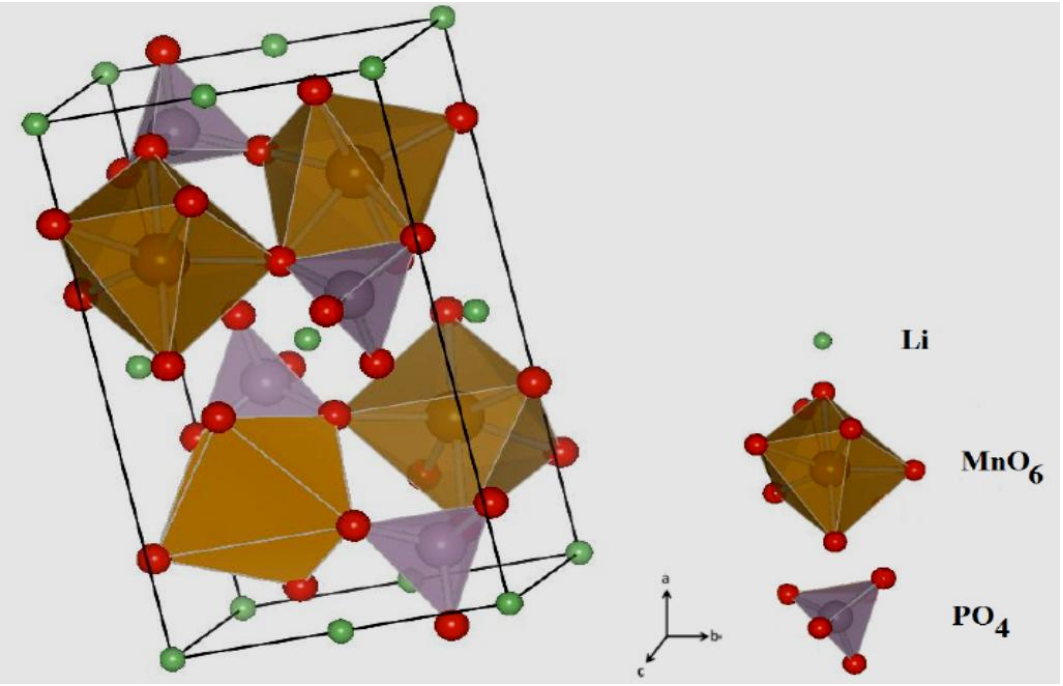

Figure 2.3: Structure of the LiMnPO4 with Pnma space group (Bakenov and Taniguchi, 2011).

Phospho-olivines have a makeup where all the oxygen ions form strong covalent bonds with P^{5+} to form PO_4^{3-} polyanion in the tetrahedral and stabilize the entire three dimensional framework (Pitchai *et al.*, 2011). This gives olivine cathode materials an advantage to work under abusive conditions but still maintain safety due to their improved stability (Yamada *et al.*, 2003). However, the electrochemical reaction kinetics is restricted in phospho-olivines because of the insulating effect of the polyanion (Bakenov and Taniguchi, 2011). $LiMnPO_4$ has a theoretical energy density at 701.1 Wh/kg which is attributed to a higher operating voltage plateau and is much higher than that of $LiFePO_4$ at 568.5 Wh/kg. It is compatible with most liquid electrolytes presently used in lithium-ion batteries (Pan *et al.*, 2013). However, $LiMnPO_4$ shows less or poor electrochemical performance due to slow lithium ion diffusion kinetics within the crystals and very low intrinsic electronic conductivity (Drezen *et al.*, 2007). For the Mn^{2+}/Mn^{3+} redox reaction to occur in $LiMnPO_4$ cathode, high ionic and electronic conductivities are necessary to enable Li^+ diffusion and electron transport (Yamada *et al.*, 2003).

In recent studies, it has been reported that morphology and structure significantly affect the electrochemical performance of $LiFePO_4$. With the development of $LiFePO_4$ paving way for $LiMnPO_4$, it could also be said that morphology and structure might as well affect the electrochemical performance of this material (Bakenov and Taniguchi, 2011). The improvement of the electrochemical kinetics has been studied and researched by many groups and it has been found that carbon coating and reduced particle size enhance the electrochemical properties of $LiMnPO_4$ (Qin *et al.,* 2012). Nano-sized $LiMnPO_4$ compared with micro-sized $LiMnPO_4$ provides shorter lithium ion diffusion path within a single particle. Several routes have been employed in the synthesis of $LiMnPO_4$ such as solid-state reaction, the polyol process, sol-gel, hydrothermal, solvothermal, precipitation, floating- zone, free-drying and electrostatic spray deposition methods.

2.2.1.1 Synthesis on high- performance $LiMnPO_4$ olivine cathode

Lithium manganese phosphate ($LiMnPO_4$) has interesting properties but suffers from poor electrochemical performance. The preparation of high performance $LiMnPO_4$ cathode requires the incorporation of conductive composites into the material. Wet chemical method could be used in the preparation as it allows perfect mixing of precursors, better homogeneity and more regular morphology of nanosized materials. However this method could lead to the complete removal of organic residuals which affects the conductivity of the synthesized material. 7 nm uniform particle sized $LiMnPO_4$ were obtained by Doi *et al*., 2009 via thermal decomposition, but the material showed poor electrochemical performance (discharge capacity 6 mAh/g) which might be due to the presence of residual oleic acid that prevented Li^+ diffusion and electron transfer (Kwon and Fromm, 2012). Using solvothermal method, $LiMnPO_4$ nanocrystals with rod-like and plate-like morphologies with superior charge-discharge capacities were obtained (Drezen *et al.,* 2007).

Coating of the cathode with a conductive carbon material allows utilizing the theoretical capacity (Kwon and Fromm, 2012) in such a way that Li^+ ions in the

active material can travel freely through the electrolyte. Minimal carbon content is required in order to increase the loading of the active material within a given volume of lithium ion batteries so as to increase the energy density (Doan and Taniguchi, 2011; Kwon and Fromm, 2012).

A combination of spray pyrolysis and wet ball milling is useful in preparing high-performance LiMnPO4 with reduced particle size. Controlled addition of carbon during the wet ball milling process helps to improve the electrical contact between the materials thereby enhancing the electrochemical properties of the active $LiMnPO_4$ (Pitchai *et al.*, 2011;Bakenov and Taniguchi 2011).

Fang *et al*. (2008) prepared $LiMnPO_4$ by hydrothermal method. Increasing the temperature depressed the Mn^{2+} disorder on Li^+ sites and the highest discharge capacity obtained was 68 mAh/g at a current density of 1.5 mAh/g. Wang *et al.* (2009) produced 30 nm thick $LiMnPO_4$ by polyol synthesis of the plate morphology (Bakenov and Taniguchi, 2011). They used trickle mode conditions, and achieved a discharge capacity of 141 mAh/g at 0.1 C at room temperature (Doan and Taniguchi 2011).

In this work, LiMnPO4 was prepared via a sol-gel synthetic route which was then followed by coating with gold nanoparticles and magnesium oxide nanowires for improved kinetics, better conductivity and enhanced electrochemical performance and possible application as a cathode material in a lithium ion cell.

2.3 Electrolytes

The electrolyte in electrochemical systems serves as the medium for the transfer of charges, which are in the form of ions, between a pair of electrodes (Whittingham, 2004). Normally the electrolyte is composed of one or more liquid solvents and one or more salts which dissociate and provide the ions. In lithium and lithium-ion batteries, the solvents used are non-aqueous and aprotic (Xu, 2004). The electrolyte has to be compatible with both (Whittingham, 2004)

positive and negative electrodes, current collectors, and separator (Whittingham 2004). It also has to be stable in contact with the strong oxidizing / reducing surface of the electrodes (chemically / electrochemically inert) (Xu, 2004) Other important factors to consider are the cost, safety, health, and environmental compatibility. From the electrochemical point of view, electrochemical stability is required and the ionic conductivity is the most important property, because it is directly connected with the specific power of the cell. The formulation of the electrolyte mostly used in commercially available lithium-ion batteries is a combination of linear and cyclic carbonates as solvents, with the presence of passivating additives, and $LiPF_6$ as electrolyte solute. The high dielectric constant of ethylene carbonate (EC) and its low viscosity (with respect to other cyclic carbonates), makes it a good candidate as electrolyte solvent. The most used linear carbonate is dimethyl carbonate (DMC). $LiPF_6$ is chosen as solute because it has a good balance between conductivity, safety and hazard for health (Scrosati and Garche, 2010). A 1M $LiPF_6$ solution of EC: DMC 1:1 (wt.) has a conductivity of 10.7 mS/cm and it is usable in the temperature range between -20 and 50 °C (Xu 2004). Apart from $LiPF_6$, $LiClO_4$ can create SEI films with enhanced ionic conductivity because of its relatively low reactivity with moisture. $LiPF_6$ reacts with moisture traces and the hydrolysis gives HF, which forms LiF in the SEI, a poor ionic conductor. Unfortunately, at high current or high temperature, the ClO^{4-} is not stable. For the purpose of this work, aqueous $LiSO_4$ electrolyte was used.

2.3.1 Aqueous electrolyte

An aqueous electrolyte has a high conductance and makes purification and drying processes during production, less stringent. The costs of aqueous electrolytes are usually much lower than suitable organic electrolytes. It should be further pointed out that the cathode material has to be developed for one or the other electrolyte and the porous structure of the electrode has to be tailored to the size and the properties of the respective electrolytes. In order to avoid electrolyte depletion during charging, the electrolyte concentration has to be kept high. If the electrolyte reservoir is too small compared to huge surface area of the electrodes,

performance of the cathode is reduced. Hence, a concentration higher than 0.2 molar are sufficient (Xu, 2004).

2.3.2 Organic electrolyte

Organic electrolytes have attracted considerable attention due to their greater electrochemical stability (>3 V) compared to aqueous systems (1 V) (Xu 2004). The wider voltage window offered by non-aqueous electrolytes provides increased energy. However, limitation of the power capability of non-aqueous electrolyte is their inherent lower conductivity (Xu, 2004). In addition, capacitance is also sensitive to the electrolyte concentration. Ionic liquids based on immidazolium salts are solidified or crystallized at below room temperature and have been applied to numerous electrochemical, photovoltaic, and synthetic fields (Xu, 2004).

2.4 Surface modification by doping and coating

Doping is the addition of quantities of an element of a semiconductor for modulating the electrical properties of the material being modified or to change its characteristics. Lightly doped semiconductors are referred to as extrinsic, while semiconductors doped to such high levels that act more like a conductor than a semiconductor is called a degenerate (Chen and Chen, 2012). Doping can also be referred to as the activation of a particular material. The surface of a material can be modified through surface doping. Doping helps to reduce manganese dissolution in $LiMnPO_4$ by decreasing the apparent contact area with the electrolyte (Liu *et al.*, 2013).

Surface coating is effective in improving the capacity retention, rate capability and even thermal stability of cathode materials for lithium ion batteries (Chen *et al.*, 2010). Different coating materials have been used for cathode materials such as carbon, metal oxide, metal carbonates, and metal phosphates as well as cathode materials with lower reactivity towards non-aqueous electrolytes (Fu *et al.*, 2006). Carbon coating has shown ability to improve performance, mostly for phosphate

based materials. Coating the surface of cathode materials can give improved electron transfer through the interface of the material's particles and therefore accelerate the heterogeneous charge transfer process on the cathode surface Coating also provides extra electro conducting pathways in the cathode material (Pitchai *et al*., 2011). The surface coating acts as a protective layer to prevent direct contact of the active core material with the electrolyte solution (Chen *et al.,* 2010).

2.5 Nanomaterials and relevance of nanotechnology

Nanomaterials are structures with dimensions in the nanoscale range, normally between 1 and 100 nm. The chemical and physical properties of substances can be considerably altered and fine-tuned when they exist on a nanoscopic scale. An increase in the specific surface area is one of such changes that could occur when the particle size of a material is scaled down to nanometer dimensions (Zhang *et al.,* 2013). Nanotechnology has made it possible to control the particle size and also apply electrically conductive coatings to improve the property of the material (Pei *et al.,* 2013). Typical applications of nanomaterials include energy conversion, electrochemistry, catalysis and environmental chemistry, where the use of nanomaterials increases efficiency, sensitivity and response time.

There are several potential advantages of nanomaterials in lithium ion battery such as: significant increase in the rate of lithium insertion/removal due to the reduced dimensions of nanomaterials; enhancement in the rate capacity as well as the cycle life (Zhang *et al.,* 2013). Electron transport is also enhanced by nanometer-sized particles; the high surface area of nanosized species allow active material to absorb lithium ions more effectively hence increase capacity with decrease in size; the chemical potentials for lithium ions and electrons may be modified resulting in a change of electrode potential (thermodynamics of the reaction) (Kwon and Fromm, 2012). Nanomaterials provide new reactions which are not possible with bulk materials. Nanoparticles of $LiMnPO_4$ can have higher electrode/electrolyte contact area leading to higher charge/discharge rates.

2.6 Gold nanoparticles and magnesium oxide nanowires for surface modification

Nanocomposites have unique chemical, physical and electronic properties different from those of bulk materials owing to the small size of nanoparticles (NPs) (1 - 100 nm). Nanocomposites are important because they can be used for catalysis (e.g. catalytic converters in automobiles), electronic, magnetic and biomedical applications. Materials with well-defined and controllable properties can be fabricated on the nanoscale by combining flexibility of inter-metallic materials (Li *et al.*, 2011). Chemical and physical properties can be tuned by varying the nanoparticles/cluster size, composition and atomic ordering. Nanostructured materials display properties distinct from pure elemental nanoparticles. In this project magnesium-gold thin film (Mg-Au) was used to enhance the performance of $LiMnPO_4$ nanoparticles for use as a cathode material in lithium ion batteries.

Gold nanoparticles (AuNPs) have gained increasing interest due to their special features. They have unusual optical and electronic properties, high stability and biological compatibility. They also have controllable morphology, size dispersion, and easy surface functionalization *(*Chae *et al*., 2009). These unique properties have been researched and utilized in high technology applications such as organic photovoltaic, sensory probes, therapeutic agents, drug delivery in biological and medical applications, electronic conductors and catalysis (EI-Sayed *et al*., 2007). Gold nanoparticles are some of the most popular metal nanoparticles. They are available in different sizes and shapes due to their ability to react and agglomerate with other nanoparticles in their surroundings. The unusual optical properties of small gold particles, their size dependent electrochemistry, and their high chemical stability have made them the model system of choice for exploring a wide range of phenomena including self-assembly, biolabeling, catalysis, electron-transfer theories, phase transfer, DNA melting and assays, and crystal growth (Hirst *et al*., 2012*)*. The range of applications for gold nanoparticles is growing rapidly as years go by. Gold nanoparticles are used as catalysts in a number of chemical reactions. The surface of gold nanoparticles can be used for

selective oxidation or in certain cases the surface can reduce a reaction (nitrogen oxides) (Ballesterp *et al.*, 2014). They are used in fuel cell applications hence gold nanotechnology would also be useful in the automotive and display industry *(*Thompson, 2007*)* where lithium ion batteries can also be used. The d electrons in transition metals play a huge role in determining the electronic, magnetic and catalytic behaviour. Nanoparticles seem to aggregate and this presents a challenge to the performance of gold nanoparticles catalysts (Carabineiro *et al.,* 2011). Choosing an appropriate support might solve the problem and enhance the performance of gold nanoparticles. Gold nanoparticles can be stabilized via intersurface interaction with the support material. For this project, MgO nanowires will be used to support gold nanoparticles to modify the surface of $LiMnPO_4$.

Magnesium is a highly reactive material, and is not found naturally on Earth. However, once produced, it is coated in a thin layer of oxide, which partly masks this reactivity. It is highly flammable and burns in water to form magnesium oxie (MgO) and hydrogen. (Mordike and Ebert, 2001). Magnesium oxide has unique properties like: very low density compared to other structural metals; high specific strength; it can be turned-milled at high speed; it is readily available and has good electrical and thermal conductivity. It has high thermal stability, low weight, good chemical resistance, non- toxicity. Magnesium oxide is an important wide-band gap insulator with high corrosion-resistant behaviour and purity (Nagashima *et al.*, 2007; Al-Ghamdi *et al.*, 2012). MgO has found interest in a variety of fields like, its use in catalysis, glass industry, pharmaceutical, toxic waste remediation, additives in refractory, paint, gas sensing and superconductor products. It is also applied in electronics, aerospace, automobiles, and biomedicine.

During the nanotechnology revolution of the past decade, one-dimensional (1D) nanostructures such as nanowires, nanotubes, nanorods and nanobelts have enjoyed prominent attention and success (Park *et al.*, 2005). 1D nanostructures have unique density of electronic states which gives them different optical, electronic and magnetic properties compared to their bulk, 2D (quantum wells) or

0D (quantum dots) counterparts (Park *et al*., 2005). Nanowires can act as building blocks for future electronics and photonics, and play important roles in the fabrication of electronics, optoelectronics, electrochemical and electromechanical nanodevices (Gyu-Chul *et al.*, 2005).

In this work, MgO nanowires were coated with gold nanoparticles for improvement of the electrochemical performance of $LiMnPO_4$ during cycling. The interaction between Mg-Au clusters can change the interplay of structure and electronic properties of the nanocomposite (Hyoun *et al.*, 2007*)*.

Chapter 3

3 Materials and methods

3.1 Reagents

Analytical reagent grade Lithium sulphate (99.9 %) trace metal basis, Lithium hydroxide monohydrate (99.995 %) trace metal basis, Manganese (II) Sulfate monohydrate, Diethylene gycol (99.0 %), magnesium acetate tetrahrate (≥99 %), Phosphoric acid, crystalline (≥99.99 %) trace metal basis, N-methyl-2-pyrrolidone, anhydrous (99.5 %). chloroauric acid ($HAuCl_4.3H_2O$), trisodium citrate dihydrate ($Na_3C_6H_5O_7.2H_2O$) were all obtained from Sigma-Aldrich; Alumina micro polishing pads were obtained from Buehler and urea (99.5 %) was obtained from Fluka.

3.2 Methodology

3.2.1 Preparation of $LiMnPO_4$ nanoparticles

$LiMnPO_4$ nanoparticles can be prepared by different techniques; in this work a sol-gel route was used to synthesize $LiMnPO_4$ nanoparticles and surface-modify them with both gold nanoparticles and magnesium Oxide nanowires. Chemical synthesis by sol-gel route was used due to its efficiency and energy saving approach. It offers rapid heating, high reaction rate and selectivity. Sol-gel synthesis can be used to prepare different lithium metal phosphate (Mn, Fe and Co) nanostructures. The preparation of $LiMnPO_4$ nanoparticles was as follows: 2.3 mL of 1 M $LiOH.H_2O$ was mixed with 6.7 mL of diethylene glycol (DEG) and 3.3 mL of distilled water. This solution was then added to a mixture of 2.3 mL of 0.3 M $MnSO_4.H_2O$ and 2.3 mL of 0.3 M H_3PO_4 which was heated to 60-75 °C to obtain a gel. After the reaction, the product was washed with water and ethanol, and then later dried overnight at 120 °C before being heated for 5 h at

350 °C under air. The powder as produced was then calcined at different incremental temperatures (400–580 °C) for 3 h in air (Li *et al*., 2013).

3.2.2 Preparation of gold nanoparticles (AuNPs)

Gold nanoparticles were synthesized through a chemical reduction method. Briefly, 50 mL of 0.01 wt% chlorauric acid ($HAuCl_4.3H_2O$) solution was heated to boiling while stirring in a 100 mL beaker. Then a few hundred microlitres (μL) of 1 wt. % trisodium citrate dihydrate ($Na_3C_6H_5O_7.2H_2O$) solution was quickly added to the auric solution. The solution changed colour within several minutes from yellow to black and then to red or purple colour depending on the size of the nanoparticles (Long *et al*., 2009).

3.2.3 Coating $LiMnPO_4$ nanoparticles with gold nanoparticles

Coating is the addition of small quantities of an element to a semiconductor to change its characteristics.The coating of gold nanoparticles allows probing the atomic sensitivity of the nanocomposite's physical and chemical properties as well as imparting the composite with new properties. Coating can improve properties such as conductivity and reactivity to overcome low solution dispersion which has been a bottleneck in their industrial application. Coating can be applied to change the surface properties of the substrate. Surface coating has proven to be effective for improving the capacity retention, rate capacity and even stability of the cathode material.

0.2 mL of gold nanoparticles was added into $LiMnPO_4$ powder sample and then the solution, under stirring, was heated to 80 ^oC and finally calcinated at 400 °C.

3.2.4 Synthesis of MgO nanowires

Magnesium oxide nanowires were synthesized by a single step hydrothermal technique. 1.61 g of magnesium acetate tetrahydrate was dissolved in 18.75 mL distilled water and stirred for 30 min at room temperature. Then, 0.3 g urea in 25 mL water was added drop wise into this aqueous solution under vigorous stirring

for 30 min. Further, the above solution was loaded into a 6.25 mL teflon-lined steel autoclave. Finally, the autoclave was sealed and maintained at 200 °C for 4 h. At the end of the reaction, the autoclave was cooled down to room temperature The products were collected by centrifugation at 8000 rpm for 10 min, and washed with distilled water and then with ethanol to reduce agglomeration. This was followed by drying at 60 °C for 24 h. Finally, the white coloured material obtained was calcined at 450 °C for 2 h (Al-Ghamdi *et al*., 2012).

.

3.2.5 MgO nanowire coated onto $LiMnPO_4$/Au

The as-prepared $LiMnPO_4$/Au was mixed with a certain amount of MgO nanowires, and then calcined at 380 °C for 3 h under furnace to form $LiMnPO_4$ /Mg-Au thin film composite.

The $LiMnPO_4$ coated with magnesium- gold composite thin film will be characterized by X-ray diffraction (XRD), energy dispersive X-ray spectroscopy (EDS), transmission electron microscopy (TEM), high resolution transmission electron microscopy (HRTEM),scanning electron spectroscopy (SEM), fourier transform infrared spectroscopy (FTIR), Raman spectroscopy, cyclic voltammetry (CV) and electrochemical impedance spectroscopy (EIS).

3.3 Material characterization techniques and instrumentation

Various techniques and instrumentations were employed to investigate the structures and electrochemical performances of the synthesized materials.

3.3.1 Structural characterisation and crystal structure identification

3.3.1.1 X-ray diffraction (XRD)

X-ray diffraction measurements were carried out with a D8 advanced diffractometer from Bruker AXS using an X-ray tube with copper K-alpha

radiation operated at 40 kV and 40 mA and a position sensitive detector vantec_1 which enables fast data acquisition. XRD is a non-destructive analytical technique for identification and quantitative determination of the various crystalline forms, known as 'phases'. Identification is achieved by comparing X-ray diffraction patterns (Novikova *et al.,* 2013). XRD consists of three basic components: an X-ray tube, a sample holder and an X-ray detector. A powdered sample or polished surface- is rotated against the centre and data collector- such as film, strip chart or magnetic medium/storage. X-rays are generated in a cathode ray tube by heating a filament to produce electrons, accelerating the electrons toward a target by applying a voltage, and bombarding the target material with electrons. The role of XRD is to identify the phase purity and phase structure of crystalline materials using Cu Kα radiation of wavelength 1.5418 Å and scanned from 80° to 10° with a step size of 0.02°. As described in the introduction, $LiMnPO_4$ has an olivine structure, where Mn and Li occupy octahedral 4*c* and 4*a* sites, and the P atom in the 4*c* site. The O atoms are in a hexagonal close-packed arrangement.

3.3.1.2 Surface morphology by SEM and HRTEM

The surface morphology and internal ultra-structure of the synthesized materials was evaluated by the use of scanning electron microscopy (SEM) and high resolution transmission electron microscopy (HRTEM), respectively. Scanning electron microscopic (SEM) images were obtained using a ZEISS ULTRA scanning electron microscope. The sample was placed on a carbon supported by alumina and then placed in a sputter coater to make the material conductive. The samples were then coated for 30 seconds using gold-palladium alloy. The high resolution transmission electron microscopic images were obtained by Tecnai G^2 F_2O X-TWIN MAT. Characterisation here was performed by coating a copper-carbon grid with a drop of the sample solution and drying with an electric lamp for 30 min.

A scanning electron microscope (SEM) is a type of electron microscope that produces images of a sample by scanning it with a focused beam of electrons (Suzuki, 2002). The electrons interact with electrons in the sample, producing various signals that can be detected and that contain information about the

sample's surface topography and composition. The electron beam is generally scanned in a raster scan pattern, and the beam's position is combined with the detected signal to produce an image. SEM can achieve resolution better than 1 nanometre. Specimens can be observed in high or low vacuum. It is used to measure the morphology and microstructure of the samples.

Transmission electron microscopy (TEM) is a microscopic technique whereby a beam of electrons is transmitted through an ultra-thin specimen which interacts with the sample as it passes through (Skoog *et al.,* 1992*)*. An image is formed from the interaction of the electrons transmitted through the specimen. This image is magnified and focused onto an imaging device, such as a fluorescent screen, on a layer of photographic film and detected by a sensor such as a charge-coupled device (CCD) camera. TEM is capable of imaging at a significantly higher resolution than light microscopes owing to the small de Broglie wavelength of electrons. This enables the instrument's user to examine fine detail even as small as a single column of atoms, which is tens of thousand times smaller than the smallest resolvable object in a light microscope. It is used to measure morphology and particle size. High resolution transmission electron microscopy (HRTEM) offers resolution to the angstrom level and enables information to be obtained on the structure (atomic packing) rather than just the morphology of the nanoalloys (shape/lattice fringes). HRTEM provides information on particle size, shape and crystallography of nanoparticles. It can measure particle sizes to as low as 1 nm. HRTEM was used to identify the size, shape and structure of the products.

3.3.1.3 Energy dispersive x-ray spectroscopy (EDS)

This is an analytical technique often used in conjunction with SEM and TEM (Harada *et al*., 1994). An electron beam (typically 10-20 keV) strikes the surface of a conducting sample, causing X-rays to be emitted, where the energies depends on the material under examination. An image of each element in the sample can be obtained by scanning the electron beam across the material. It is a high-resolution variant of electron microprobe analysis/x-ray microanalysis whereby

information can be obtained on the chemical composition of individual nanoparticles Characterisation here was performed by coating a copper- carbon grid with a drop of the sample solution and drying with an electric lamp for 30 min.

3.3.1.4 Fourier transform infrared spectroscopy (FTIR)

The electronic (vibrational and rotational) properties of the materials were determined by fourier transform infrared (FTIR) spectroscopy. FTIR spectra were obtained using a perkin elmer spectrum 100 series attenuated total reflection (ATR) FTIR spectrometer. Infrared spectroscopy reveals information about the vibrational states of a molecule. Intensity and spectral position of IR absorptions allow the identification of structural elements of molecules, typically functional groups. Typical vibrations of functional groups make infrared spectroscopy also an important analytical tool. In the gas phase, a rotational fine structure can often be observed from which the moment of inertia of the molecule can be determined. When a spectrum is recorded using a conventional, dispersive IR spectrometer, each data point reveals the transmitted light at the respective frequency. The signal provided by the FTIR technique, however, contains information about the complete spectrum of the probe. This signal has to be transformed from the time-domain into the frequency-domain in order to reveal the spectrum. The characterisation was performed by placing a small amount of solid sample onto the FTIR stand.

3.3.1.5 Raman spectroscopy

Raman scattering intensity of molecules is greatly enhanced (by as much as 5 orders of magnitude) when they are absorbed on certain metals. The effect (which again probes vibrational structure) has been used to study the binding of adsorbents on metallic nanoparticles and the cluster formation process. It is a spectroscopic technique used to observe vibrational, rotational, and other low-frequency modes in a system. Raman spectra were recorded with a laser-spectrometer LABRAM HRVIS (model Jobin-Yvon) fitted with an olympus

BX41 optical microscope (from France). Raman spectra are usually excited using the 532 nm laser. Spectra can be collected over the range 0–4000 cm^{-1}. Standard photon-counting techniques were utilized for detection. In a typical spectral acquisition, ten spectra, each recorded with a resolution of 2 cm^{-1} were averaged to increase the signal-to-noise ratio. To avoid sample photodecomposition during collection of Raman spectra, care has been taken to use a power density of 10 W/cm^2.

3.3.2 UV-Vis spectroscopy

Ultra violet-visible (UV-Vis) absorption measurements were made with a Nicolet Evolution 100 UV-visible spectrometer (Thermo Electron, UK), using a quartz cuvette. UV-Vis was used to examine the properties of the synthesized materials in UV-visible region of the electromagnetic spectrum. This spectroscopy measures the absorption, transmission and emission of ultraviolet and visible light wavelength by matter. UV-Vis spectroscopy is applied in analytical chemistry for the quantitative determination of different analytes, such as highly conjugated organic compounds, transition metal ions and biological macromolecules with analyses usually carried out in solutions.

3.3.3 Electrochemical techniques

3.3.3.1 Cyclic voltammetry (CV)

Cyclic voltammetry experiments were carried out using a BAS 100 W integrated and automated electrochemical work station from bio analytical systems (BAS), lafayette, USA. All cyclic voltammograms were recorded with a computer interfaced to the BAS 100 W electrochemical workstation. A 10 mL electrochemical cell with a conventional three electrode set up was used. The electrodes were: (1) glassy carbon working electrode (GCE) (A = 0.071 cm^2) from BAS, modified with $LiMnPO_4$; (2) glassy carbon (GCE) working electrode (A = 0.071 cm^2) from BAS modified with $LiMnPO_4$/Mg-Au thin film composite; (3) platinum wire, from Sigma Aldrich was the counter electrode and (4) Ag/AgCl (3

M KCl) from BAS was the reference electrode. Alumina micro polish and polishing pads were obtained from Buehler, IL, USA and were used for polishing the GCE before any modification. Cyclic voltammetry (CV) is a technique which is widely used in the study of oxidation/reduction reactions and the detection of reaction intermediates (Manjunatha *et al*., 2012). This technique indicates the potentials at which processes occur while from the sweep rate dependence. Because of these capabilities, CV is nearly always the technique of choice when studying a system for the first time. In a cyclic voltammetry experiment the working electrode potential is ramped linearly versus time. When cyclic voltammetry reaches a set potential, the working electrode's potential ramp is inverted. This inversion can happen multiple times during a single experiment. The most important parameters in a cyclic voltammogram are the peak potentials (E_{pc}, E_{pa}) and peak currents (I_{pc},I_{pa}) of the cathodic and anodic scans, respectively. If the electron transfer process is faster compared with other processes (such as diffusion), the reaction is said to be electrochemically reversible, and the peak separation is given by:

$$\Delta E_p = \left| E_{pa} - E_{pa} \right| = 2.303\frac{RT}{nF} \quad (9)$$

Thus, for a reversible redox reaction at 25 °C with n electrons ΔE_p should be: $0.0592/nV$.

The formal reduction potential (E^o) for a reversible couple is given by:

$$E^o = \frac{(E_{pa} + E_{pc})}{2} \quad (10)$$

The modified working electrode (GCE) was prepared by first polishing it repeatedly with 1.0, 0.3 and 0.05 μm alumina slurries respectively, rinsed thoroughly with water and sonicated in ethanol for 5 min. 2 mg of synthesized material was dissolved in 1 mL of N-methyl-2-pyrrolidone and 1.5 μL of this mixture was drop-coated on the polished surface of the GCE and then allowed to dry. Cyclic voltammograms were obtained by cycling the potential of the GCE

against that of the Ag/AgCl electrode from -1000 mV to +1000 mV at scan rates between 1 and 10 mV/s and recording the resultant current flow.

3.3.3.2 Electrochemical impedance spectroscopy (EIS)

Electrochemical impedance spectroscopy (EIS) measurements were recorded with Zahnner IM6 electrochemical work station from MeBtechnik at a bias potential of 0.222 V, amplitude of 5 mV and frequency range of 100 mHz to 100 kHz. A 10 mL electrochemical cell with a conventional three electrode set up was used. EIS is an electrochemical technique which can be used in corrosion, biosensors, battery development, fuel cell development, paint characterization, sensor development, and physical electrochemistry. EIS provides a more thorough understanding of an electrochemical system than any other electrochemical technique. Its operating principle involves the measurement of the impedance between the current and the potential at a fixed direct current (DC) potential during frequency scan with a fixed superimpose alternating current (AC) signal of small amplitude. EIS measures the dielectric properties of a medium as a function of frequency. The impedance of a system over a range of frequencies, and therefore the frequency response of the system, including the energy storage and dissipation properties, is revealed during measurement. Often, data obtained by EIS is expressed graphically in a Nyquist plot as shown in **Fig. 3.1** or a Bode plot as shown in **Fig. 3.2**. Unfortunately, to make such measurements takes relatively long, somewhere between about 30 min and a few hours, depending on the frequency range and the stability of the electrochemical system because the frequency needs to be scanned for the measurements. The imaginary impedance (Z_{Im}) and the real impedance (Z_{Re}) are recorded as a function of the applied frequency with the result that the Nyquist plots (Z_{Im} vs. Z_{Re}) is fitted to simple electrical equivalent circuits (EECs) as shown in **Fig. 3.3**. A Randles circuit is an equivalent electrical circuit that consists of an active electrolyte resistance R_s in series with the parallel combination of the double-layer capacitance C_{dl} and an impedance of a Faradaic reaction. It is commonly used in EIS for the interpretation of impedance spectra, often with a constant phase element (CPE) replacing the double layer capacitance (C_{dl}). By fitting EECs, important

information of the interface such as solution resistance (R_s), electron transfer resistance (R_{ct}), Warburg element (R_w) and double layer capacitance (C_{dl}), are measured (Chang *et al*., 2010). EIS in the fully discharged state is used to evaluate the Li-ion diffusion coefficient in $LiMnPO_4$.

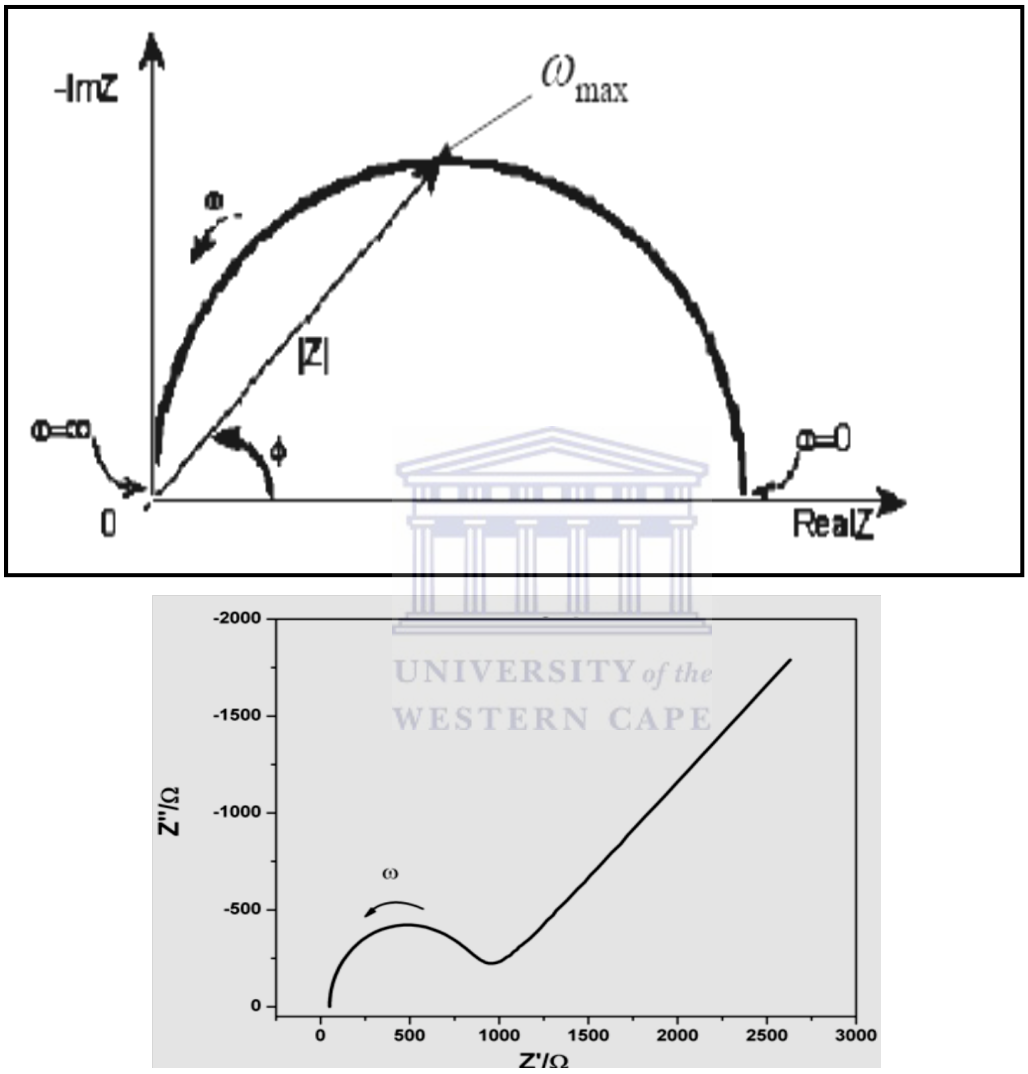

Figure 3.1: Nyquist Plot with impedance vector (Barsoukov and Macdonals 2005).

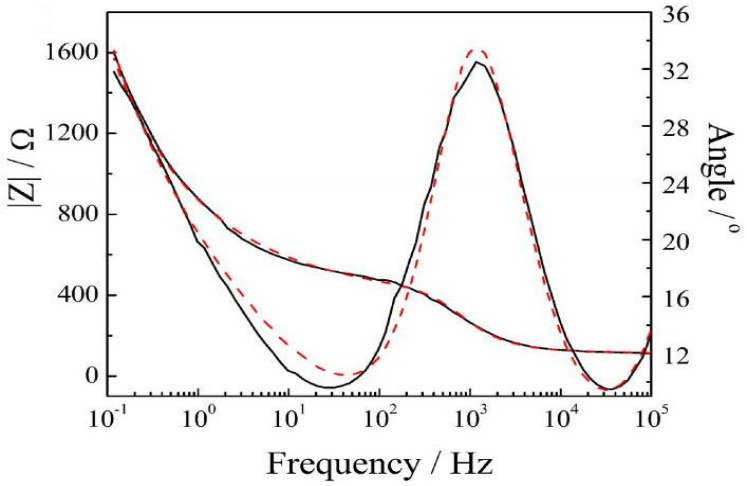

Figure 3.2: Typical Bode plot (Barsoukov and Macdonals 2005).

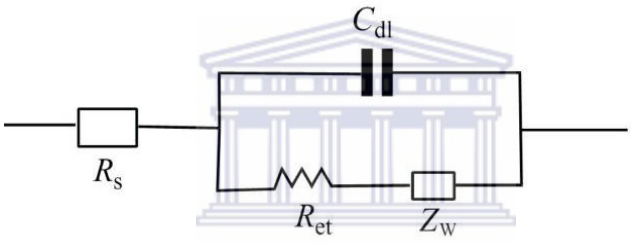

Figure 3.3: Randles circuit equivalent electrical circuit**.**

Chapter 4:

4 Results and discussion

4.1 Characterisation and analysis of nano-$LiMnPO_4$ olivine cathode

4.1.1 Particle morphology and chemical composition

The particle size and morphology of $LiMnPO_4$ calcined at 580 °C was investigated by high resolution scanning electron microscopy (HRSEM). The HRSEM micrograph is shown in **Fig. 4.1**. Spherically-shaped, pure $LiMnPO_4$ has primary particles size of ~ 100 nm. The secondary particles of $LiMnPO_4$ that form from aggregation of the primary particles are random in size and range between 200 - 350 nm indicating that the crystals of the olivine $LiMnPO_4$ grow very well and have inter-particles boundaries(Chen et al., 2008).

TEM and EDS results of $LiMnPO_4$ are shown in **Fig. 4.2 and 4.3**, respectively. The micrographs of the prepared sample of $LiMnPO_4$ derived from sol- gel procedure and calcined at 580 °C are displayed. **Fig. 4.2** shows the TEM images of $LiMnPO_4$ nanoparticles which correspond to those of the single-crystals with orthorhombic structure and particle size of about ~ 150 nm (Ramar and Balaya, 2013). The $LiMnPO_4$ particles are randomly-sized crystals with dimensions ranging from some tens of nanometres to several micrometers in size, and the particles appear to be interconnected with an individual particle size in the range 100 nm - 200 nm. **Fig. 4.2 (b)** is a typical high-resolution electron microscopic (HRTEM) image and **Fig. 4.2 (c)** is an enlarged section of the areas shown in **Fig. 4.2 (b)**. The HRTEM of the powdered samples showed clear lattice fringes indicating formation of pure crystallites of $LiMnPO_4$. The observed d-spacing at 2.8 Å of neighbouring lattice fringes corresponds to the (031) plane of $LMnPO_4$ indicating that highly ordered crystallites were formed. The crystallite has a typical, well-defined orthorhombic symmetry (Zhao *et a*l., 2012). **Fig. 4.2 (d)** shows the selected area electron diffraction (SAED) of $LiMnPO_4$ which reveals

highly ordered crystalline particles. The diffraction patterns were indexed according to the Pnmb space group with the selected area diffraction (SAD) pattern corresponding to the (011) facet plane of the orthorhombic lattice of $LiMnPO_4$. **Fig. 4.3** shows the EDS spectrum indicating that the $LiMnPO_4$ were composed of elemental Mn, P and O. The signals of Cu and C in the EDS spectrum were due to the C-coated Cu grids.

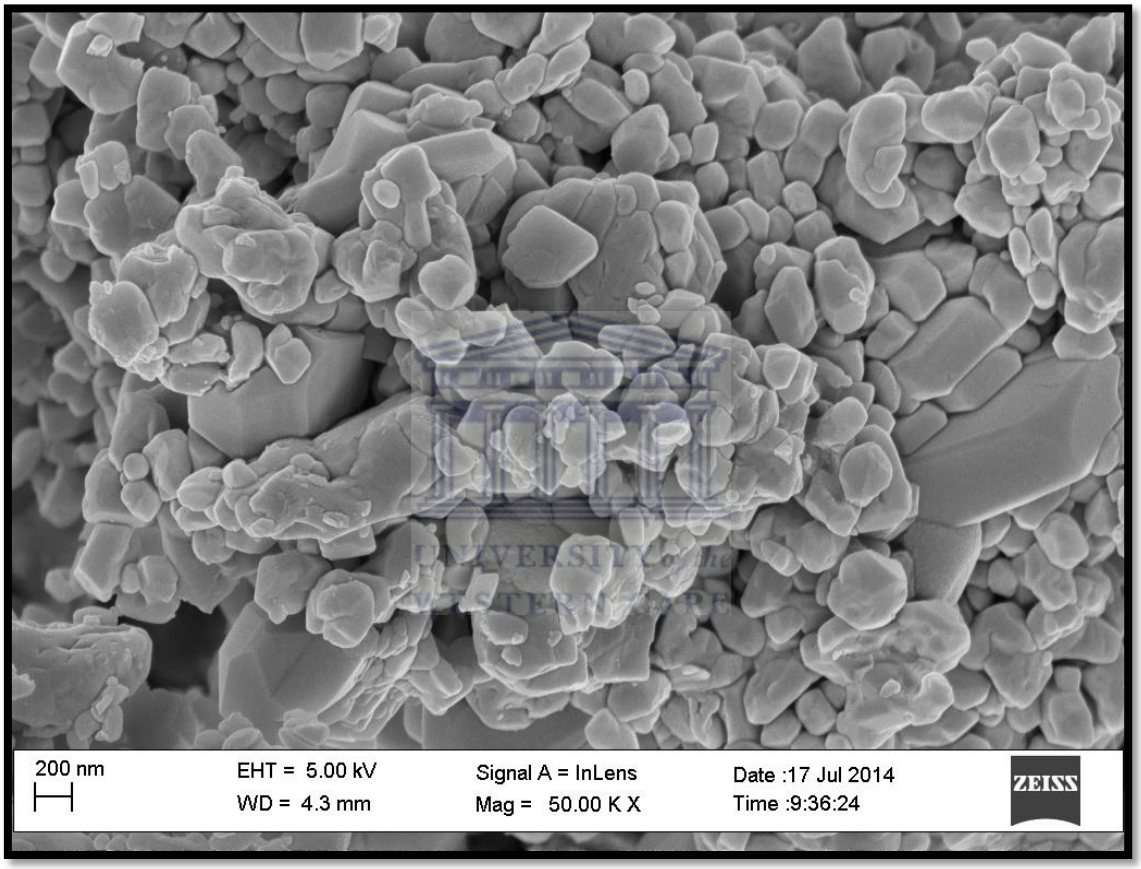

Figure 4.1: High resolution scanning electron micrographs (HRSEM) of $LiMnPO_4$ powder calcined at 580 °C**.**

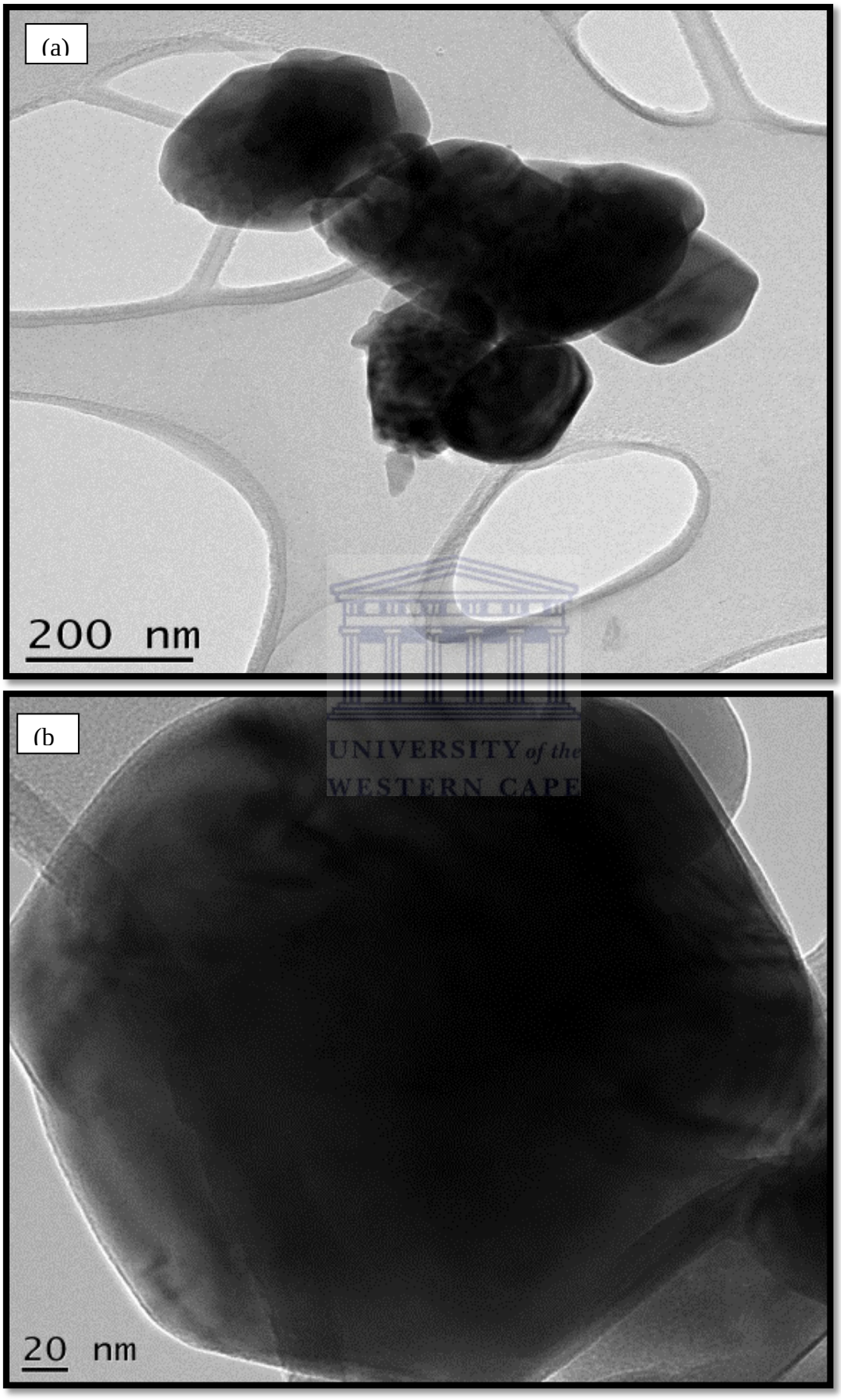

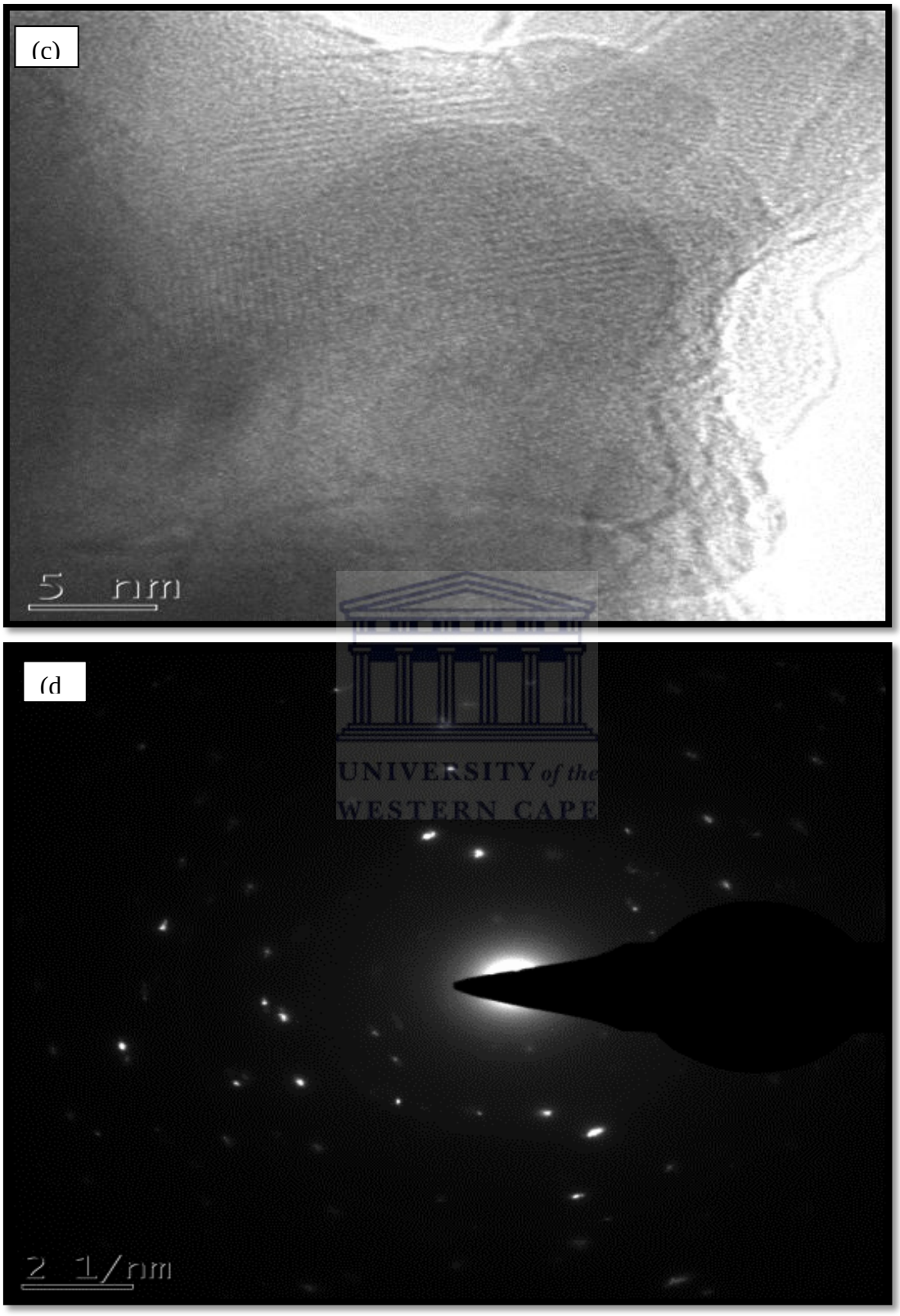

Figure 4.2: TEM images of $LiMnPO_4$ powders calcined at 580 °C at (a) - (b) with lattice image or HRTEM (c) and selected area electron diffraction (SAED) patterns (d).

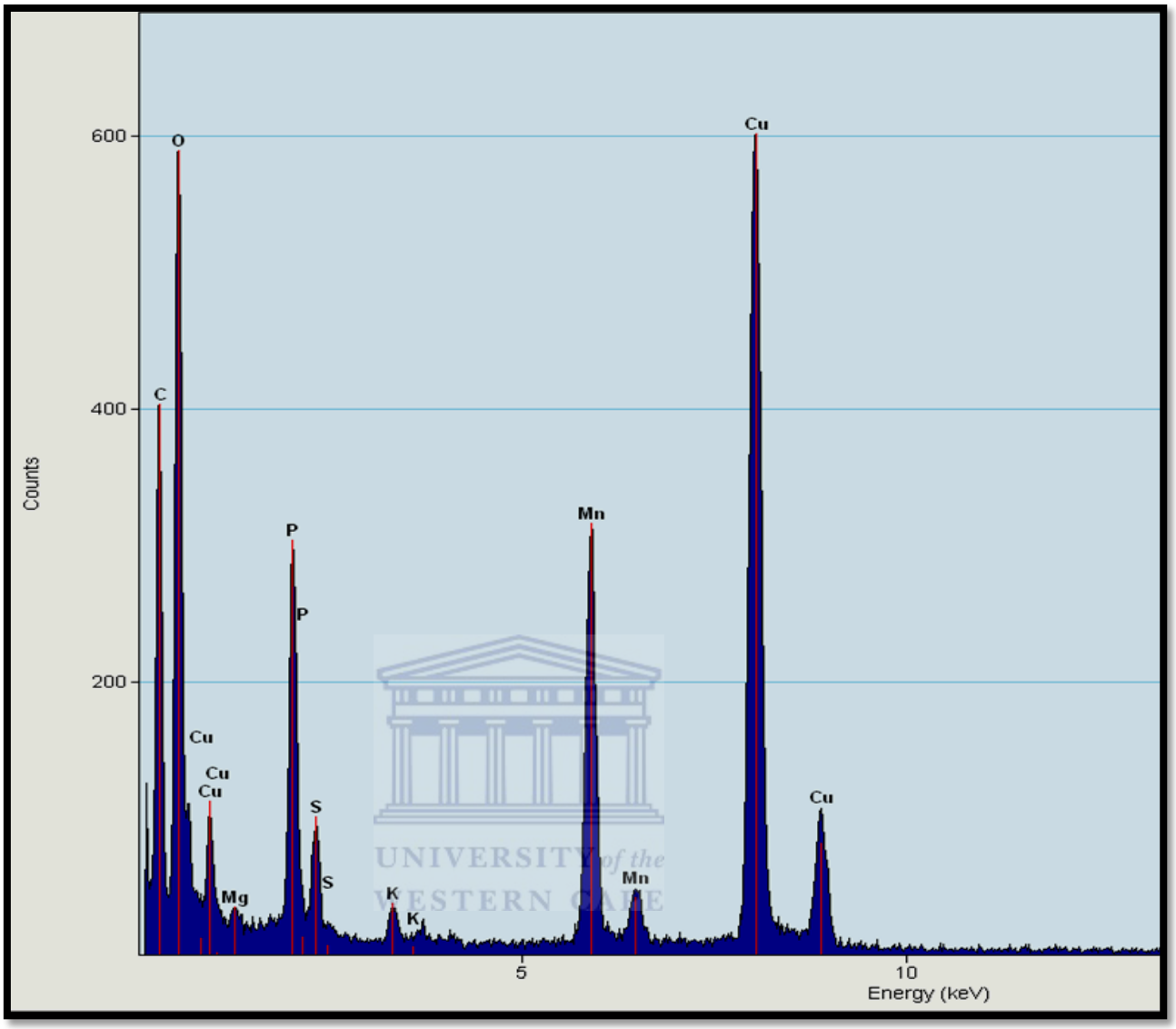

Figure 4.3: EDS of the synthesized nano-$LiMnPO_4$ on the copper grid.

4.1.2 Crystal structure and phase composition analyses by X-ray diffraction (XRD)

X-ray powder diffraction (XRD) is a rapid analytical technique primarily used for phase identification of a crystalline material and provides information on unit cell dimensions. The sample was finely ground, homogenized, and average bulk composition determined. XRD reveals information on the structure, crystallinity and lattice spacing of the material. XRD was done to investigate the effects of different sintered temperatures and time on crystal structure of $LiMnPO_4$. **Fig. 4.4** shows the XRD patterns of $LiMnPO_4$ samples synthesized at different calcination

temperatures. **Fig. 4.4 (a)** shows the ambiguous XRD patterns of the as-prepared $LiMnPO_4$ sample calcined at 400 °C. The intensity here is too low, due to low calcination temperature. The diffraction peaks of $LiMnPO_4$ calcinated between 500 - 580 °C, **Fig. 4.4 (c) to (e)**, are sharper and narrower. These peaks were further analysed by Rietveld refinement which confirmed the presence of $LiMnPO_4$ and $Mn_2P_2O_7$ phases. In **Fig. 4.4 (e)**, the composition was found to be 95 wt% $LiMnPO_4$ and 5 wt% $Mn_2P_2O_7$, which showed that the dominant phase is stoichiometric $LiMnPO_4$. The peaks for this extra phase decrease as we move from **Fig. 4.4 (a)** to **(e)**. The olivine phase was formed at a temperature as low as 400 °C even though the peak intensity was very low. The peak intensity increased with reaction temperature, indicating improved crystallization and particle growth. In **Fig. 4.4 (e)**, the crystal phase of $LiMnPO_4$ sample was identified to be an ordered olivine structure indexed by orthorhombic Pnmb, with fewer impurities (Kumar *et al*., 2011). The XRD patterns revealed that the samples annealed at different temperatures are in the same phase, except that the peaks are gradually sharpened and intensified. This suggests an increase in the crystallinity and ordering of olivine $LiMnPO_4$ phase as well as the release of lattice strain at higher temperature. Thus, powders sintered at higher temperature are more suitable for battery assembly. XRD, HRTEM and SAED confirmed with literature that $LiMnPO_4$ has orthorhombic crystalline phase with space group of Pnmb and that $LiMnPO_4$ nanostructure is single – crystalline.

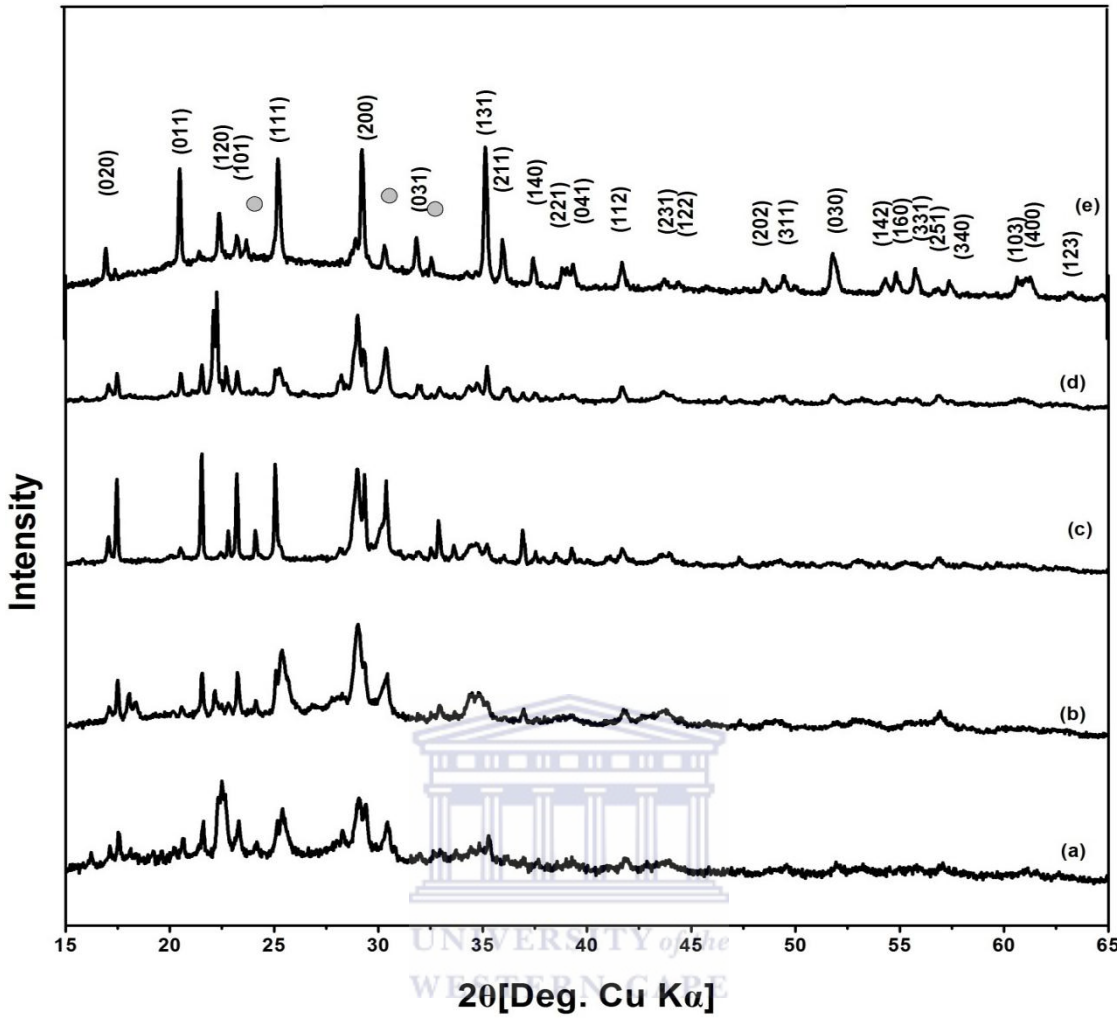

Figure 4.4: XRD patterns of $LiMnPO_4$ samples calcined at different temperatures for 3 h: (a)400 °C; (b) 450 °C; (c) 500 °C;(d) 550 °C and (e) 580 °C.

4.1.3 $LiMnPO_4$ fourier-transform infrared and Raman vibrational spectroscopic analysis

Fig. 4.5 shows the FTIR spectra of dry $LiMnPO_4$ powder calcinated at 580 °C. The IR spectral features of $LiMnPO_4$ have been previously assigned based on group theory analysis, isotope studies, and direct comparison to similar olivine structures ($LiMePO_4$; Me = Fe, Mg, Ni) (Burba and Frech, 2006). The spectra are dominated by the intramolecular vibrations of the PO_4^{3-} anion which confirm the presence of phospho-olivine phase in $LiMnPO_4$. These internal vibrations consist of three components; the antisymmetric PO_4^{3-} stretching mode at 1065 cm^{-1}, the symmetric PO_4^{3-} stretching mode around 974 cm^{-1} and the antisymmetric bending

mode between 650 cm^{-1} and 530 cm^{-1} (Norberg and Kostecki, 2001, Kumar *et al*., 2011). Several other absorption bands were observed at 2941, 1671 and 1437 cm^{-1}, respectively. The 2941 cm^{-1} band is attributed to the O-H stretching vibration, and the 1671 and 1437 cm^{-1} absorption bands are normally attributed to O-H bending vibrations combined with Mn atoms.

Fig. 4.6 shows the Raman spectra of the $LiMnPO_4$ nanoparticles measured at wavelength 532 nm. From **Fig 4.6** the Raman spectra of the $LiMnPO_4$ is dominated by a strong and broad band at 943 cm^{-1} corresponding to the symmetric mode of PO_4^{-3}, and the two low intensity bands at 980 and 1005 cm^{-1} are due to the asymmetric stretching modes of the PO_4^{-3} anion (Kumar et al, 2011). These bands are associated with the two intense absorption bands in the FTIR spectrum at approximately 974and 1065 cm^{-1}. The other peaks between 600-950 cm^{-1} corresponds to PO_4^{3-} stretching mode.

The results from XRD, FTIR and Raman spectroscopy confirmed that olivine $LiMnPO_4$ was produced.

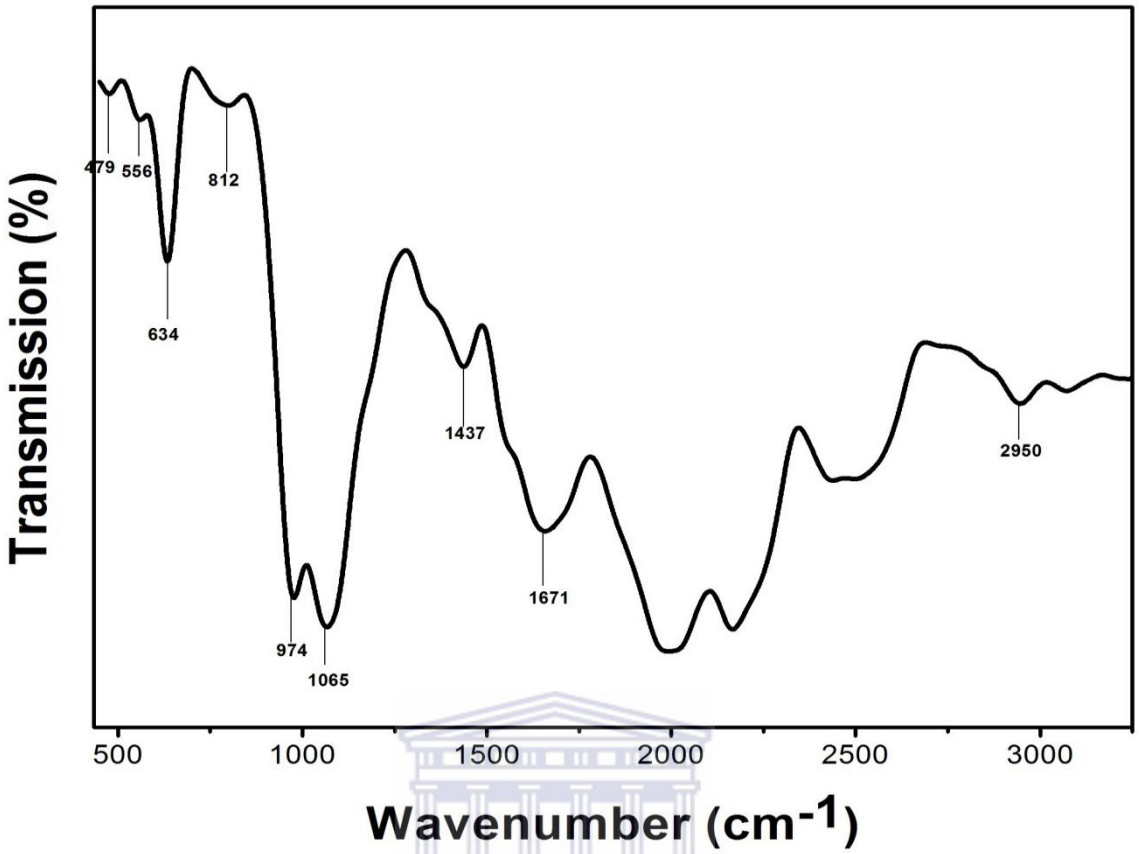

Figure 4.5: FTIR spectra of olivine $LiMnPO_4$ calcinated at 580 °C.

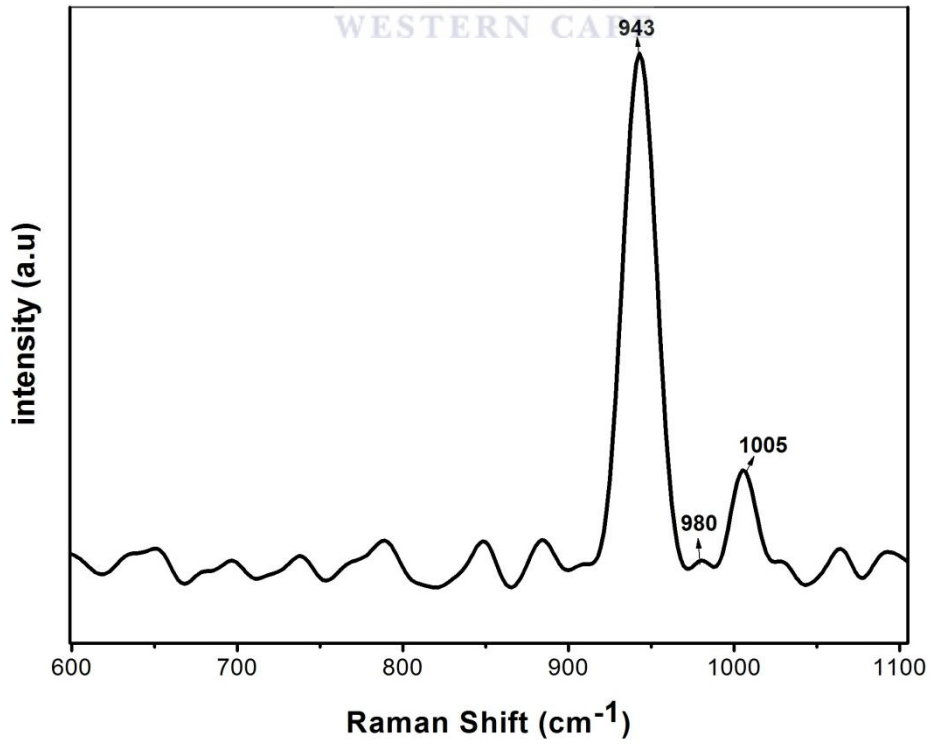

Figure 4.6: Raman spectra of olivine $LiMnPO_4$.

4.1.4 Electrochemical characterisation of $LiMnPO_4$

4.1.4.1 Redox reaction analysis

The cyclic voltammogram (CV) at **Fig. 4.7**, shows the characterization of the cathode material, $LiMnPO_4$, on glassy carbon electrode (GCE) in 1 M Li_2SO_4 electrolyte which was carried out at 10 mV/s at an electrochemical potential window of -1000 mV/s to 1000 mV/s. As expected, the bare GCE did not exhibit any electrochemistry since there was nothing immobilized on the electrode surface. However the GCE modified with $LiMnPO_4$ have two redox couples at low scan rates. The anodic and cathodic peaks correspond to lithium de-intercalation and intercalation (Manjunatha *et al*., 2012). The CV profile consists of reduction peak C_1 at -494 mV which correspond with anodic peak A_1 at 364 mV, at a formal potential, $E°$ = -65 mV. The peak to peak separation (E_{pa} - E_{pc}), ΔE_p = 858 mV. These sets of peaks were due to the redox reaction of Mn^{2+}/Mn^{3+} couple. The corresponding reaction equations for redox peaks of $LiMnPO_4$ can be written as follows:

Oxidation: $LiMnPO_4 \rightarrow Li^+ + MnPO_4^-$ (11)

Reduction: $Li^+ + MnPO_4^- \rightarrow LiMnPO_4$ (12)

The additional peak which is a reduction peak C_2 was observed at 124 mV, the cathodic peak is associated with the initial Li^+ ion insertion in the octahedral site (Manjunatha *et al*., 2012). The redox peaks of the $LiMnPO_4$ electrode are sharp with well-defined splitting, which indicates good crystallinity of the product. In theory extremely small scan rate was applied to get the true separation between the anodic and cathodic peaks, practically we applied 1 mV/s as the lowest scan rates (Ramar and Balaya, 2013). The sharp peaks which were observed in **Fig. 4.7** for GCE modified with $LiMnPO_4$ indicates a facile lithium ion transfer resulting in better reaction kinetics compared with bare GCE.

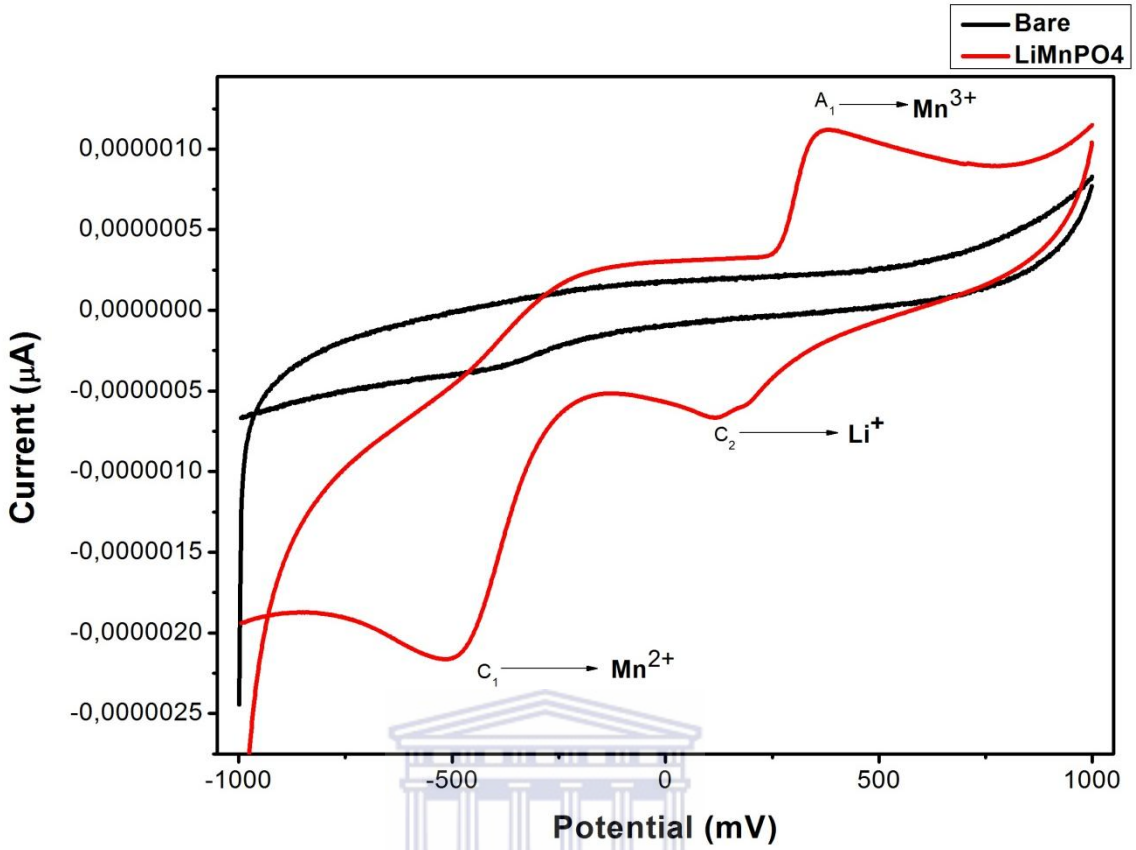

Figure 4.7: Cyclic voltammograms of the bare GCE and that of GCE modified with the $LiMnPO_4$ in 1 M Li_2SO_4. Scan rate 10 mV/s (voltage range: -1000 – 1000 mV).

Fig. 4.8 shows the CV profiles of LiMnPO4-modified GCE in 1 M Li_2SO_4 at different scan rates. It can be seen that Li_2SO_4 electrolyte provides a stable electrochemical window for the lithium intercalation/de-intercalation in $LiMnPO_4$ and therefore all electrochemical studies were based on it. When scanned from 1 - 10 mV/s, the anodic peak current increases with scan rate. This shows a linear dependence of the peak current on scan rates. It also shows that $LiMnPO_4$ is an electro-active material undergoing a rapid reversible electron transfer reaction in Li_2SO_4 electrolyte. Though $LiMnPO_4$ is electroactive, it still suffers from poor conductivity and the next chapter presents the results obtained upon coating the cathode material with a thin film of magnesium-gold composite in order to enhance its conductivity (Kwon and Fromm, 2012).

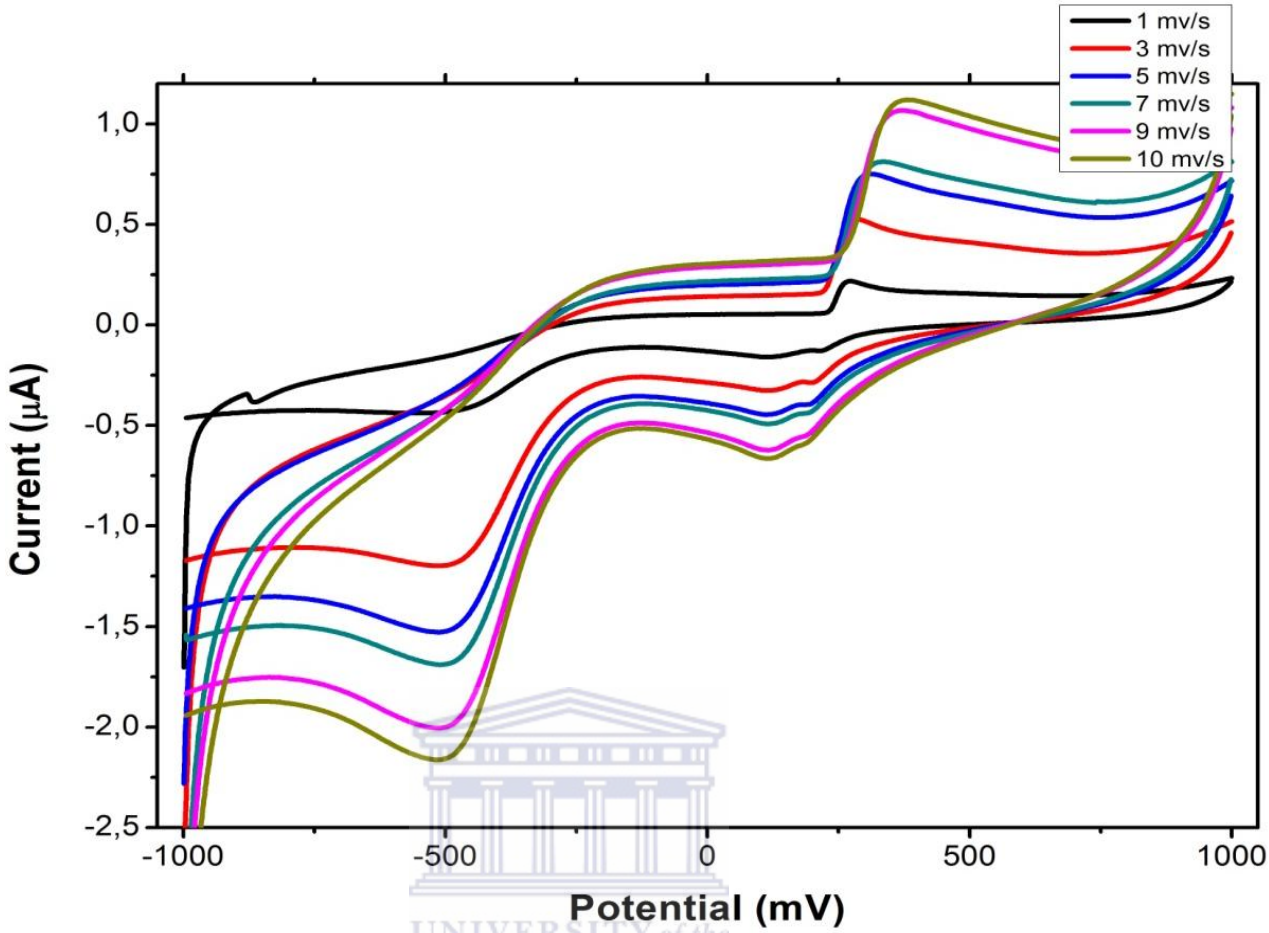

Figure 4.8: Cyclic voltammetry of $LiMnPO_4$ in 1 M $LiSO_4$ electrolyte at different scan rates between 1 - 10 mV/s.

.

Chapter 5

5 Analysis of lithium manganese phosphate coated with magnesium-gold composite thin film

The synthesized $LiMnPO_4$ nanoparticles were modified through surface modification by the use of MgO nanowire and gold nanoparticles to form a composite of $LiMnPO_4$/Mg-Au thin film which was further analyzed and characterized**.**

5.1 Magnesium nanowire and gold nanoparticles.

5.1.1 Synthesis and characterisation of magnesium oxide nanowires

MgO nanowires were synthesised by hydrothermal synthesis and characterised with SEM, TEM, UV-Vis and XRD, for morphology, particle size, structure and spectroscopic characteristics of the material. **Fig. 5.1** Shows the typical SEM images of MgO consisted of uniform, ultrafine nanowire-like structures with high yield. The length is in the range of several hundred nm to more than 10 µm while the height ranges from 20 µm to more than 100 µm. **Fig. 5.2 (a)** shows the TEM image of the nanowire which confirms the straight-line morphology with no spherical droplets or nanoparticles at the tip which agrees with SEM. **Fig. 5.2 (b)** shows a selected area diffraction pattern (SAED) of MgO nanowire, which shows well- spotted MgO nanowires, revealing the highly ordered single crystalline nature of the nanomaterial. The diffraction patterns were indexed according to the crystal structure of single phase face centered cubic and the structure of MgO is polycrystalline in nature. The figure also shows a spotty ring pattern and the strong (200) and (220) diffraction arcs which confirm what was observed in XRD with (200) and (220) having high intensity peaks (Al-Ghamdi *et al*., 2012). **Fig. 5.3** shows the EDS spectrum indicating that the nanowires were composed of Mg and O, with the magnesium showing a very strong peak around 1.5 keV. The signals of Cu and C in the EDS spectrum were due to the TEM C-coated Cu grids.

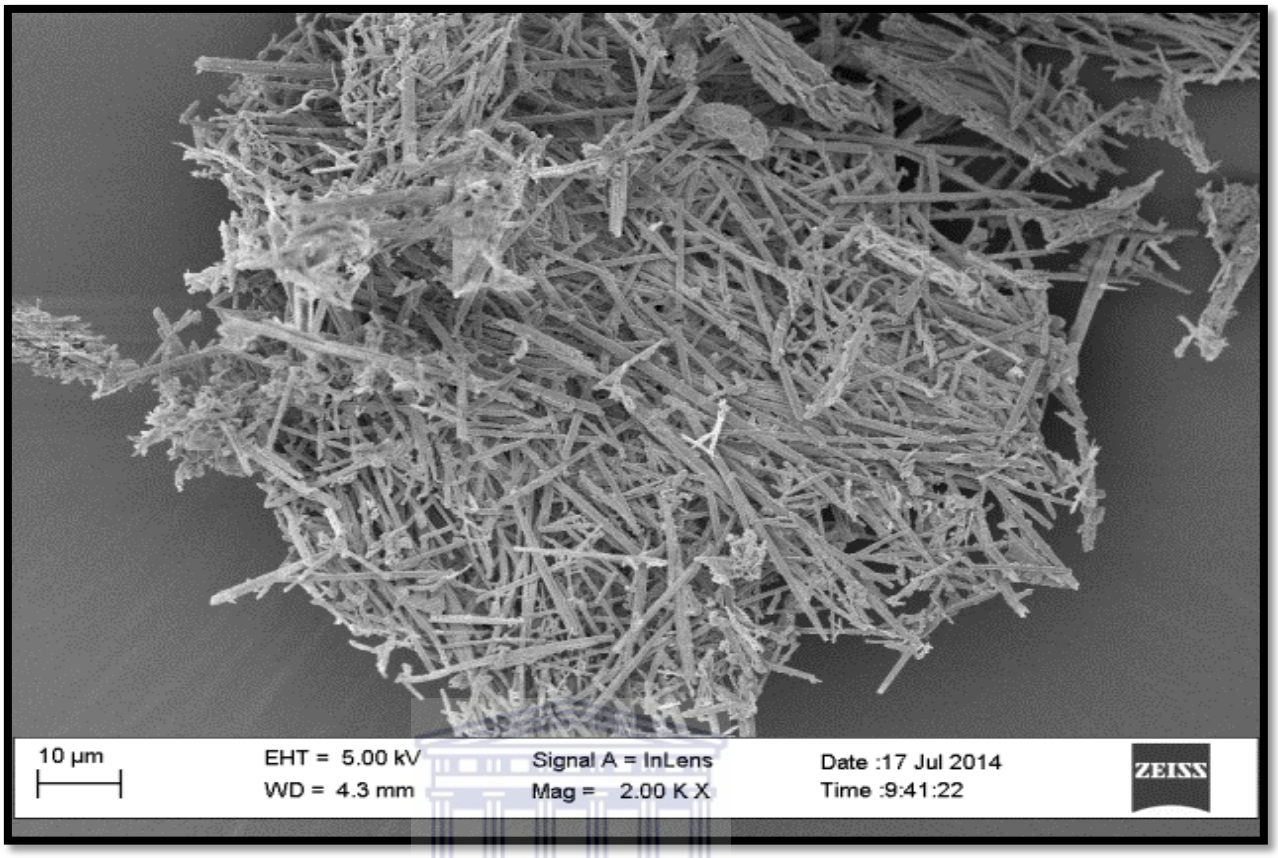

Figure 5.1: SEM images of the MgO nanowires.

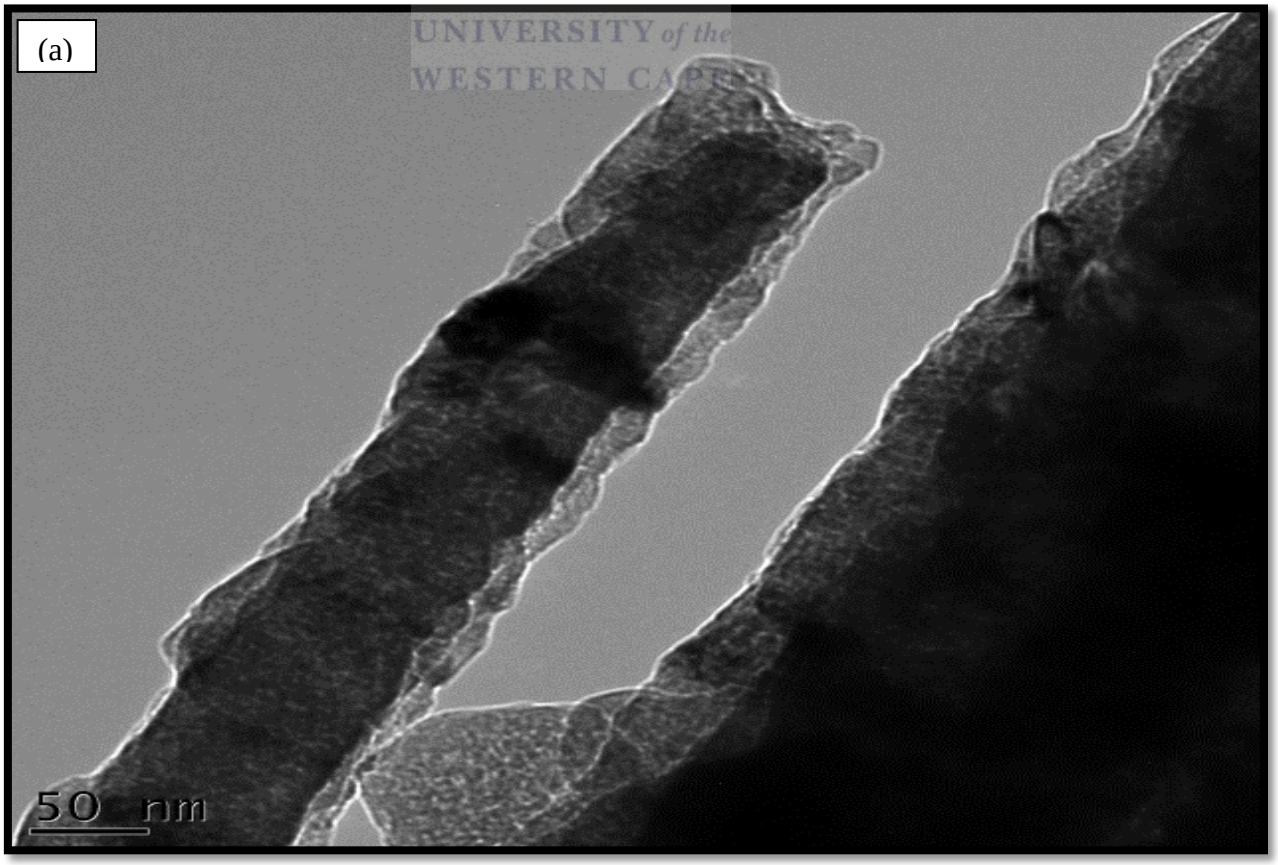

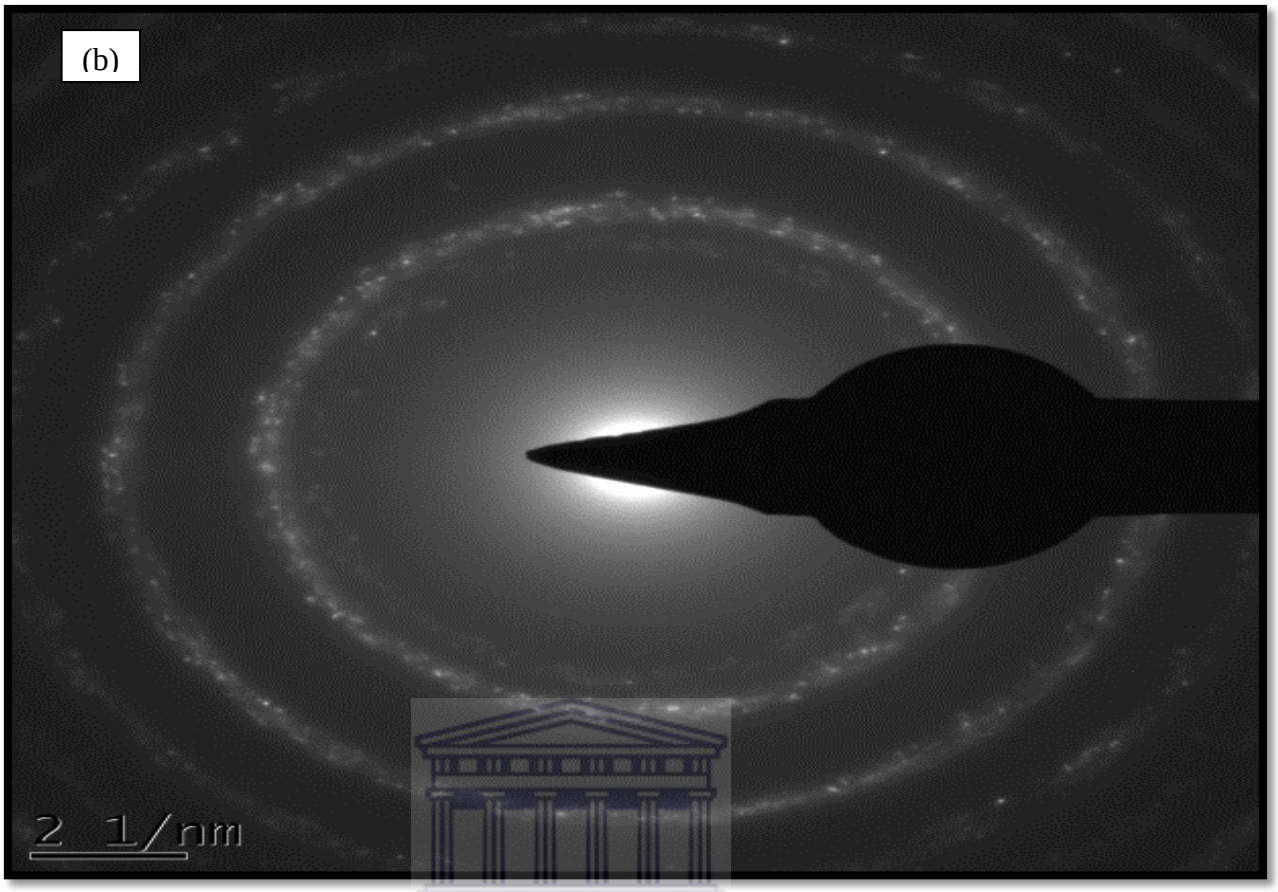

Figure 5.2: (a) TEM image of the MgO nanowires and (b) SAED pattern of the MgO nanowires.

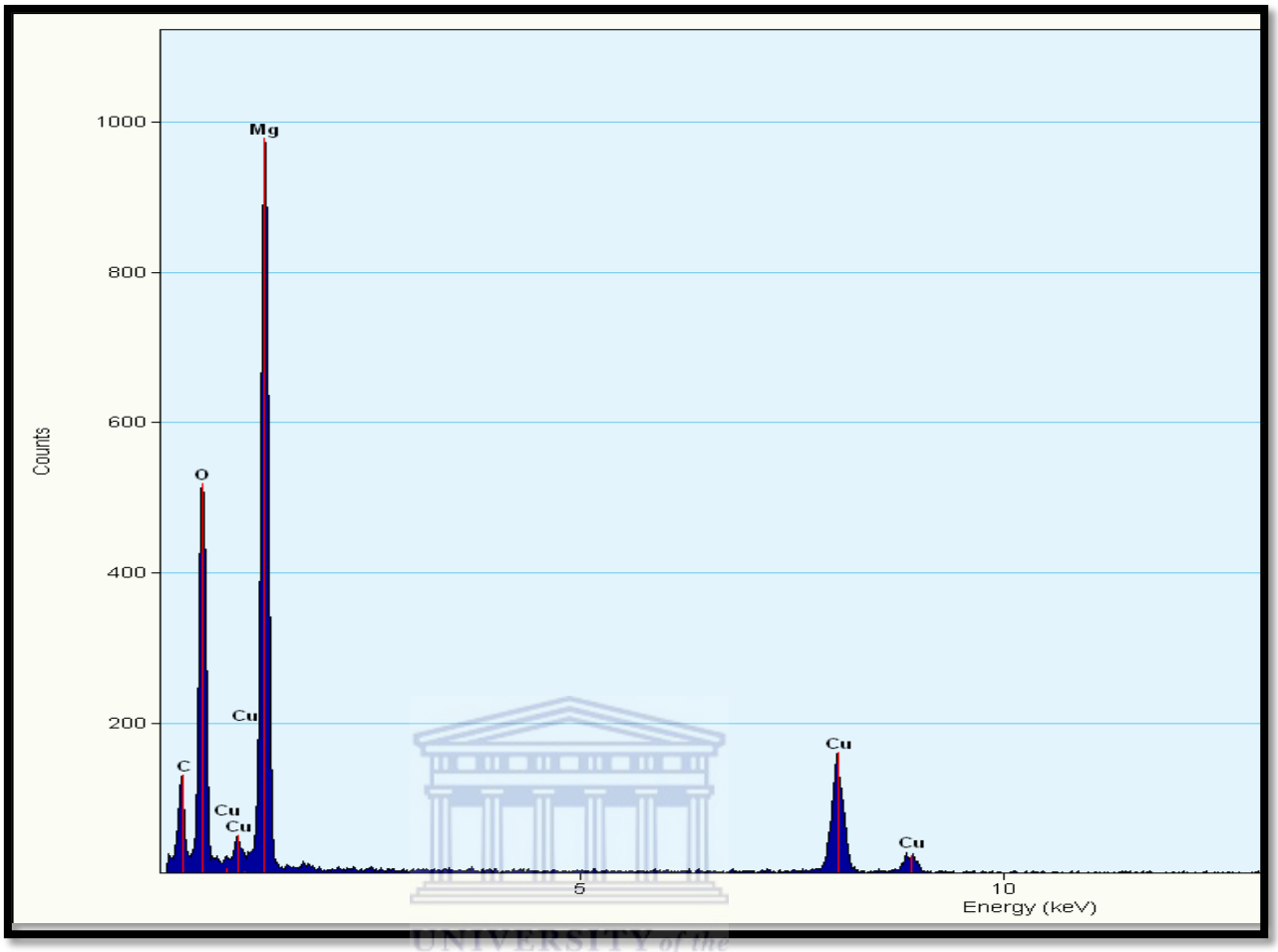

Figure 5.3: MgO nanowires TEM energy dispersive x-ray (EDS).

Fig. 5.4 Shows the XRD results of all recognizable reflection peaks of MgO including (111), (200),(220), (311) and (222).The crystal structure of the sample is attributed to the single phase face centred cubic with a lattice constant of a = 0.421 nm. The sharp and intense peaks further confirm that the MgO nanowires are well crystallized. Other phases were not observed in the diffraction pattern of the MgO nanowires thus indicating that there was no un-reacted Mg or other magnesium oxides. This clearly shows that the synthesized MgO nanowires have high purity which corroborates the TEM-EDS results where only Mg and O were present in the spectrum. **Fig. 5.5** Shows the UV-visible absorption spectra of MgO nanowires at room temperature, where the absorption intensity was observed at the lower wavelength region. An absorption peak in the UV regime with a wavelength of 215 nm is attributed to the band to- band transition in the band gap region (Al-Ghamdi *et al*., 2012). From these sets of results, it has been proven that

MgO nanowires were successfully synthesized and can then be coated onto the surface $LiMnPO_4$.

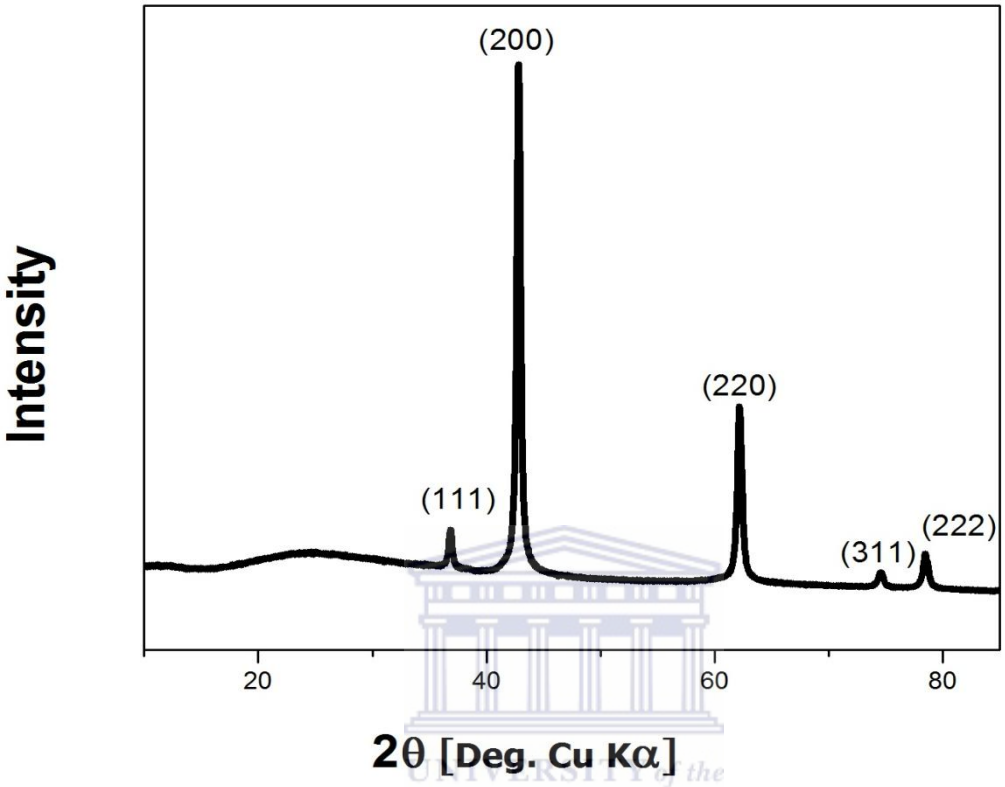

Figure 5.4: X-ray pattern of the MgO nanowire network.

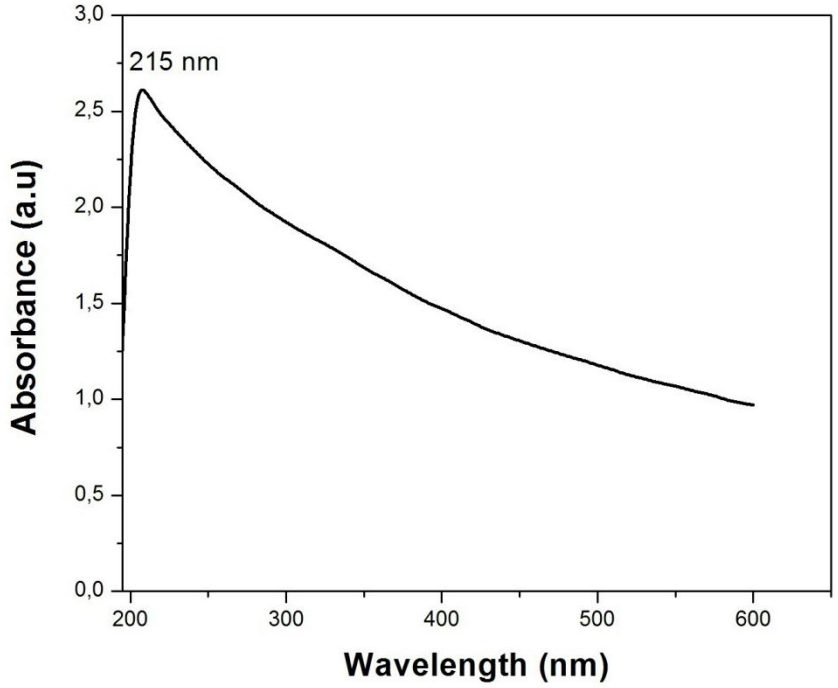

Figure 5.5: UV-Vis absorption spectra of the MgO nanowires.

5.1.2 Characterisation of gold nanoparticles

Transmission electron microscopy (TEM) is a powerful and straightforward method for the determination of size and shape of nanoparticles. The shapes and sizes of the deposited particles were measured using transmission electron microscopy (TEM). The darker circular particles in the images **Fig. 5.6** are gold nanoparticles which are spherical in shape. The size of the synthesized gold nanoparticles was found to be between 60 -30 nm. The size of the nanoparticles decreases with increase in trisodium citrate amount. In other words, the more the quantity of trisodium citrate, the smaller the size of the nanoparticles. **Fig. 5.7** shows the EDS spectrum of Au nanoparticles. The Si and Ni might be due impurities from the precursors. The signals of Cu and C in the EDS spectrum were due to the TEM C-coated Cu grids.

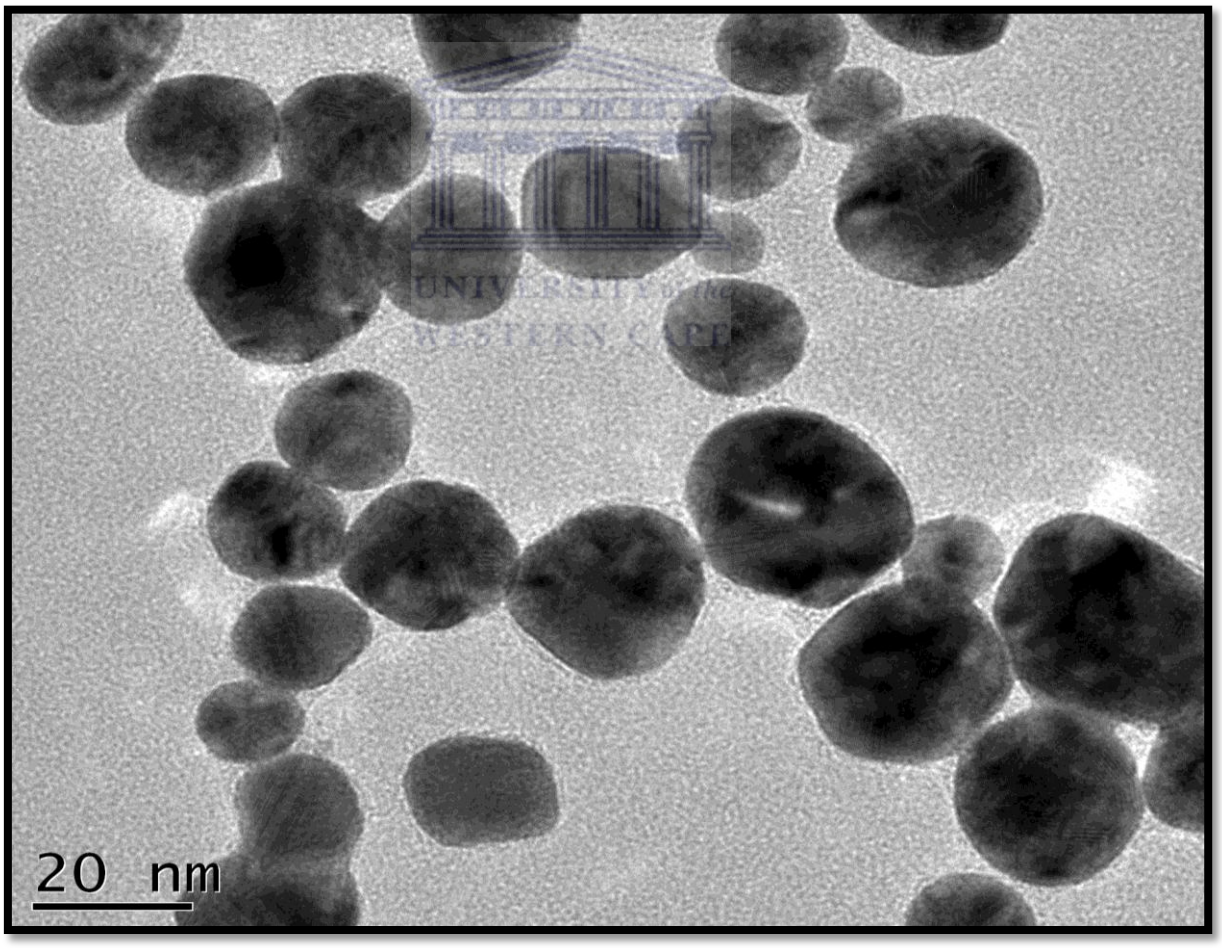

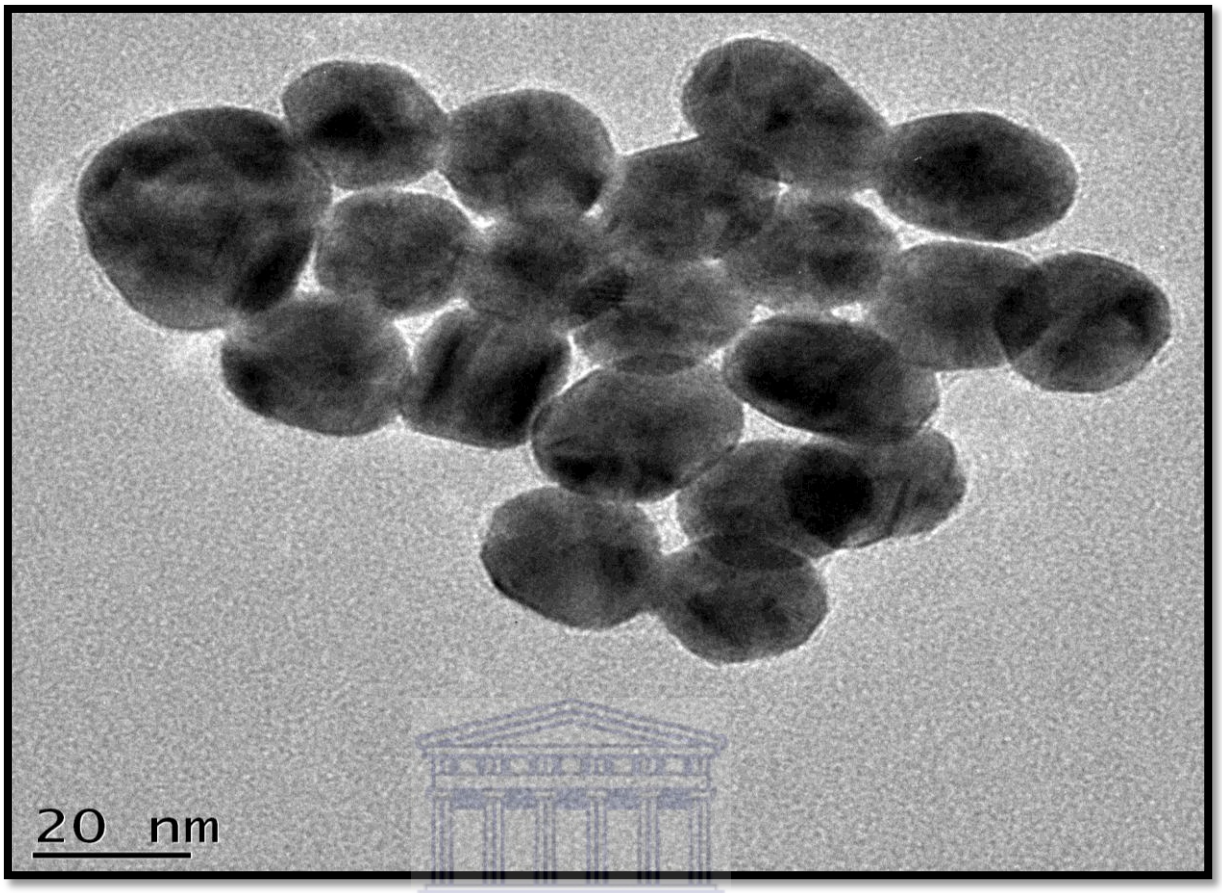

Figure 5.6: TEM images of the gold nanoparticles.

Different molecules absorb radiation of different wavelengths. **Fig. 5.8** shows the UV-Vis absorption spectra of the gold nanoparticles. An absorption spectrum will show a number of absorption bands corresponding to structural groups within the molecule. Absorption of UV radiation by a molecule excites it from a vibrational level in the electronic ground state to one of the many vibrational levels in the electronic excited state. The optical properties of gold nanoparticles such as absorption maxima and absorption intensity are particle size dependent. The UV-Vis which was carried out showed an intense absorption peak at 524 nm which is generally attributed to surface plasmon excitation of small spherical gold nanoparticles (Long *et al.,* 2009). From these sets of results it can be proven that gold nanoparticles were successfully synthesized and can then be coated onto $LiMnPO_4$.

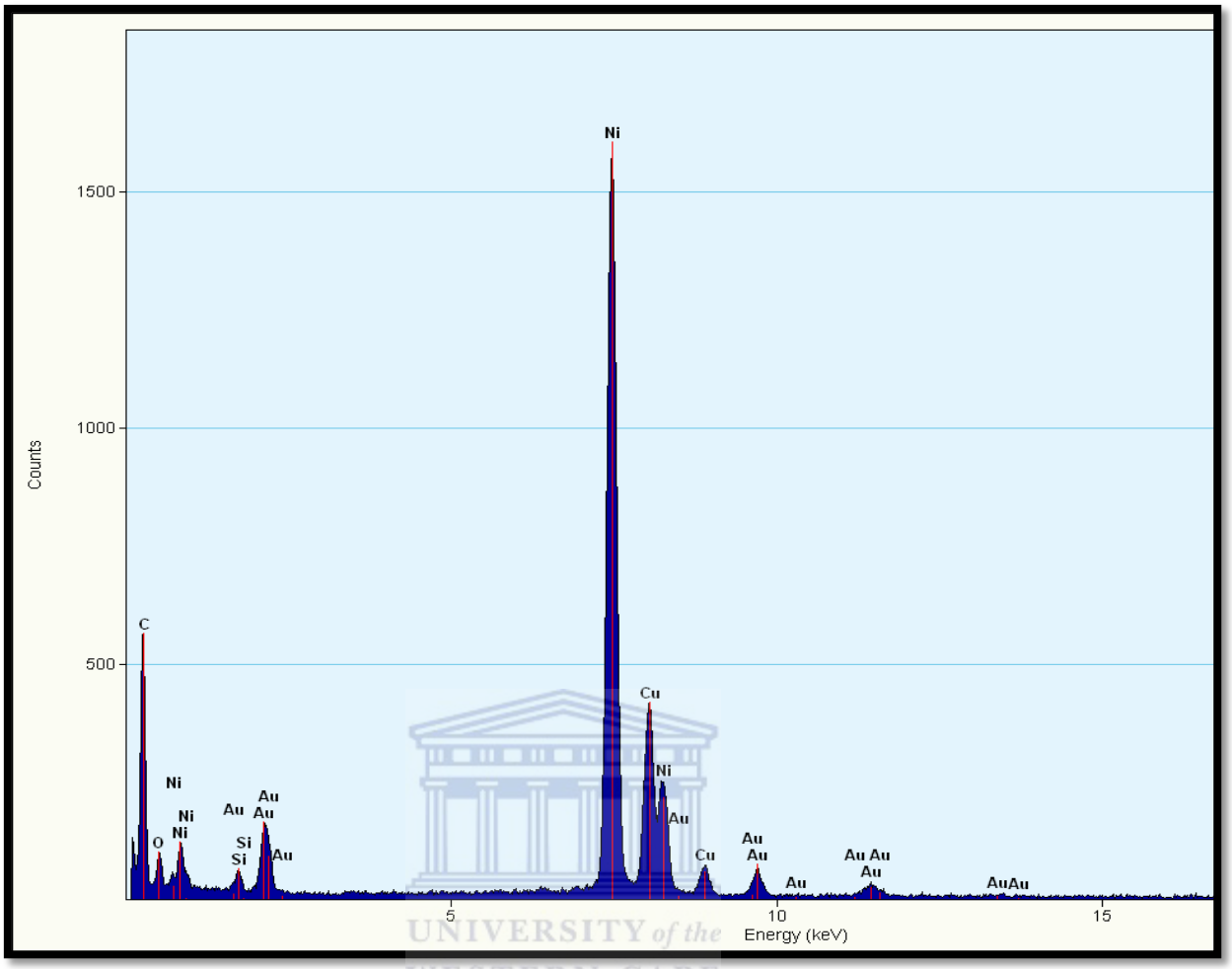

Figure 5.7: TEM/EDS of the gold nanoparticles**.**

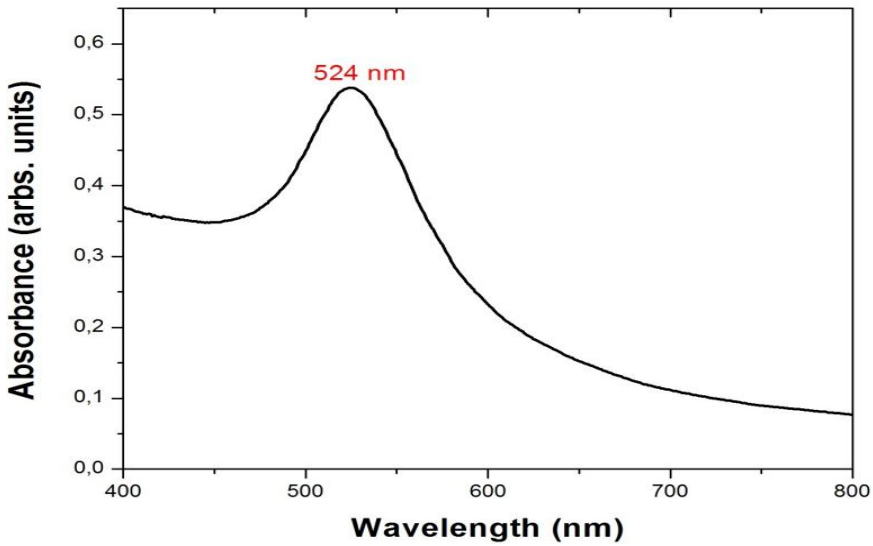

Figure 5.8: Gold nanoparticles UV-Vis absorption.

5.2 Lithium manganese phosphate coated with magnesium-gold composite thin film

5.2.1 Particle morphology and chemical composition of composite of $LiMnPO_4$/Mg-Au

High resolution scanning electron microscopy (HRSEM) was used to show the morphology of the synthesized $LiMnPO_4$ coated with gold-magnesium composite thin film. The SEM micrographs are shown in **Figs. 5.9, Fig. 5.10** and **Fig. 5.11** where different magnifications and detectors were used to investigate the particles size and distribution. **Fig. 5.9** shows the HRSEM image of $LiMnPO_4$ coated with gold-magnesium composite thin film (LiMnPO4/Mg-Au). The Figure reveals different geometrical structures with the plate-like crystalline structure corresponding to $LiMnPO_4$ with apparent secondary particles of ~250 nm and primary particles having sizes of ~ 100 nm sitting on top of the big crystals. The nanowires were also observed in the micrograph but more obvious at 44.11 KX magnifications where images were captured by zooming into the nanostructure as shown in **Fig. 5.10**. A typical morphology of MgO nanowires as discussed previously was observed. The spherical nanoparticles aligned on top of the nanostructure confirm the presence of gold nanoparticles.

Fig 5.11 shows the SEM images of the $LiMnPO_4$/Mg-Au nanostructure acquired with the use of secondary electron (SE) detector so as to observe the coated nanoparticles on the material. The micrograph shows white-spotted spherical gold nanoparticles coated on the surface of the $LiMnPO_4$ crystal structure. Therefore, HRSEM confirms the presence of the gold nanoparticles as well as magnesium oxide nanowires coatings on the parent cathode material.

Fig. 5.12 provides the EDS spectra of the composite cathode material which shows peaks of elemental magnesium (Mg), oxygen (O), manganese (Mn), phosphorus (P), gold (Au) and some sulphur (S) - which was due to the precursors. Thus the Mg-Au thin film coating on the surface of the $LiMnPO_4$ olivine cathode material is confirmed.

Table 4.1 shows the elements and their atomic percentages in the nanocomposite with oxygen having the largest composition. The smaller percentages of magnesium and gold confirmed the fact that a thin film of these nanomaterials was coated on the parent LiMnPO4 cathode material. It is expected that the electrochemical performance of the composite cathode will be greatly enhanced over that of the pristine cathode (Drezen *et al*., 2007).

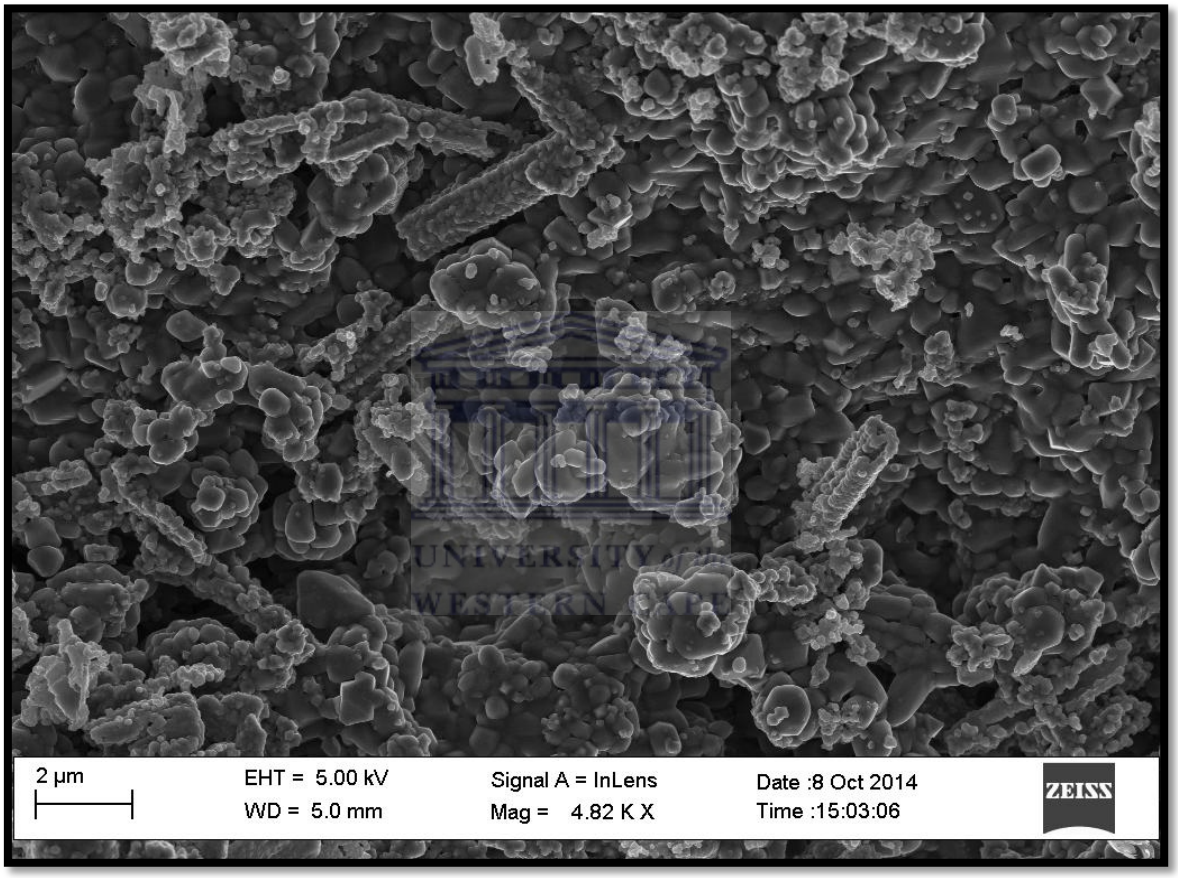

Figure 5.9: HRSEM of $LiMnPO_4$/Mg-Au nanoparticles at magnification of 4.82 KX using SEM InLens Detector.

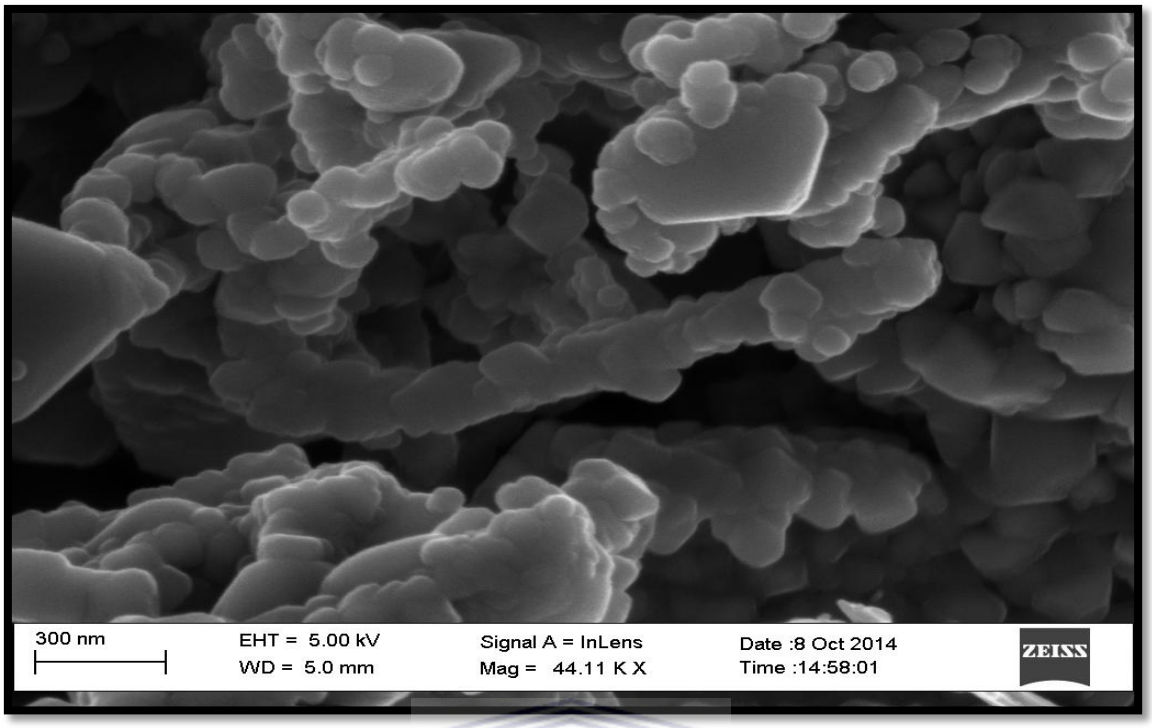

Figure 5.10: HRSEM of $LiMnPO_4$/Mg-Au nanoparticles at magnification of 44.11 KX using SEM InLens Detector.

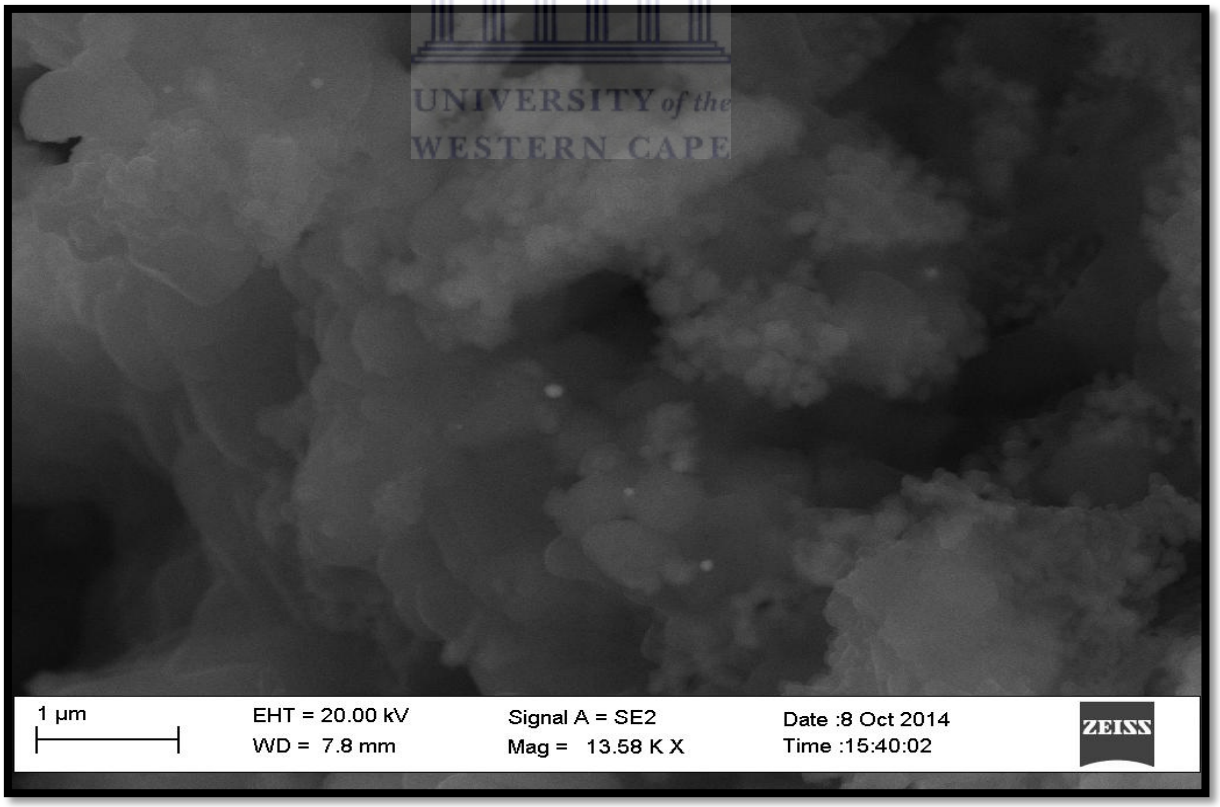

Figure 5.11: HRSEM of $LiMnPO_4$/Mg-Au nanoparticles at magnification of 13.58 KX with the use of Secondary Electron Detector.

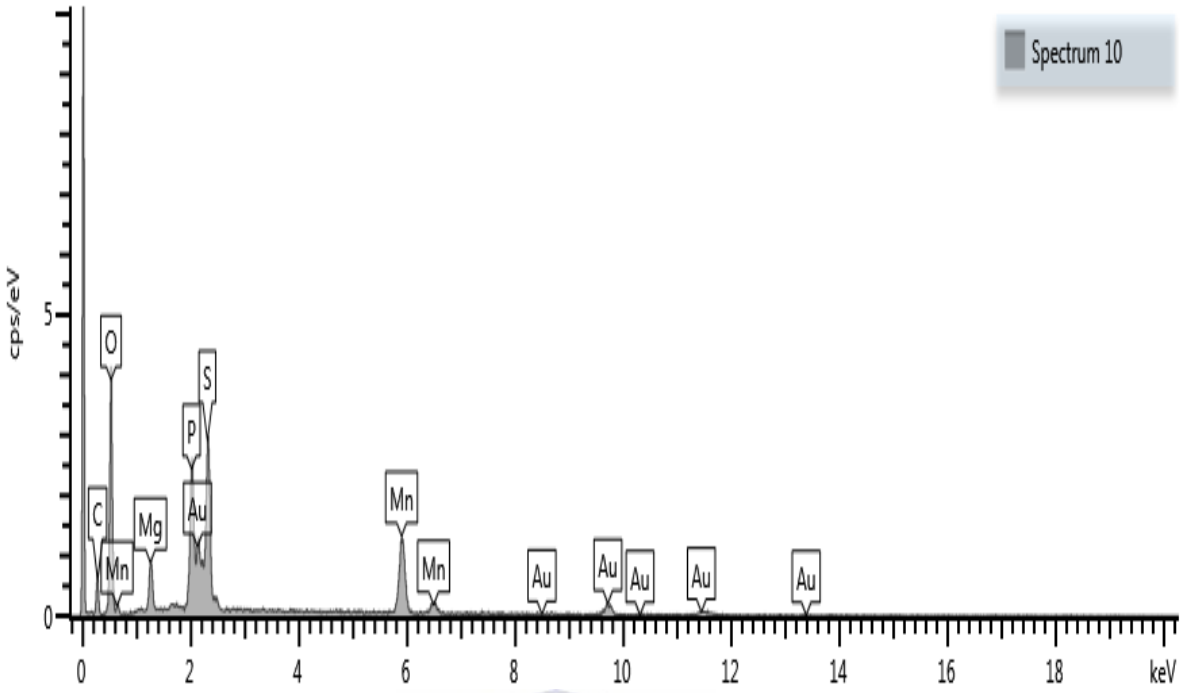

Figure 5.12: Energy dispersive x-ray (EDS) of $LiMnPO_4$/Mg-Au nanoparticles.

Elements	Atomic %
O	**62.69**
Mn	**10.19**
P	**8.63**
Mg	**4.4**
Au	**1.83**

Table 5.1: Chemical composition of $LiMnPO_4$/Mg-Au composite by EDS/SEM.

5.2.2 Crystal structure and phase composition analysis by x-ray diffraction (XRD) for the composite of $LiMnPO_4$/Mg-Au thin film

Fig. 5.13 shows the XRD pattern recorded from the product synthesized by MgO and gold coating onto the surface of $LiMnPO_4$ to form $LiMnPO_4$/Mg-Au composite. The olivine structure of $LiMnPO_4$ was maintained after modification and a solid LiMnPO4/Mg-Au was formed as shown in **Fig. 5.13**. It can be seen that the intensities of the peaks and sharpness increase in the modified material compared to the pristine meaning there was an increase in the crystallinity which was also observed from HRSEM results. The XRD Pattern did show peaks of

MgO and Au. It confirmed the presence of Mg-Au composite with diffraction peaks which are closer to each other. All reflection peaks for MgO was observed, including (111), (200), (220), (311) and (222) and can be well indexed to the cubic MgO structure with a lattice constant of a = 0.421120 nm (JCPDS: 045-0946). An Au layer was observed with diffraction peaks (111), (200), (220) and (311) diffraction peaks indexed to the cubic Au structure with lattice constant of a = 0.407860 nm (JCPDS: 0004-0784). XRD analysis revealed that olivine $LiMnPO_4$ does still retain its orthorhombic structure. The presence of MgO and Au diffraction peaks confirms that the thin film has been coated onto $LiMnPO_4$ and the nanoparticles are crystalline in nature. The diffraction results demonstrate a high degree of crystallinity and uniformity.

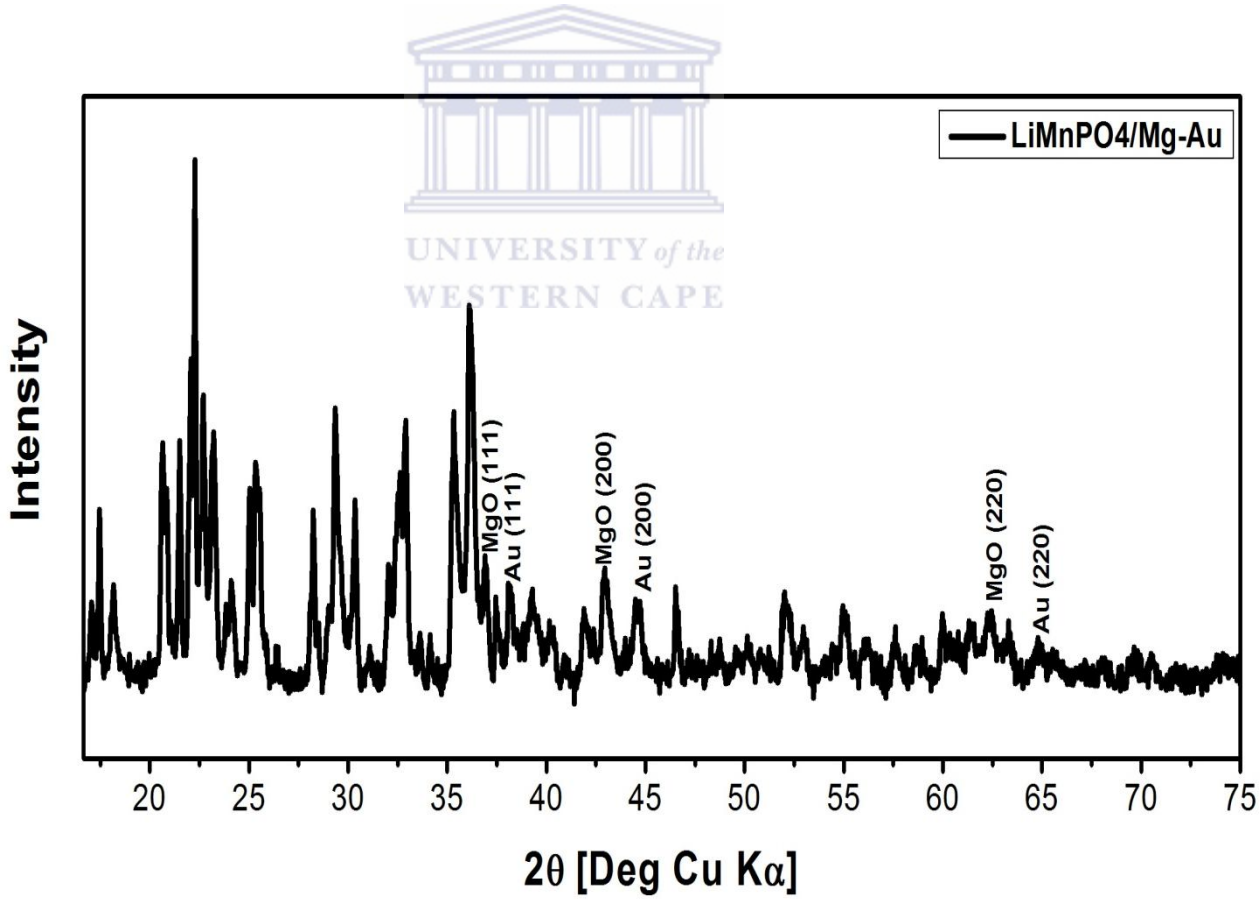

Figure 5.13: XRD pattern of $LiMnPO_4$ coated Mg-Au composite thin film**.**

5.2.3 Fourier-transform infrared $LiMnPO_4$ coated with Mg-Au thin film analysis

Fig. 5.14 shows the FTIR spectra of pure $LiMnPO_4$ and the modified LiMnPO4/Mg-Au thin film .The change in the band shapes is apparently not noticeable from the spectra. There is a change in peak intensity in the modified cathode material meaning the functional group PO_4^{3-} was not affected by the modification with magnesium oxide nanowire as well as gold nanoparticles. There are no peaks related to gold or magnesium, so it is more likely that Mg-Au composite was well incorporated into the matrix. The FTIR results confirm that the structure of $LiMnPO_4$ was still maintained and this implies that the material is stable as was also observed in the XRD result.

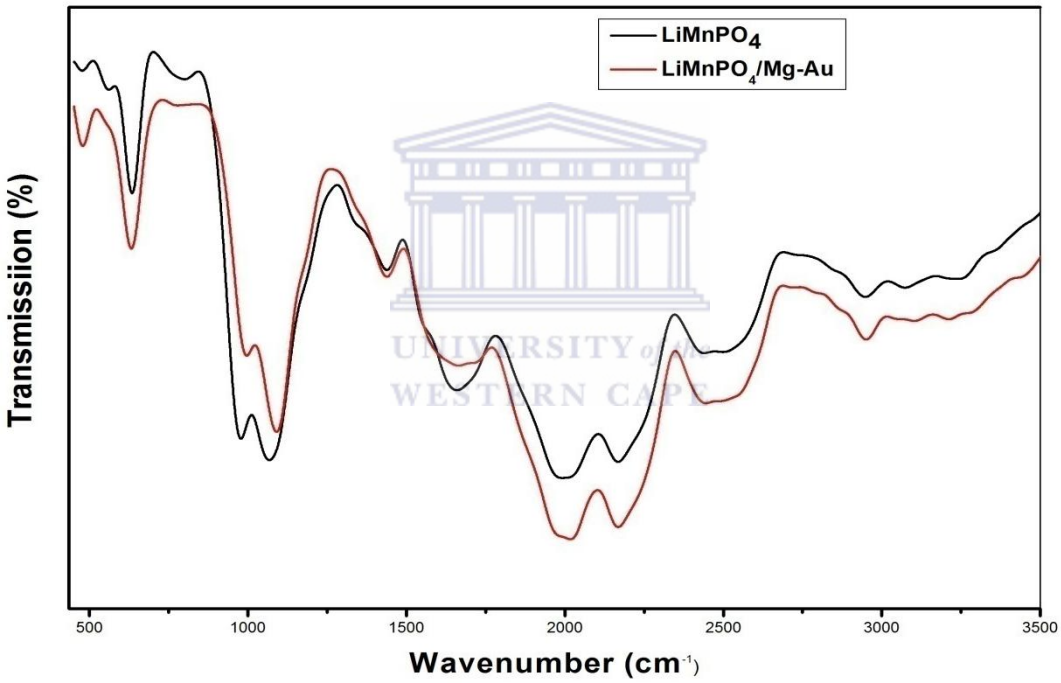

Figure 5.14: FTIR spectra for olivine $LiMnPO_4$/Mg-Au composite.

.

5.2.4 Electrochemical characterisation for composite of $LiMnPO_4$ coated with magnesium-gold composite

The $LiMnPO_4$ coated magnesium-gold composite thin films were investigated by cyclic voltammetry and electrochemical impedance spectroscopy to study the electrochemical performance.

5.2.4.1 Cyclic voltammetry for redox reaction analysis

Fig. 5.15 shows that the cyclic voltammograms of the unmodified $LiMnPO_4$ and the modified composite were well defined pair of redox peaks and are related to the electrochemical lithium ion insertion/deinsertion within the octahedral sites of $LiMnPO_4$ structure (Manjunatha *et al*., 2012). In both materials, the redox process primarily involves a change in the oxidation state of manganese in $LiMnPO_4$. It can be clearly observed that the peak currents in $LiMnPO_4$/Mg-Au composite were higher than in the pristine cathode; an indication that the conductivity of $LiMnPO_4$ has been improved and more facile lithium ion transfer will result in better reaction kinetics. The oxidation and reduction peaks for $LiMnPO_4$/Mg-Au are observed at: A_1 (I_{pa}= 1, 91 µA, E_{pa} = 191 mV), C_1 (I_{pc} = -3.43 µA, E_{pc} = -477 mV) the oxidation and reduction peaks correspond to Mn^{3+}/Mn^{2+} (Ramar and Balaya, 2013). In addition to the cathodic peak C_1, a small peak was at C_2 (I_{pc}= -1.911µA, E_{pc} = 95.63 mV) during a scan in the cathodic direction. This cathode peak is associated with the initial Li^+ ion insertion in the octahedral site and it is not reversible. The peak potential difference (ΔE_p) in the redox peaks of $LiMnPO_4$/Mg-Au composite is ($\Delta E_p = E_{pa} - E_{pc}$ = 668 mV) while it was found out that for $LiMnPO_4$, ΔE_p = 868 mV, from the ΔE_p values, it can be seen that $LiMnPO_4$/Mg-Au has a smaller peak to peak separation than $LiMnPO_4$ therefore, there is better electrochemical reversibility in $LiMnPO_4$/Mg-Au composite than in $LiMnPO_4$. This decrease is due to the presence of the Mg-Au conductive coating on the composite cathode material.

Cyclic voltammetry was also used to calculate the charge and discharge for $LiMnPO_4$ and $LiMnPO_4$/Mg-Au composite. The charge/discharge capacities obtained from the integrated area under the anodic peak at the scan rate of 10 mV/s indicate that the composite $LiMnPO_4$/Mg-Au composite cathode exhibited a charge capacity of 259 mAh/g and a discharge capacity of 157 mAh/g for the insertion of lithium and reduction of Mn^{3+} to Mn^{2+}, and the corresponding values for $LiMnPO_4$ were for charge capacity 115 mAh/g and discharge capacity 44 mAh/g respectively. The calculated capacities show that $LiMnPO_4$/Mg-Au composite has higher capacity compared with $LiMnPO_4$. For the purpose of this

research work, the cathodic capacity is our main interest and it was found out to be 157 mAh/g this was close to the theoretical capacity of 170 mAh/g for $LiMnPO_4$ (Wu *et al*., 2012). Therefore $LiMnPO_4$/Mg-Au composite exhibits better electrochemical performance and it can be proposed to be used in lithium ion batteries as cathode material.

The capacities were calculated according to the following steps:
The integration of the Area peak obtained at 10 mV/s scan rate from $LiMnPO_4$/Mg-Au thin film gave the area under the current-potential curve as 9.7 x10^{-4} Ampere-Volt (AV).

But charge, $Q = \frac{Area\ (AV)}{Scan\ rate\ (\frac{V}{s})}$ (13)

Thus $Q = \frac{9.7x10^{-4}\ (AV)}{0.01(\frac{V}{s})}$ (14)

$Q = 0.097\ As$ = 0.097 coulombs

However, in battery system, the capacity units are Ampere-hour (Ah). Since 3600 As = 1 Ah.

Therefore: $Q = \left(\frac{0.097\ As}{3600}\right)$Ah (15)

$Q =$ 2.7 x10^{-5} Ah

The interest is on specific capacity so the calculation for Q (electric charge) was done so that it can help in the calculation for specific capacity, which is defined as the capacity per gram of the active cathode material. The active mass = 1.71x10^{-4} g.

Specific capacity = $\frac{Q}{active\ mass}$ (16)

$$= \frac{2.7x10^{-5}Ah}{1.71x10^{-4}g} = 0.157 \text{ Ah/g} \quad (17)$$

Specific capacity is usually expressed in mAh/g. therefore, the specific capacity becomes 0.157 Ah/g x 1000 = 157 mAh/g, the same procedure was adopted for all other capacity calculations with data obtained from cyclic voltammetry.

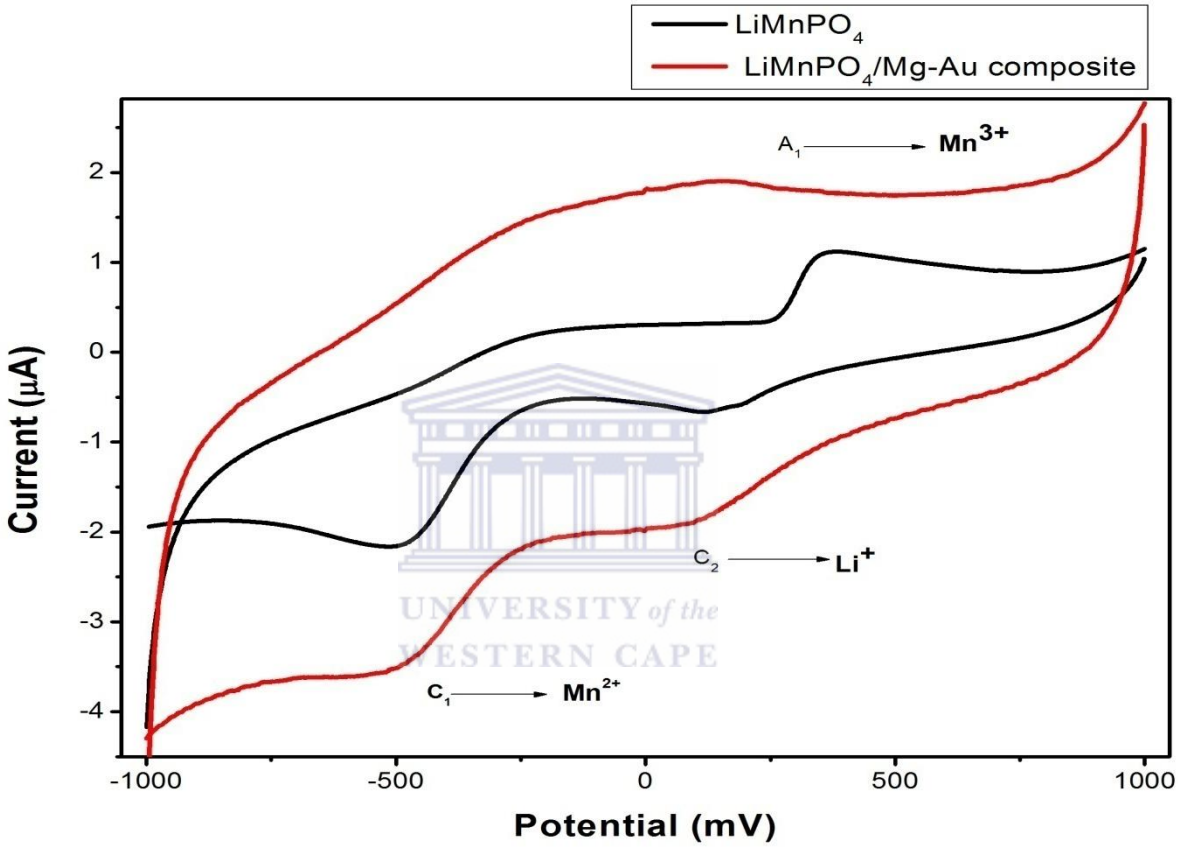

Figure 5.15: Comparative cyclic voltammograms of $LiMnPO_4$/Mg-Au thin film composite and pristine $LiMnPO_4$ in 1 M Li_2SO_4. Scan rate 10 mV/s (voltage range: -1000 mV/s – 1000 mV/s).

The effects of scan rates

The study of reversibility of $LiMnPO_4$ and $LiMnPO_4$/Mg-Au composite system was conducted by change in scan rates from 1 – 10 mV/s. As stated previously, the pair of peaks consists of anode and cathodic peaks, corresponding to the two-phase charge –discharge reaction of the Mn^{2+}/Mn^{3+} redox couple and an extra peak at the cathodic direction which is related to proton insertion and is not

reversible. The peak potential difference between the anodic and the cathodic processes increases with increasing scan rate, indicating a quasi-reversible system (Chen *et al*., 2012).

From **Fig. 5.16** it can be seen that there is a linear relationship between peak current and scan rates, the peak separation increases with increase in scan rate. All the CV profiles overlap regardless of the scan rate at the beginning of charging and discharging. $LiMnPO_4$/Mg-Au composite electrode presents a larger peak current and a larger enclosed area as well as a smaller peak potential difference compared with those of the $LiMnPO_4$ (**Fig. 5.15**) electrode at the same scan rate. These results indicate that the $LiMnPO_4$/Mg-Au composite electrode has better reversibility and higher specific capacity in comparison with the $LiMnPO_4$ electrode. The improvement of the composite electrode over $LiMnPO_4$ is due to the kinetic effects of the conductive gold nanoparticles and MgO nanowire additive on the surface of $LiMnPO_4$ which increases its electrochemical activity.

The infused magnesium-gold thin film on the crystal lattice tends to have good effects by increasing the surface area of the electrode. Gold in these manner works as the host for lithium ion intercalation and extraction and provides good electronic contact between the electrode which has $LiMnPO_4$ particles and the current collector through an overlap of the electrochemically active energies of the conductive gold particles *(*Chae *et al*., 2009). MgO nanowires being in the nanoscale will help in enhancing the mobility of electrons between the adjacent $LiMnPO_4$ particles during the lithiation/delithiation process (Gyu-Chul *et al.*, 2005). The nanowires will interact with $LiMnPO_4$ nanoparticles to form a 3D network which will easily facilitate lithium ion transport. Having a linear relationship between current and scan rates proves that $LiMnPO_4$ and $LiMnPO_4$/Mg-Au composite are both electroactive. However, $LiMnPO_4$/Mg-Au composite has better conductivity.

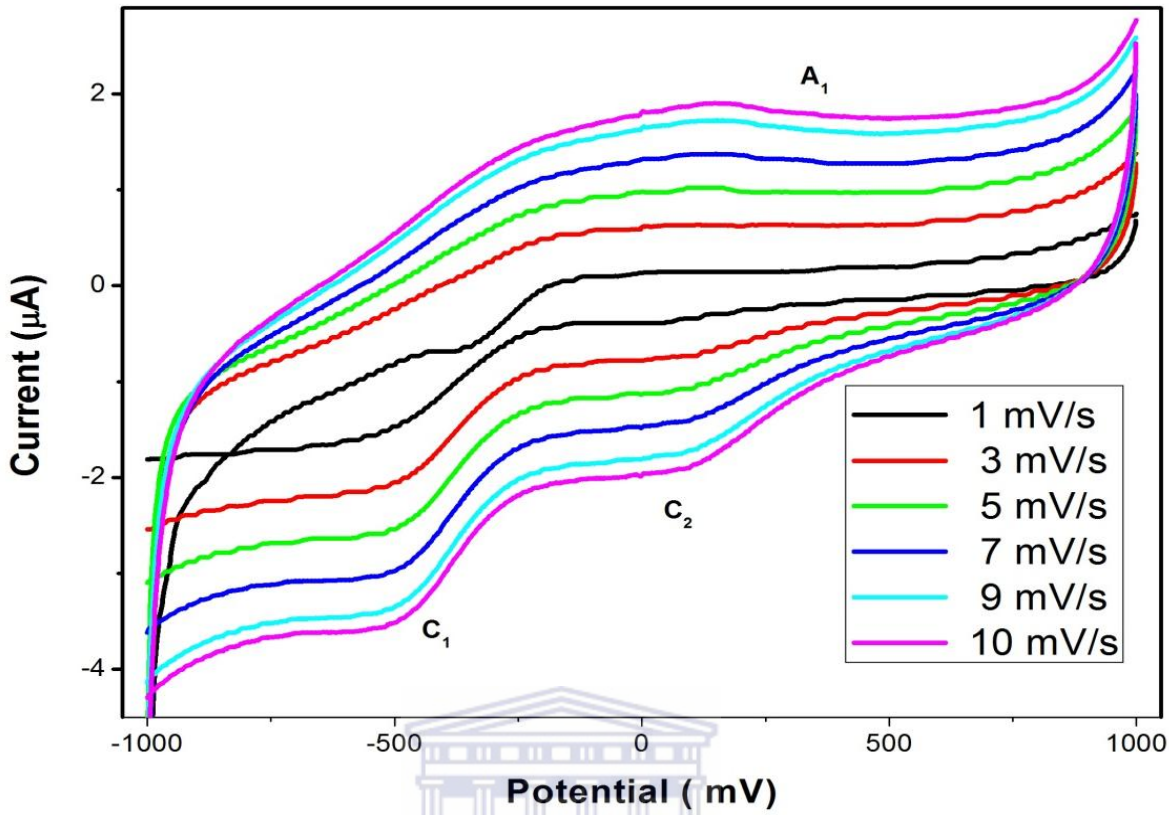

Figure 5.16: The effect of potential scan rate on the cyclic voltammograms of $LiMnPO_4$/ Mg-Au composite in 1 M $LiSO_4$ 1 – 10 mV/s. Voltage range: -1000–1000 mV.

A linear dependence of peak current on square root of scan rate was investigated. **Fig. 5.17** and **Fig. 5.18** were taken from the redox reactions of Mn^{2+}/Mn^{3+} and illustrate the scan rate dependence of the peak potentials (E_{pa} and E_{pc}) and peak currents (I_{pa} and I_{pc}) for $LiMnPO_4$ and $LiMnPO_4$/Mg-Au composite. E_{pa} and E_{pc} increases as scan rate increases. **Fig. 5.17** and **5.18** were used to calculate the Li^+ diffusion coefficient.

For reversible reaction, the concentration is related to peak current by the Randles-Sevčik equation (at 25 °C). The Randles –Sevcik equation (Monk, 2001):

$$I_p = (2.69 \times 10^5)\, n^{3/2} A D^{1/2} C V^{1/2} \qquad (18)$$

where n (1) is the number of electrons transferred, A (0.071 cm^2) is the area of the electrode, C (1 x 10^{-3} mol/cm^3) is the concentration of the bulk electrolyte solution and $I_p/v^{1/2}$ (0.7616 x 10^{-6}A $s^{1/2}$/ $V^{1/2}$) is the slope of the I_p versus $v^{1/2}$ linear plot (cathodic plots of **Fig. 5.17**) for $LiMnPO_4$ and 0.9809 x 10^{-6}A $s^{1/2}$/ $V^{1/2}$) is the slope of the I_p versus $v^{1/2}$ linear plot (cathodic plots of Fig. 5.18) for $LiMnPO_4$/Mg-Au composite. The diffusion coefficient, D, calculated for $LiMnPO_4$ and $LiMnPO_4$/Mg-Au composite was found to be 4.81 x 10^{-10} cm^2/s and 2 x 10^{-9} cm^2/s respectively which is close to the reported data for $LiMnPO_4$ in organic electrolyte (Molenda *et al*., 2006). Hence, the electrochemical processes are diffusion controlled. The diffusion coefficient between the pristine and modified showed little difference even though the $LiMnPO_4$/Mg-Au composite showed higher diffusion by an order of magnitude, meaning diffusion of lithium ions does not change much since it occurs in the solid bulk of the electrode materials which remains the same $LiMnPO_4$ in the modified and pristine and in aqueous and non-aqueous electrolyte.

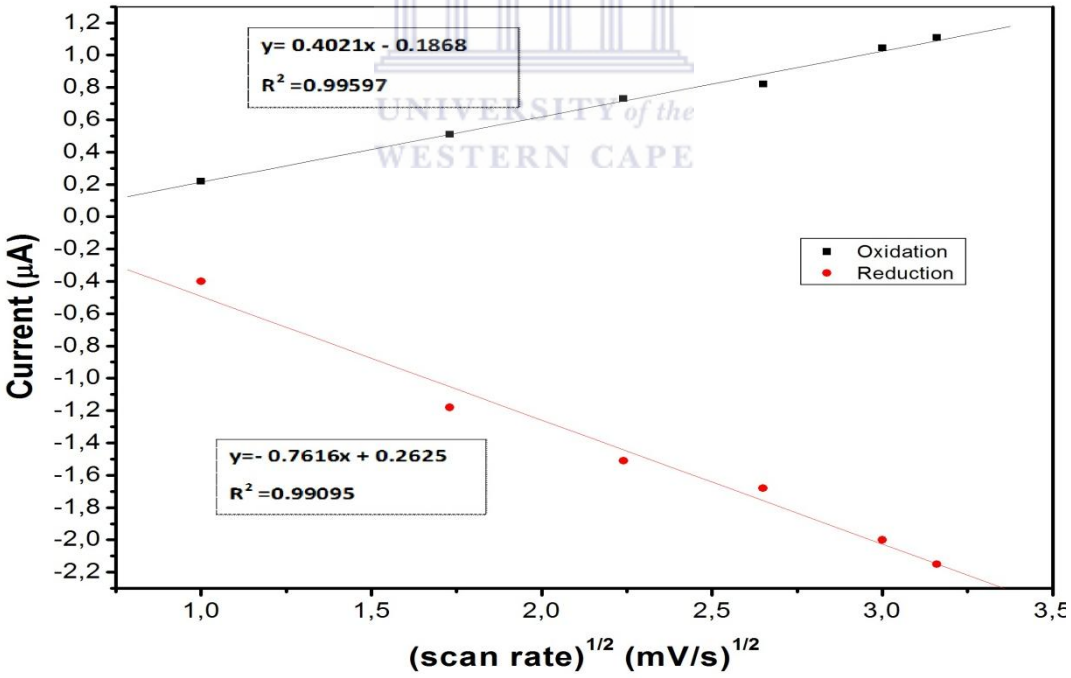

Figure 5.17: The plots of the anodic peak current as a function of potential scan rates and cathodic current as a function of potential scan rate for $LiMnPO_4$.

.

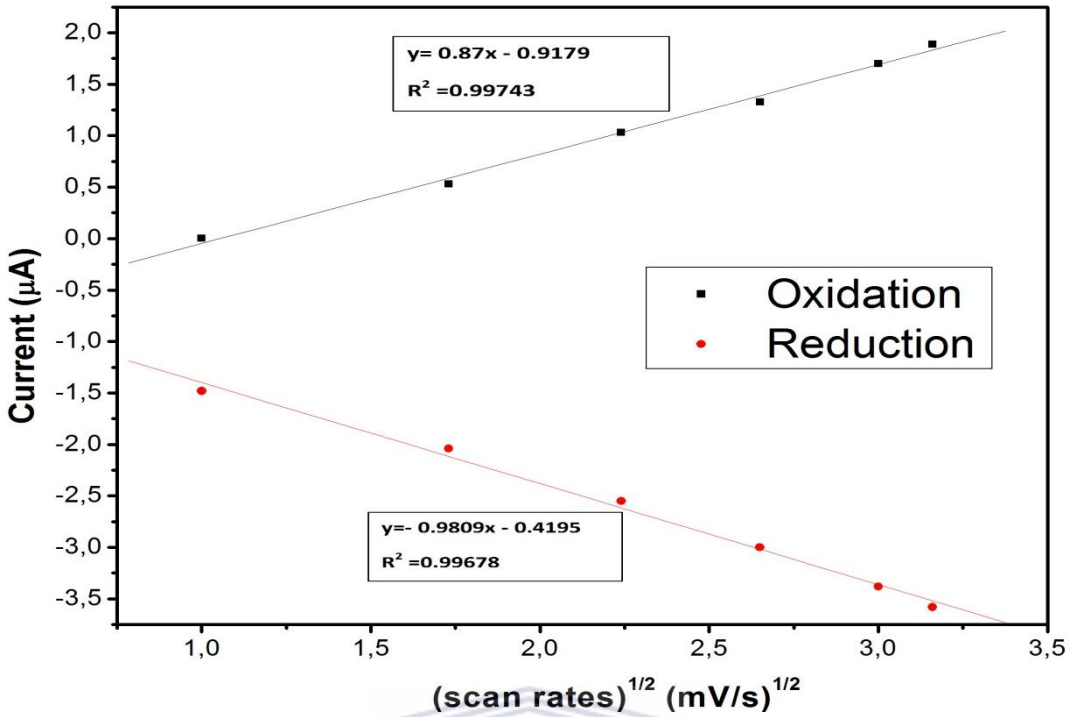

Figure 5.18: The plots of the anodic peak current as a function of potential scan rates and cathodic current as a function of potential scan rate for $LiMnPO_4$/Mg-Au thin film composite.

5.2.4.2 Electrochemical impedance spectroscopy

Electrochemical impedance spectroscopy (EIS) can provide information on impedance changes of the electrode surface after each modification step. In EIS, the semicircle diameter of impedance equals the electron transfer resistance (R_{ct}) which controls the transfer kinetics at the electrode interface. This resistance reflects the electron transfer kinetics of the redox probe at the electrode interface. **Fig. 5.19** shows curves of $LiMnPO_4$ electrode and the $LiMnPO_4$/Mg-Au composite on the Nyquist plot. Each plot gave a well-defined single semi-circle at high frequency and an inclined line at low frequency attributed to Warburg impedance associated with lithium ion diffusion in the bulk of the electrode. This is an indication that during lithium deinsertion/insertion, the kinetics of the electrode process is controlled by the diffusion process in the low frequency region and by the charge transfer in the high frequency region (Franger *et al.*, 2002, Zhang *et al.*, 2009, Feng, 2010). An intercept of the semi-circle with the *Z*′-axis in the very high frequency region identifies the Ohmic resistance (R_s) of the

electrolyte and electrodes. Both the $LiMnPO_4$ and the $LiMnPO_4$/Mg-Au composite electrode show the impedance semi-circle however, the electron transfer resistance of the $LiMnPO_4$/Mg-Au composite electrode was smaller than that of the $LiMnPO_4$ electrode. The R_{ct} values were obtained from equivalent electrical circuit fitting using Zplot software. The R_{ct} for $LiMnPO_4$/Mg-Au composite electrode was found to be 138.2 Ω and the one for $LiMnPO_4$ electrode was found to be 467.6 Ω, suggesting that the modified electrode has better charge transfer kinetics than the $LiMnPO_4$ electrode meaning the Mg-Au thin film coated on the surface of $LiMnPO_4$ facilitates the transfer of electrons hence, presents a more efficient electrochemical system (Ikpo et al., 2013). The observation proved that the $LiMnPO_4$/Mg-Au composite electrode has better conducting properties with enhanced electron transfer mediation than the $LiMnPO_4$ electrode. The poorer conductivity of $LiMnPO_4$ leads to more severe Li^+ ions jamming at the surface of the particles and accumulation of undesired Mn^{2+} upon cycling thus increasing the charge transfer resistance. The wider conduction bands of Au nanoparticles contributed in the enhancement of the electrochemical performance of $LiMnPO_4$/Mg-Au composite.

This observation from the Nyquist plot is correlated with the Bode phase-impedance plots (**Fig. 5.20**) where the pristine electrode exhibited higher impedance to electron transfer than the composite electrode as evidenced by the impedance and phase angle values ($LiMnPO_4$: 25.12 kΩ and 64°; $LiMnPO_4$/Mg-Au composite: 14.13 kΩ and 46°) at low frequency regimes where disturbances to the equilibrium positions of the systems are minimal. The change or the decrease in impedance for $LiMnPO_4$/Mg-Au composite at lower frequency, shows that the rate of electron transfer (flow of current) is greater This shows that facile electrode kinetics takes place on the composite cathode than on the $LiMnPO_4$. An improved rate of Li^+ in the electrolyte solution is therefore expected for $LiMnPO_4$/ Mg-Au composite. The lower R_{ct} observed from the EIS Nyquist plot corresponds to the shift of phase angle to high frequency which was observed from Bode plots of $LiMnPO_4$/Mg-Au composite and therefore, associated with fast electron transfer.

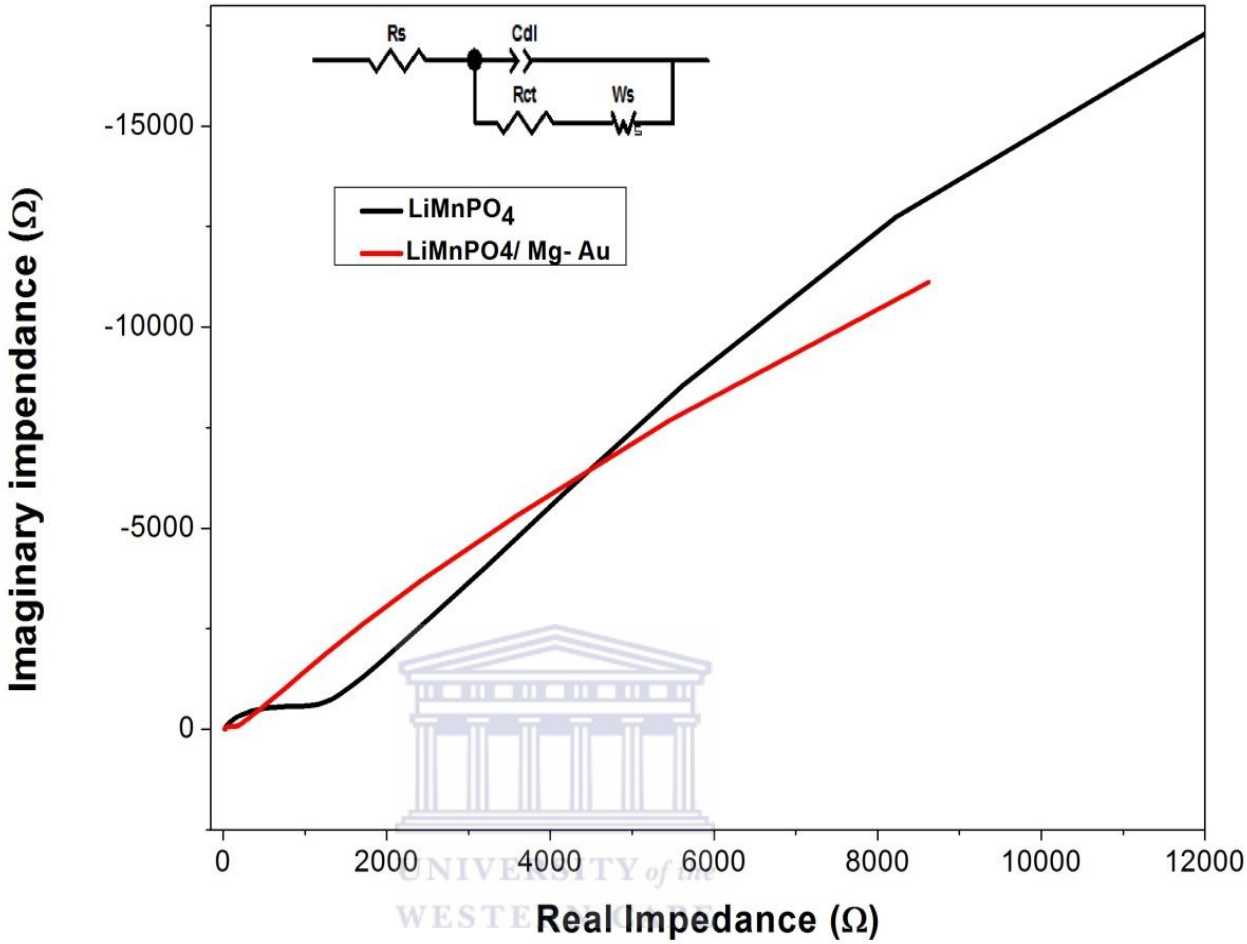

Figure 5.19: Comparative Nyquist plots of $LiMnPO_4$ and $LiMnPO_4$/Mg-Au thin film composite at formal potential.

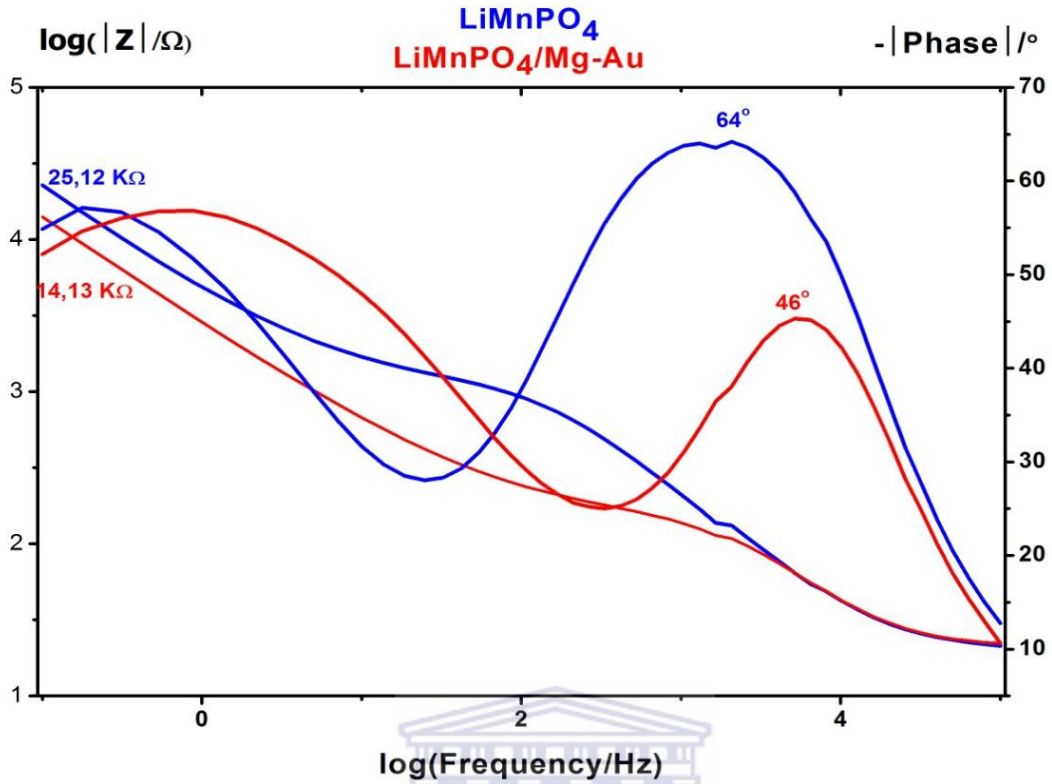

Figure 5.20: Comparative Bode phase-impedance diagrams of $LiMnPO_4$ and $LiMnPO_4$/Mg-Au composite at formal potential.

Table 5.2 shows the parameters of the equivalent circuit from Randles equivalent electrical circuit (inset) in the experimental impedance data of $LiMnPO_4$ and $LiMnPO_4$/Mg-Au composite electrode taken at the formal potential of the Cyclic voltammetry. The values of the parameters in **Table 5.2** show that electrode reactions are kinetically more facile in the $LiMnPO_4$/Mg-Au composite cathode system than in the $LiMnPO_4$ as a result of the presence of the conductive additives in the $LiMnPO_4$. R_{ct} value was found to be 407.6 Ω and 138.2 Ω for $LiMnPO_4$ and $LiMnPO_4$/Mg-Au respectively, which proved faster electrochemical transduction for $LiMnPO_4$/Mg-Au composite compared with $LiMnPO_4$. The time constant (τ); exchange current (I_o) (a measure of the rate of exchange charge between oxidized and reduced species at any equilibrium potential without net overall change) and heterogeneous rate constant of electron transfer ($k_{et)}$ were calculated according to the equations (Bard and Faulkne, 2001, Park and Yoo, 2003):

$$:\tau = \frac{1}{\omega_{max}} \quad (19)$$

$$R_{\mathrm{ct}} = \frac{RT}{nFI_{\mathrm{o}}} \quad (20)$$

$$I_o = nFAk_{\mathrm{et}}C \quad (21)$$

$$K_{\mathrm{et}} = \frac{I_{\mathrm{o}}}{nFAC} \quad (22)$$

$$\omega = \frac{1}{R_{\mathrm{ct}}+R_{\mathrm{s}}} \quad (23)$$

$$\sigma = (R_{\mathrm{s}} + R_{\mathrm{ct}})\omega^{\frac{1}{2}} \quad (24)$$

$$D = \frac{2(RT)^2}{(\sigma n^2 F^2 AC)^2} \quad (25)$$

where ω_{max} (frequency at maximum imaginary impedance of the semicircle in Hz), R_s is the solution resistance, R_{ct} is the charge transfer resistance, T is room temperature (K), *C* is the concentration (mol/cm^3), *R* is the gas constant (8.314 J /molK), *F* is the Faradays constant (96 486 C/ mol), *n* is the number of electrons, and k_{et} is the heterogeneous rate constant (cm^2/s).

From the value of R_{ct} we can be able to calculate the value for the exchange current (I_o) and then from this value, electron transfer rate constant (k_{et}) was calculated. It is evident from **Table 5.2** that the composite, with lower value of the Warburg coefficient (σ), has a higher diffusion coefficients (*D)* value thus confirming the earlier observations that faster lithium ion diffusion takes place on the $LiMnPO_4$/Mg-Au composite (modified) electrode than on the ($LiMnPO_4$) pristine cathode due to the presence of the conductive additives. The calculated values of the diffusion coefficients are close or in the magnitude of the value reported for $LiMnPO_4$ in organic electrolyte. The values of *D* from the two different techniques (CV: $D_{\mathrm{LiMnPO4/Mg\text{-}Au}}$ = 2. x 10^{-9} cm^2/s; D_{LiMnPO4} = 4.81 x 10^{-10}

cm^2/s; and EIS: $D_{LiMnPO4/Mg\text{-}Au} = 1.39 \times 10^{-13}$ cm^2/s; $D_{LiMnPO4} = 2.21 \times 10^{-17}$ cm^2/s), from these values both the CV and EIS showed an increase in the value of diffusion for $LiMnPO_4$/Mg-Au composite. The conductive additives facilitated lithium ion diffusivity thereby increasing the kinetics of the phase transformation between the charged phase and discharged phase. The value for electron transfer kinetics (k_{et}) calculated revealed that $LiMnPO_4$/Mg-Au composite has higher value compared with $LiMnPO_4$. All the results above were due to conductive Mg-Au thin films which were present in the composite cathode system.

	LiMnPO4	**$LiMnPO_4$/Mg-Au composite**
τ/ s/rad	2.35×10^{-4}	1.21×10^{-5}
R_{ct}/ Ω	407.6	138.2
I_o/ A	6.30×10^{-5}	1.86×10^{-4}
K_{et}/ cm/s	9.2×10^{-6}	2.72×10^{-5}
σ/ $\Omega/S^{1/2}$	22.65	14.18
D/ cm^2/s	2.21×10^{-17}	1.4×10^{-13}

Table 5.2: Kinetic parameters of composite $LiMnPO_4$ and $LiMnPO_4$ obtained from electrochemical impedance spectroscopy.

Chapter 6

6 Conclusion and Recommendations

6.1 Conclusion

The goal of this project was to explore lithium manganese phosphate ($LiMnPO_4$) modified by being coated with magnesium-gold composite thin film as cathode materials and study the conductivity of the $LiMnPO_4$ vs. $LiMnPO_4$/Mg-Au composite for possible use as cathode material in lithium ion batteries. Lithium manganese phosphate ($LiMnPO_4$) was synthesized via sol-gel approach which formed nanomaterials in a range 100-350 nm. The nanoscale dimensions enhance the electrochemical performance and the Li-ion diffusion, meaning smaller dimension can shorten the diffusion length of Li ion in the discharge and charge procedures to improve ion conductivity of the material. The conductivity of $LiMnPO_4$ can be further influenced by surface coating with gold nanomaterials and magnesium nanowires. Magnesium oxide nanowire and gold nanoparticles were successfully synthesized and proven by morphological studies. In the present work, pristine ($LiMnPO_4$) and $LiMnPO_4$ coated with Mg-Au composite thin film were synthesized successfully and characterized. The formation of the nanocrystalline phase and structure of the pristine and Mg-Au coated $LiMnPO_4$ nanoparticles were confirmed from the analysis of the XRD and FTIR results, respectively which showed that both $LiMnPO_4$ and $LiMnPO_4$/Mg-Au composite samples were identified as a single-phase olivine, confirming that the $LiMnPO_4$ olivine structural integrity was maintained after modification. The characterizations have also proven that all the $LiMnPO_4$/Mg-Au composite materials possess the olivine structure (*Pnmb* space group) which is related to the pristine $LiMnPO_4$ and further XRD analysis revealed that olivine $LiMnPO_4$ does still retain its orthorhombic structure in the presence of MgO and Au diffraction peaks, which confirms that the thin film has been coated onto $LiMnPO_4$ and the nanoparticles are crystalline in nature. The diffraction results demonstrate a high degree of crystallinity and uniformity. Raman and FTIR confirmed that the

material contain phosphate group which is present in the structure of olivine cathode material $LiMnPO_4$.The morphology, structure, shape and size of both $LiMnPO_4$ and $LiMnPO_4$/Mg-Au was confirmed by both the SEM and TEM images and the presence of Mn, P, O, Au and Mg elements in the $LiMnPO_4$/Mg-Au composite were confirmed from HRSEM–EDS. This means that surface coated layers due to Mg-Au thin film was also observed from surface morphology characterisation techniques. The combination of these techniques indicates that the Mg-Au composite has been infused into the crystal lattice and subsequently increased the active surface area of the electrode. It is expected that the existence of Mg-Au thin film would have a positive impact on the electrochemical performances of $LiMnPO_4$ at high rate. The formation of nanostructures can enhance the electrical conductivity of a cathode material. EIS and CV results revealed that $LiMnPO_4$/Mg-Au composite exhibited better electrochemical activity characterized by low charge-transfer resistance and well defined redox couples. From the CV, it was observed that $LiMnPO_4$ and $LiMnPO_4$/Mg-Au composite can be described as reversible reaction systems with resistive behaviour. The diffusion coefficients as well as the charge/discharge capacities were calculated using cyclic voltammetry and it showed that $LiMnPO_4$/Mg-Au composite has higher diffusion coefficient. The charge and discharge capacities of $LiMnPO_4$/Mg-Au composite and $LiMnPO_4$ were calculated using CV at 10 mV/s scan rates and it proved that $LiMnPO_4$/Mg-Au composite possesses higher charge/discharge capacities. The discharge capacity is about 93% closer to the value reported for theoretical $LiMnPO_4$ cathode material. The potential gap calculated from oxidation and reduction peaks proved that $LiMnPO_4$/Mg-Au composite has small potential gap than $LiMnPO_4$, meaning that in $LiMnPO_4$/Mg-Au composite, there is a faster electron transfer process. The higher conductivity observed in the $LiMnPO_4$/Mg-Au composite compared to the pristine is attributed to the presence of magnesium and gold thin film. The observations which were confirmed by both CV and EIS proved that the $LiMnPO_4$/Mg-Au composite electrode has better conducting properties with enhanced electron transfer mediation than the $LiMnPO_4$ cathode electrode. The wider conduction bands of gold nanoparticles coated on the surface contributed to the enhancement in the

electrochemical performance of $LiMnPO_4$/Mg-Au composite. Higher electronic conductivity supports faster charge transportation at high current rates, and is useful to prevent the pronounced pile-up of Li^+ ions and undesired Mn^{2+} ions on the surfaces of the particles during discharge. The composite cathode material demonstrated good electrochemical properties and is a promising cathode material for lithium ion batteries. This study suggests that the modification of $LiMnPO_4$ with Mg-Au thin film provides a new low cost approach for producing alternative $LiMnPO_4$ cathode material for lithium ion batteries with improved electrochemical properties.

$LiMnPO_4$ properties have been influenced by carbon coating in the previous studies of olivine cathode $LiMnPO_4$, but carbon tends to be not electrochemically active. Carbon amount must be minimized in order to increase the loading of active material within a given volume of lithium ion batteries, so as to increase the energy density. The novelty of this work is mainly in the use of gold nanomaterials and magnesium nanowires as surface coating materials for the enhancement of the electrochemical performance $LiMnPO_4$ cathode material. Gold works as the host for lithium ion intercalation and extraction and provides good electronic contact between the electrode which has $LiMnPO_4$ particles and the current collector through an overlap of the electrochemically active energies of the conductive gold particles. MgO nanowires being in the nanoscale will help in enhancing the mobility of electrons between the adjacent $LiMnPO_4$ particles during the lithiation/delithiation process. The nanowires will interact with $LiMnPO_4$ nanoparticles to form a 3D network which will easily facilitate lithium ion transport. The surface coating acts as a protective layer to prevent cathode corrosion during cycling.

This is the first time that $LiMnPO_4$/Mg-Au composite will be produced. The fabrication of battery coin cells with the $LiMnPO_4$/Mg-Au as cathode was however, not done. Hence, the material was not proven to be a better cathode material than the commercialised ones. It can be concluded from the investigations conducted that the $LiMnPO_4$/Mg-Au composite material

synthesized presents good electrochemical properties for applications in lithium ion batteries as well as in supercapacitors, as was seen from the calculations of charge/discharge capacities obtained from CV and improved conductivity obtained from EIS data.

6.2 Recommendations

A coin cell assembly is needed to be designed for battery testing; and the use of organic electrolyte in cyclic voltammetry and EIS is also necessary for further comparisons with previous works. Furthermore, this research work has however not explored the electronic configurations in olivine structure and the presence of all the elements in the synthesized materials. EDS which was used cannot detect alkaline metals like lithium. In future work, X-ray photoelectron spectroscopy (XPS) which can measure the elemental composition at the parts per thousand range, empirical formula, chemical state and electronic state of the elements that exist within a material, will be employed. Results obtained may be further used to verify the present proposed mechanism for enhanced electronic conductivity, and also to provide more insight for new cathode material design.

References

Al-Ghamdi, A., et al. (2012). *"A new facile synthesis of ultra fine magnesium oxide nanowires and optical properties."* Journal of Electroceramics **29**(3): 198-203.

Alotto, P., et al. (2014). *"Redox flow batteries for the storage of renewable energy: A review."* Renewable and Sustainable Energy Reviews **29**(0): 325-335.

Aravindan, V., et al. (2013). *"$LiMnPO_4$ - A next generation cathode material for lithium-ion batteries."* Journal of Materials Chemistry A **1**(11): 3518-3539.

Aricò A.S., et al. (2005).” Nanostructured materials for advanced energy conversion and storage devices”Nature Materials **4**: 366 – 377.

Ballestero, D., et al. (2014). "*Novel methodology for gold nanoparticles deposition on carbon monolith supports."* Colloids and Surfaces A: Physicochemical and Engineering Aspects **441**(0): 91-100.

Bakenov Z. and Taniguchi I. (2011). *“$LiMnPO_4$ Olivine as a Cathode for Lithium Batteries”* The Open Materials Science Journal ***5*** *:*222-227.

Bard, A.J. and L.R. Faulkne. (2001). “*Electrochemical methods fundamentals and applications”*. Second edition : John Wiley and Sons, Inc.

Barré, A., B. et al. (2013). *"A review on lithium-ion battery ageing mechanisms and estimations for automotive applications."* Journal of Power Sources **241**(0): 680-689.

Barsoukov, E and J.R. Macdonald (2005) “*Impemdamce spectroscopy: Theory, Experiment and Applications”*. Second edition. Hoboken, New Jersey: John Wiley & Sons, Inc.595

Burba,C.M. and R. Frech (2006) *Vibrational spectroscopic investigation of structurally-related $LiFePO_4$, $NaFePO_4$, and $FePO_4$ compounds*. Spectrochimica. Acta A :65 44.

Carabineiro, S., et al. (2011). *"Gold nanoparticles supported on magnesium oxide for CO oxidation."* Nanoscale Research Letters **6**(1): 435.

Chae Kyu Kim , et al (2008) . "*Gold nanoparticles in delivery applications*". Advanced Drug Delivery Reviews **60**: 1307–1315

Chang B. and Park S. (2010) "*Electrochemical Impedance Spectroscopy"* (2010) Annual Review of Analytical Chemistry **3**: 208-209.

Chen, J. (2013). *"Recent Progress in Advanced Materials for Lithium Ion Batteries."* Materials **6**(1): 156-183.

Chen, J. et al. (2008). "*The hydrothermal synthesis and charactarization of olivines and related compounds for electrochemical applications*". Solid State Ionics **178** (31-32): 1676-1693.

Chen Ya-Wen and Chen Jenn-Shing. (2012). *"A Study of Electrochemical Performance of $LiFePO_4$/C Composites Doped with Na and V*". International Jornal of Electrochemical Science**, 7**: 8128 - 8139

Chen, Z., et al. (2010). *"Role of surface coating on cathode materials for lithium-ion batteries."* Journal of Materials Chemistry **20**(36): 7606-7612.

Doan, T. N. L. and I. Taniguchi. (2011). *"Cathode performance of $LiMnPO_4$/C nanocomposites prepared by a combination of spray pyrolysis and wet ball-milling followed by heat treatment."* Journal of Power Sources **196**(3): 1399-1408.

Doi T., et al. (2009) "*Cathodic performance of $LiMn_{1-x}M_xPO_4$ (M = Ti, Mg and Zr) annealed in an inert atmosphere"*. Electrochimica Acta; **54**: 3145-51.

Drezen, T., et al. (2007). *"Effect of particle size on $LiMnPO_4$ cathodes."* Journal of Power Sources **174**(2): 949-953.

EI-Sayed I.H., et a.l (2007) "*Gold nanoparticles:interesting optical properties and recent applications in cancer diagnostics and therapy*". Nanomedicine **2**(5): 681-693.

Fang H, Z. Pan and L. Li (2008). "*The possibility of manganese disorder in $LiMnPO_4$ and its effect on the electrochemical activity"*. Electrochemistry Communocations; **10**: 1071-1073.

Fergus, J. W. (2010). *"Recent developments in cathode materials for lithium ion batteries."* Journal of Power Sources **195**(4): 939-954.

Franger,S, et al. (2002). "*$LiFePO_4$ Synthesis Routes for Enhanced Electrochemical Performance"*. Electrochemical Solid-State Letters., **5**: A231.

Fu, L., et al. (2006). *"Surface modifications of electrode materials for lithium ion batteries."* Solid State Sciences **8**(2): 113-128.

Gyu-Chul Yi, et al. (2005). "*ZnO nanorods: synthesis, characterization and applications"*.Semiconductor Science. Technology.

Hadjipaschalis, I., et al. (2009). *"Overview of current and future energy storage technologies for electric power applications."* Renewable and Sustainable Energy Reviews **13**(6–7): 1513-1522.

Harada M. et al. (1994). "*Structural analysis of polymer-protected platinum/rhodium bimetallic clusters using extended x-ray absorption fine structure spectroscopy. Importance of microclusters for the formation of bimetallic clusters*". Journal of Physical Chemistry ***98***, 2635.

Huang, M. R., C.W. Lin, and H.Y. Lu. (2001). "*Crystallographic facetting in solid-state reacted $LiMn_2O_4$ spinel powder."* Applied Surface Science **177**(1-2): 103-113.

Hirst D. G, S. Jain and J.M. O'Sullivan (2012) "*Gold nanoparticles as novel agents for cancer therapy*". The British Journal of Radiology **85**:101–113.

Ikpo, C. O., *et al. (2013)* "*Novel Iron-Cobalt Derivatised Lithium Iron Phosphate Nanocomposite for Lithium Ion Battery Cathode*." International Journal of Electrochemical Science,. **8**: 753-772.

Jacobson, Mark Z. and M. A. Delucchi. (2009). *"A Path to Sustainable Energy by 2030" (PDF).* Scientific American **301** (5): 58–65.

Jenkel J. et al. (1994) "*Analytical Chemistry for Technicians"*. Lewis Publishers, Boca Raton, United States of America.

Kim, D. K., et al. (2008). "*Spinel $LiMn_2O_4$ Nanorods as Lithium Ion Battery Cathodes."* Nano Letters **8**(11): 3948-3952.

Kumar, P.R., et al. (2011). "*Carbon coated $LiMnPO_4$ nanorods for lithium batteries*".Journal of The Electrochemical Society, **158** (3) A227-A230.

Kwon, N. H. and K. M. Fromm (2012). *"Enhanced electrochemical performance of and lt;30and #xa0;nm thin $LiMnPO_4$ nanorods with a reduced amount of carbon as a cathode for lithium ion batteries."* Electrochimica Acta **69**(0): 38-44.

Li, Y.-F., et al. (2011). "*Geometries, stabilities, and electronic properties of gold–magnesium (Au-Mg) bimetallic clusters."* Physics Letters A **375**(18): 1877-1882.

Li, L., et al. (2013). "*Effect of different carbon sources on the electrochemical properties of rod-like LiMnPO4-C nanocomposites."* RSC Advances **3**(19): 6847-6852.

Liu, J., et al. (2013). "*Synthesis of nano-sized $LiMnPO_4$ and in situ carbon coating using a solvothermal method."* Journal of Power Sources **229**(0): 203-209.

Long, N. N., et al. (2009) "*Synthesis and optical properties of colloidal gold nanoparticles*". Journal of Physics: Conference Series **187** 012026.

Mann, P., L. Gahagan and M.B. Gordon. (2009)"*Tectonic setting of the world's giant oil and gas fields,"* in Michel T. Halbouty (ed.) Giant Oil and Gas Fields of the Decade, 1990–1999, Tulsa, Okla.: American Association of Petroleum Geologists, p. 50.

Manjunatha, H. et al. (2012). "*Electrochemical studies of $LiMnPO_4$ as aqueous rechargeable lithium–ion battery electrode"*.Journal of Solid State Electrochemistry,**16**:1941–1952.

Manthiram, A., et al. (2008). "*Nanostructured electrode materials for electrochemical energy storage and conversion."* Energy & Environmental Science **1**(6): 621-638.

Molenda J. et al. (2006). *"Diffusional mechanism of deintercalation in LiFe1 − yMnyPO4 cathode material"*. Solid State Ionics **177**:2617–2624

Moncada, A., et al. (2014). *"High-performance of PbO_2 nanowire electrodes for lead-acid battery."* Journal of Power Sources **256**(0): 72-79.

Monk, P.M.S. (2001) *Fundamentals of electroanalytical Chemistry*. Analytical Techiques in the Sciences (AnTS), ed.

Mordike, B. L. and T. Ebert (2001). "*Magnesium: Properties — applications — potential."* Materials Science and Engineering: A **302**(1): 37-45.

Nagashima, K., et al. (2007). *"Control of magnesium oxide nanowire morphologies by ambient temperature."* Applied Physics Letters **90**(23).

Norberg, N. S. and Kostecki, R. (2011). " *FTIR spectroscopy of a LiMnPO4 composite cathode.*" Electrochimica Acta **56** (25): 9168-9171.

Novikova, S., et al. (2013) *"$LiFe_{1-x}M_xPO_4/C$ (M=Co, Ni, Mg) as cathode materials for lithium-ion batteries."* Electrochimica Acta(0).

Ramar, V. and P., Balaya (2013). "*Emhancing the electrochemical Kinetics of high voltage olivine LiMnPO4 by isovalent co-doping".*Physical Chemistry Chemical Physics. **15**(40): 17240-17249.

Rand, D. A. J. and P. T. Moseley (2009). Secondary batteries – lead– acid systems | overview. Encyclopedia of Electrochemical Power Sources. J. Garche. Amsterdam, Elsevier**:** 550-575.

Pan, X.-L., et al. (2013). "*Hydrothermal synthesis of well-dispersed $LiMnPO_4$ plates for lithium ion batteries cathode."* Electrochimica Acta **87**(0): 303-308.

Park, S.-M. and J.-S. Yoo. (2003) "*Electrochemical impendance spectroscopy: for better electrochemical measurements Analytical chemistry"*. **75**(21): 455-461.

Park, J., et al. (2005). *"Generalized Synthesis of Metal Phosphide Nanorods via Thermal Decomposition of Continuously Delivered Metal−Phosphine Complexes Using a Syringe Pump."* Journal of the American Chemical Society **127**(23): 8433-8440.

Pitchai, R., et al. (2011). *"Nanostructured cathode materials: a key for better performance in Li-ion batteries."* Journal of Materials Chemistry **21**(30): 11040-11051.

Qin, Z., et al. (2012). *"Morphology controlled synthesis and modification of high-performance $LiMnPO_4$ cathode materials for Li-ion batteries."* Journal of Materials Chemistry **22**(39): 21144-21153.

.Salah, A. A., et al. (2006) "*Doping Effects on Electronic Conductivity and Electrochemical Performance of $LiFePO_4$"*. Spectrochimica. Acta A 65 1007.

Shukla, A. K., et al. (2001). "*Nickel-based rechargeable batteries."* Journal of Power Sources **100**(1–2): 125-148.

Shaju, K., et al. (2003). *"X-ray photoelectron spectroscopy and electrochemical behaviour of 4 V cathode, Li (Ni< sub> 1/2</sub> Mn< sub> 1/2</sub>) O< sub> 2</sub>."* Electrochimica Acta **48**(11): 1505-1514.

Scrosati, B. and J. Garche (2010). *"Lithium batteries: Status, prospects and future."* Journal of Power Sources **195**(9): 2419-2430.

Skoog D. A., et al. (1992). "*Fundamentals of Analytical Chemistry"*(1992) Saunders College Publishing, Fort Worth, United States of America :100-200.

Suzuki, E. (2002).0 "*High-resolution scanning electron microscopy of immunogold-labelled cellsby the use of thin plasma coating of osmium"*. Journal of Microscopy **3**(208): 153-157.

Thompson, D. *T. (*2007)*Nano Today*, ***2***: 40-43.

Wang K., et al. (2009). "*Optimized carboncoated $LiFePO_4$ cathode material for lithium-ion batteries"*. Electrochimica Acta; **54:** 2861-8.

Wang, G. X., et al. (2006). "*A study on $LiFePO_4$ and its doped derivatives as cathode materials for lithium-ion batteries."* Journal of Power Sources **159**(1): 282-286.

Wu, L. et al. (2013). "*Synthesis of Cr-doped $LiMnPO_4$/C cathode materials by sol–gel combined ball milling method and its electrochemical properties*". Ionics **19**: 1061–1065.

Whittingham, M. S. (2004). *"Lithium Batteries and Cathode Materials."* Chemical Reviews **104**(10): 4271-4302.

Winter, M. and R. J. Brodd (2005). "*What Are Batteries, Fuel Cells, and Supercapacitors?* (Chem. Rev. 2003, 104, 4245−4269. Published on the Web 09/28/2004.)." Chemical Reviews **105**(3): 1021-1021.

Woo Kim H.,et al (2007) "*Controlled Growth and Characterization of MgO Nanowires by Varying the Thickness of the Underlying Au Layers".* Journal of the Korean Physical Society, **51** (1): 204_208.

http://www.nexergy.com/media/BatteryGraph.JPG (last access 10.02.2011).

http://tuprints.ulb.tu-darmstadt.de/1864/1/Dissertation_Stefan_Laubach.pdf (last access 10.02.2011).

Xu, K. (2004). "*Nonaqueous Liquid Electrolytes for Lithium-Based Rechargeable Batteries."* Chemical Reviews **104**(10): 4303-4418.

Yamada, A., et al. (2003). "*Olivine-type cathodes: Achievements and problems."* Journal of Power Sources **119–121**(0): 232-238.

Zhang, Q., et al. (2013). *"Nanomaterials for energy conversion and storage."* Chemical Society Reviews **42**(7): 3127-3171.

Zhao, M., et al. (2012). "*Characteristics and electrochemical performance of* $LiFe_{0.5}Mn_{0.5}PO4/C$ *used as cathode for aqueous rechargeable lithium battery*." Journal of Power Sources. **211**: 202-207.